

HADES RV Programme with HARPS-N at TNG[★]

XII. The abundance signature of M dwarf stars with planets

J. Maldonado¹, G. Micela¹, M. Baratella^{2,3}, V. D’Orazi³, L. Affer¹, K. Biazzo⁴, A. F. Lanza⁴, A. Maggio¹, J. I. González Hernández^{5,6}, M. Perger^{7,8}, M. Pinamonti⁹, G. Scandariato⁴, A. Sozzetti⁹, D. Locci¹, C. Di Maio^{10,1}, A. Bignamini¹¹, R. Claudi³, E. Molinari¹², R. Rebolo^{5,6}, I. Ribas^{7,8}, B. Toledo-Padrón^{5,6}, E. Covino¹³, S. Desidera³, E. Herrero^{7,8}, J. C. Morales^{7,8}, A. Suárez-Mascareño^{5,6}, I. Pagano⁴, A. Petralia¹, G. Piotto², and E. Poretti^{14,15}

¹ INAF - Osservatorio Astronomico di Palermo, Piazza del Parlamento 1, 90134 Palermo, Italy
e-mail: jesus.maldonado@inaf.it

² Dipartimento di Fisica e Astronomia Galileo Galilei, Vicolo Osservatorio 3, 35122 Padova, Italy

³ INAF - Osservatorio Astronomico di Padova, vicolo dell’Osservatorio 5, 35122 Padova, Italy

⁴ INAF - Osservatorio Astrofisico di Catania, Via S. Sofia 78, 95123, Catania, Italy

⁵ Instituto de Astrofísica de Canarias, 38205 La Laguna, Tenerife, Spain

⁶ Universidad de La Laguna, Departamento Astrofísica, 38206 La Laguna, Tenerife, Spain

⁷ Institut de Ciències de l’Espai (ICE, CSIC), Campus UAB, Carrer de Can Magrans s/n, 08193 Bellaterra, Spain

⁸ Institut d’Estudis Espacials de Catalunya (IEEC), 08034 Barcelona, Spain

⁹ INAF - Osservatorio Astrofisico di Torino, Via Osservatorio 20, 10025 Pino Torinese, Italy

¹⁰ Università degli Studi di Palermo, Dipartimento di Fisica e Chimica, via Archirafi 36, Palermo, Italy

¹¹ INAF - Osservatorio Astronomico di Trieste, Via Tiepolo 11, 34143 Trieste, Italy

¹² INAF - Osservatorio Astronomico di Cagliari & REM, Via della Scienza, 5, 09047 Selargius CA, Italy

¹³ INAF - Osservatorio Astronomico di Capodimonte, Salita Moiariello 16, 80131 Napoli, Italy

¹⁴ Fundación Galileo Galilei-INAF, Rambla José Ana Fernández Pérez 7, 38712 Breña Baja, TF, Spain

¹⁵ INAF - Osservatorio Astronomico di Brera, Via E. Bianchi 46, 23807 Merate, Italy

Received September 15, 1996; accepted March 16, 1997

ABSTRACT

Context. Most of our current knowledge on planet formation is still based on the analysis of main-sequence, solar-type stars. Conversely, detailed chemical studies of large samples of M-dwarf planet hosts are still missing.

Aims. We aim to test whether the correlations between the metallicity, individual chemical abundances, and mass of the star and the presence of different type of planets found for FGK stars still holds for the less massive M dwarf stars. Methods to determine in a consistent way stellar abundances of M dwarfs from high-resolution optical spectra are still missing. The present work is a first attempt to fill this gap.

Methods. We analyse in a coherent and homogeneous way a large sample of M dwarfs with and without known planetary companions. We develop for the first time a methodology to determine stellar abundances of elements others than iron for M dwarf stars from high-resolution, optical spectra. Our methodology is based on the use of principal component analysis and sparse Bayesian’s methods. We made use of a set of M dwarfs orbiting around an FGK primary with known abundances to train our methods. We applied our methods to derive stellar metallicities and abundances of a large sample of M dwarfs observed within the framework of current radial velocity surveys. We then used a sample of nearby FGK stars to cross-validate our technique by comparing the derived abundance trends in the M dwarf sample with those found on the FGK stars.

Results. The metallicity distribution of the different subsamples shows that M dwarfs hosting giant planets show a planet-metallicity correlation as well as a correlation with the stellar mass. M dwarfs hosting low-mass planets do not seem to follow the planet-metallicity correlation. We also found that the frequency of low-mass planets does not depend on the mass of the stellar host. These results seem in agreement with previous works. However, we note that for giant planet hosts our metallicities predict a weaker planet metallicity correlation but a stronger mass-dependency than photometric values. We show, for the first time, that there seems to be no differences in the abundance distribution of elements different from iron between M dwarfs with and without known planets.

Conclusions. Our data shows that low-mass stars with planets follow the same metallicity, mass, and abundance trends than their FGK counterparts, which are usually explained within the framework of core-accretion models.

Key words. techniques: spectroscopic – stars: abundances – stars: late-type – planetary systems

1. Introduction

More than twenty-five years after the first exoplanets discoveries (Wolszczan & Frail 1992; Mayor & Queloz 1995) it is now

* Based on observations collected at the European Southern Observatory, Chile under programme ID 0102.D-0119(A) and 0102.D-0119(B)

well-established that planetary systems are found around a wide variety of stellar hosts from brown dwarfs and low-mass stars to red giants, pulsars and probably white dwarfs (see e.g. Perryman 2018, and references therein). However, the vast majority of known planets are found to orbit around Sun-like stars (see e.g. <http://exoplanet.eu/> or <http://exoplanets.org/>). Therefore, our un-

derstanding of the dependence of planet formation on the stellar mass is still far from being complete.

The study of chemical abundances in Sun-like planet host stars has been crucial for our understanding of planet formation with the finding that the frequency of gas-giant planets is a function of the host star metallicity (e.g. Gonzalez 1997; Santos et al. 2004; Fischer & Valenti 2005; Sozzetti et al. 2009) while stars with orbiting low-mass planets do not seem to be preferentially metal-rich (e.g. Ghezzi et al. 2010; Mayor et al. 2011; Sousa et al. 2011; Buchhave et al. 2012). This trend is explained within the framework of core-accretion models, which assume that the timescale needed to form an icy or rocky core is largely dependent on the metal content of the protostellar cloud (e.g. Pollack et al. 1996; Ida & Lin 2004; Hubickyj et al. 2005; Mordasini et al. 2009, 2012).

Besides the gas-giant planet metallicity correlation any other claim of a chemical trend in planet hosts has been controversial or at least disputed. Most studies show that planet hosts have abundances similar to those of stars without planets (e.g. Bodaghee et al. 2003; Ecuivillon et al. 2006; Gonzalez 2006; Gilli et al. 2006; da Silva et al. 2011; Adibekyan et al. 2012b). For instance, it has been suggested that the α -elements enhancement found in planet hosts of intermediate metallicity (Adibekyan et al. 2012b) or the small depletion on refractory elements with respect to volatiles found in the Sun and other solar analogues (e.g. Meléndez et al. 2009; Ramírez et al. 2009) can be effects of galactic chemical evolution (e.g. González Hernández et al. 2010, 2013) or related to an inner Galactic origin of the planet hosts (e.g. Adibekyan et al. 2014; Maldonado & Villaver 2016).

At the low end of the stellar mass scale, low-mass stars (e.g. M dwarfs) are promising targets in the search for small, rocky planets with the potential capabilities of hosting life (e.g. Dressing & Charbonneau 2013). Unlike their FGK counterparts, detailed chemical studies of samples of M dwarf planet hosts have focused only on the iron content, or metallicity and are based on a relatively small number of planet hosts. Furthermore, metallicity values are often based on photometric values which makes difficult a comparison with the spectroscopic results from Sun-like stars. As example, the stellar sample analysed in Johnson et al. (2010a) comprises only five planets around M dwarfs while Neves et al. (2013) studied a sample with 13 stars hosting 20 planets (seven stars hosting gas-giant planets, and six stars with only low-mass planet hosts). The sample in Rojas-Ayala et al. (2012) includes a total of 113 M dwarfs, but only 11 planet hosts. Montet et al. (2014) analysed a sample of 111 M dwarfs with only eight planet hosts. These numbers contrast dramatically with the large number of FGK planet hosts for which detailed chemical abundances have been performed (e.g. Bodaghee et al. 2003; Adibekyan et al. 2014; Maldonado et al. 2015b).

Despite the small number statistics, several interesting trends regarding the planet-metallicity correlation in M dwarfs have already been discussed. It is known that there is a systematically lower fraction of Jovian planets around M dwarfs than around FGK stars (Endl et al. 2003, 2006; Butler et al. 2006; Bonfils et al. 2007; Cumming et al. 2008; Johnson et al. 2010b). On the other hand, low-mass planets seem to be common around M dwarfs (Bonfils et al. 2013; Howard et al. 2012; Mulders et al. 2015a,b). Previous works also suggest that the gas-giant planet metallicity correlation is also apparent in the M dwarf sample but the correlation is not present when Neptunian and smaller planets are considered (Bonfils et al. 2007; Johnson & Apps 2009; Schlaufman & Laughlin 2010; Rojas-Ayala et al. 2012; Terrien et al. 2012; Neves et al. 2013; Courcol et al. 2016). More re-

cently, Pinamonti et al. (2019) found a moderate-to-weak dependence of the planetary minimum mass on the stellar metallicity for M dwarfs.

Regarding other chemical abundances besides iron, and to the very best of our knowledge, a detailed analysis has not been performed yet. This is because the accurate determination of the stellar parameters and abundances of M dwarfs is a difficult task as these stars are faint at optical wavelengths and their optical spectra are largely covered by molecular bands that blend or hide most of the atomic lines. Whilst spectral synthesis has been tested in several works, it is computationally expensive and requires a good knowledge of the atomic and molecular data. It has been tested usually on small number of stars, focusing on strong atomic lines, and on spectral windows known to be less affected by molecular lines or in the near infrared (e.g. Woolf & Wallerstein 2005; Bean et al. 2006; Önehag et al. 2012; Souto et al. 2017), that is, at wavelengths redder than the spectral coverage of many spectrographs especially designed to achieve accurate radial velocities and used on current planetary surveys of M dwarfs.

We believe that the analysis of a homogeneous and large sample of M dwarfs hosting planets is needed before a confirmation or rejection of preliminary trends or a proper comparison with FGK stars is invoked. Several radial velocity projects have been working on different methodologies to derive stellar abundances of M dwarfs using the same spectra that are used for the radial velocity determinations. Within the framework of the CARMENES (Quirrenbach et al. 2018) collaboration, Passegger et al. (2018, 2019); Schweitzer et al. (2019) derived stellar parameters for almost 300 M dwarfs by applying spectral synthesis to both visible and near-infrared spectra. For the HARPS GTO M dwarf survey (Bonfils et al. 2013), a technique based on the use of pseudo-equivalent widths of spectral features identified in optical high-resolution spectra was developed by Neves et al. (2014). In a recent work, machine learning methods applied to pseudo-equivalent widths have been developed by Antoniadis-Karnavas et al. (2020). A different technique, although also based on pseudo-equivalent widths, was presented in Maldonado et al. (2015a) within the framework of the HADES survey (Affer et al. 2016).

In this paper we present a completely different methodology. Unlike previous works it has the advantage that it can be used to determine the elemental abundances of different elements besides iron. Our approach is based on the use of principal component analysis and sparse Bayesian's fitting methods. A set of M dwarfs in binary systems orbiting around an FGK primary was observed and is used to train our method.

We use our derived abundances to revisit the correlation between the presence of planets around M dwarfs and the stellar properties, namely the stellar mass and the chemical composition. One of the motivations is the increase with respect to previous works of the number of M dwarfs known to host a planet. In particular we analyse the properties of at least five times more M dwarfs hosting low-mass planets ($\text{msin } i \lesssim 30 \text{ M}_\oplus$) than previous works. We made use of the available high-resolution HARPS and HARPS-N échelle spectra as well as our spectroscopic tools specifically designed for the analysis of M dwarfs spectra to homogeneously determine stellar properties and chemical abundances. This allows us to increase consistently the stellar sample analysed in this work.

The paper is organised as follows. Sect. 2 describes the stellar sample analysed in this work and how stellar parameters are obtained. We describe our technique to measure stellar abundances for M dwarf stars from optical spectra in Sect. 3. Detec-

tion limits for our target stars are discussed in Sect. 4. The mass, metallicity, and individual abundance distributions are presented in Sect. 5. Our conclusions follow in Sect. 6.

2. Spectroscopic data

A list of late-K and M dwarf stars observed within the framework of radial velocity surveys was compiled by carefully checking the stars within the California Planet Survey (CPS) late-K and M-type dwarf sample (Rauscher & Marcy 2006), the HARPS GTO M dwarf sample (Bonfils et al. 2013), and the HADES radial velocity program sample of M dwarfs (Affer et al. 2016).

In order to derive homogeneous stellar properties, only stars with HARPS (Mayor et al. 2003) and HARPS-N (Cosentino et al. 2012) data were considered. HARPS data were obtained from the ESO Science Data Products Archive¹, while HARPS-N data were taken from the public archive of the Telescopio Nazionale Galileo (TNG)². The instrumental setup of HARPS and HARPS-N is almost identical. The spectra cover the range 383–693 nm (HARPS-N) and 378–691 nm (HARPS). Both instruments provide a resolving power of $R \sim 115000$. The spectra are provided already reduced using HARPS/HARPS-N standard calibration pipelines. For each star a coadded spectrum combining all the available observations was made. Typical values of the signal-to-noise ratio (measured around 605 nm) for the combined spectra are from 45 to 99 with a median value of 67.

Stellar effective temperatures and metallicities were determined for each star by using the code msdlines³ (Maldonado et al. 2015a) which is based on the use of spectral features and their ratios. The iron abundance values given by the code msdlines are based on the photometric M_K -[Fe/H] relationship by Neves et al. (2012, hereafter N12) while the effective temperatures are based on the revised scale by Mann et al. (2013b). Physical parameters namely, surface gravity, stellar mass, stellar radius, and luminosity are derived from the derived stellar effective temperature and metallicity values by using the empirical calibrations provided in the msdlines code. The stellar masses provided by this code are based on near-infrared photometry (Henry & McCarthy 1993) and have typical uncertainties of the order of 13%. We note that for eight targets our methodology provides unrealistic low stellar masses (below $0.10 M_{\odot}$). In these particular cases, photometric masses were considered using the calibration by Henry & McCarthy (1993). These calibrations are provided in the CIT photometric system. We therefore converted the 2MASS (Cutri et al. 2003) magnitudes into CIT magnitudes before applying these calibrations, following the transformations provided by Carpenter (2001). Stellar radius is computed using the mass-radius relationship provided in Maldonado et al. (2015a), surface gravities are derived from the stellar masses and radii, and luminosities by applying the Stefan-Boltzmann law. We note that this is exactly the procedure followed in Maldonado et al. (2015a) to derive the empirical calibrations of the physical parameters as a function of T_{eff} and metallicity.

Galactic spatial-velocity components (U, V, W) were computed using *Gaia* DR2 (Gaia Collaboration et al. 2018) proper motions and parallaxes, together with radial velocities from Soubiran et al. (2018) and *Gaia* DR2. When no values from these sources were available, data from the *Simbad*⁴ database were considered. To compute (U, V, W) the procedure of Montes

et al. (2001) was followed. This procedure updates the original algorithm (Johnson & Soderblom 1987) to epoch J2000 in the International Celestial Reference System (ICRS). When possible, the full covariance matrix was used in computing the uncertainties in order to take the possible correlations between the astrometric parameters into account. Finally, stars were classified as belonging to the thin/thick disk applying the methodology described in Bensby et al. (2003, 2005).

Stellar age is one of the parameters more difficult to determine in an accurate way, especially when dealing with low-mass stars. An estimate of the age of our stars was obtained by interpolating parallaxes and stellar parameters within a grid of Yonsei-Yale isochrones (e.g. Yi et al. 2001; Kim et al. 2002). The code *q2*⁵ was used for the interpolation (Ramírez et al. 2014). However, we caution that the use of isochrones for M dwarf stars shows important limitations. Indeed, for roughly $\sim 20\%$ of the stars we were not able to recover a reliable age estimate.

The final number of stars with available spectra is 204. They are listed in Table A.1 while the corresponding HR diagram is shown in Figure 1. The kinematic properties of the stars are also listed in Table A.2. In order to identify those stars hosting planets the available information in the NASA exoplanets archive⁶ was carefully checked (up to June 2020). Five stars host at least one giant planet, one (or more) low-mass planets are found orbiting around 29 stars, while four stars host simultaneously both giant and low-mass planets. Table A.3 shows the planet hosts, number of planets, and planetary properties taken from the NASA exoplanets archive.

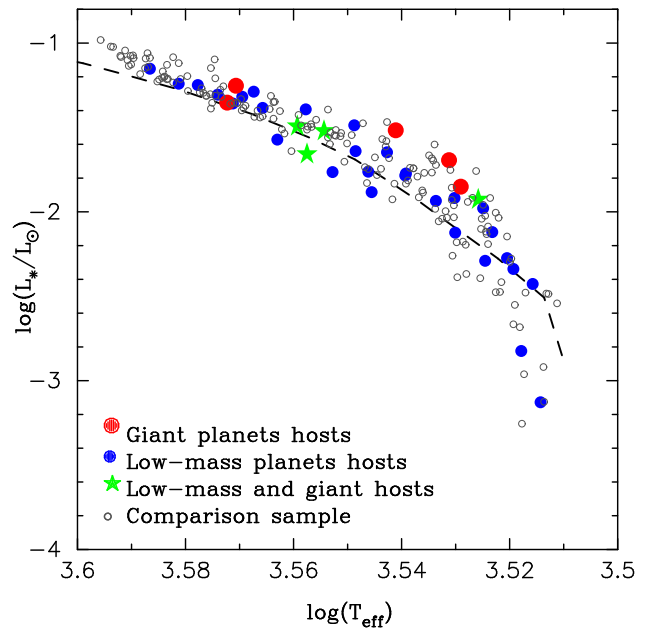


Fig. 1. Luminosity versus T_{eff} diagram for the stars analysed. Stars with gas-giant planets are shown with red filled circles, while low-mass planet hosts are shown with blue filled circles. Stars harbouring simultaneously gas-giant and low-mass planets are shown with green stars. A 5 Gyr isochrone from Spada et al. (2013) is also shown for comparison.

¹ http://archive.eso.org/wdb/wdb/adp/phase3_spectral/form?

² <http://archives.ia2.inaf.it/tng/faces/search.xhtml?dswid=4905>

³ <https://github.com/jesús-maldonado-prado/msdlines>

⁴ <http://simbad.u-strasbg.fr/simbad/sim-fid>

⁵ <https://github.com/astroChasqui/q2>

⁶ <https://exoplanetarchive.ipac.caltech.edu/>

3. Abundance determination in M dwarfs

3.1. Spectroscopic observations

The common procedure used in the literature to derive chemical abundances of M dwarfs is to search for M stars in common proper motion pairs orbiting around solar-type stars for which the accurate determination of spectroscopic abundances is possible. The list provided by Mann et al. (2013a) was used as a starting reference. Several additional M dwarfs in binary systems were selected from Montes et al. (2018). After searching the lists of possible calibrators available in the ESO and TNG archives, HARPS/HARPS-N data were found for only six stars. As these data were not sufficient to try kind of calibration, additional observations were performed.

Spectroscopic observations of 14 M dwarfs (and 12 FGK primaries) were performed in an observing run between the 9th and 13rd of November, 2018. Observations were performed using the HARPS spectrograph (Mayor et al. 2003) at La Silla ESO observatory. By adding the data already public in the ESO/TNG archives the total number of M dwarfs amounts to 20. Typical values of the signal-to-noise ratio (S/N measured at ~ 605 nm) for the FGK primaries are between 40 and 130. The sample of M dwarfs is significantly fainter and even using relatively long integration times (up to two hours for some targets) the achieved S/N ratio is rather modest between 30 and 70 in the best cases. The star NLTT11500 (primary HIP17076) was excluded as a calibrator as the primary is a spectroscopic binary with both components clearly visible in our spectra.

3.2. Stellar parameters and chemical abundances of the FGK primaries

Basic stellar parameters (T_{eff} , $\log g$, microturbulent velocity, and [Fe/H]) for the primary stars were determined by using the code TGVIT⁷ (Takeda et al. 2005) which applies the iron ionisation and excitation equilibrium conditions to a set of 302 Fe I and 28 Fe II lines. The input stellar equivalent widths (EWs) were measured automatically using the code ARES⁸ (Sousa et al. 2007, 2015). The *reject* parameter was adjusted according to the signal-to-noise ratio of the spectra as described in Sousa et al. (2008). Uncertainties in the stellar parameters are computed by progressively changing each stellar parameter from the converged solution to a value in which any of the conditions (excitation equilibrium, match of the curve of growth, ionisation equilibrium) are no longer fulfilled. We note that this procedure only evaluates statistical errors (see for details Takeda et al. 2002a,b). The uncertainties due to the errors in the measurement of the EWs were also computed and added in quadrature to the ones derived by the TGVIT code. Other sources of uncertainties, such as the choice of the model atmosphere, the list lines used, or the adopted atomic parameters are not taken into account. The derived parameters are provided in Table 1.

Chemical abundance of individual elements, C, O, Na, Mg, Al, Si, Ca, Sc, Ti, V, Cr, Mn, Co, Ni, and Zn are obtained using the 2017 version of the code MOOG⁹ (Sneden 1973) together with ATLAS9 atmosphere models (Kurucz 1993a). The used line list is given in Maldonado et al. (2015b, and references therein). Hyperfine structure (HFS) was taken into account for V I, and Co I, using the MOOG driver *blends*. Our derived abundances are provided in Table 2. They are expressed relative to the so-

lar values derived in Maldonado et al. (2015b), using the same methodology and similar spectra. We do not consider HFS effects on Mn abundances, as Maldonado et al. (2015b) found an offset between the HFS abundances of Mn when using different lines. The uncertainties take into account the line-to-line scatter errors as well as the uncertainties due to the propagation of the errors in the stellar parameters and the equivalent widths (computed using the star HIP116906 as reference).

Carbon abundances were derived by spectral synthesis of the CH molecular band at 430 nm using the CH line list provided in Masseron et al. (2014). They are expressed relative to the solar value obtained in Baratella et al. (2020). Oxygen abundances were derived by spectral fitting of the [O I] 630 nm line. However, reliable abundances were obtained only for seven stars. Carbon and oxygen uncertainties are those due to the fitting procedure.

3.3. M dwarf abundances: Methodology

In order to derive the abundances of the M stars we initially tried to proceed as in Maldonado et al. (2015a) where a large dataset of spectral features and ratios of features were identified as temperature and metallicity diagnostics. However, in spite of the fact that many of these features are found to correlate with the elemental abundances, a quick inspection of the plots of pseudo-equivalent width measurements versus [X/H] reveals flat curves or complex patterns difficult to fit. Therefore, we conclude that even if the pseudo-equivalent width of a given spectroscopic feature might show a significant correlation with a specific ion abundance, the values of pseudo-equivalent widths depend on other parameters such as effective temperature, surface gravity, the global metallicity content, or the abundance of alkali metals. In addition, many of the features are likely to be a blend of different atomic or molecular lines. In other words, pseudo-equivalent widths values contain too much information to deal with.

A common technique to reduce the dimensionality of the data and find the variables in which the spread or variance of the data is larger is the so-called principal component (PCA) analysis. The PCA technique (e.g. Francis & Wills 1999) is used to extract information of correlated data sets and find a new basis in which the largest amount of variance is explained with the least number of basis vectors. This methodology has been successfully applied to samples of FGK stars even with spectroscopic data at moderate resolution (e.g. Muñoz Bermejo et al. 2013; Xiang et al. 2017; Giribaldi et al. 2019).

We initially tried to identify spectral regions sensitive to the elemental abundance of different ions. For this purpose we made use of atmospheric models together with the lists of lines used in the chemical analysis of solar-type stars and already identified spectral indexes sensitive to metallicity and other elements (e.g. Ghezzi et al. 2014). We made use of ATLAS9 models together with the spectral synthesis code SYNTHE (Kurucz 1993a,b) as it is easy to change the abundances of different elements and compute spectra with the desired abundances. We are aware that other sets of models (PHOENIX, MARCS) are usually considered to better reproduce the atmospheres of low-mass stars (e.g. Bertone et al. 2008; Sinclair et al. 2010; Maldonado 2012). However, we found that better results were obtained if the full spectral range was considered (from 534 nm, to avoid the bluest region of the spectra which suffers from a lower S/N and the gap between the two CCDs in HARPS spectra).

Before applying the PCA, each coadded spectrum was rebinned to a common wavelength grid and smoothed to a lower resolution using a Gaussian filter of a 12 nm width. To estimate

⁷ <http://www2.nao.ac.jp/~takedayi/tgv/>

⁸ <http://www.astro.up.pt/~sousasag/ares/>

⁹ <http://www.as.utexas.edu/~chris/moog.html>

Table 1. Spectroscopic properties of the primaries FGK stars.

Primary	Secondary	SpType	V (mag)	T _{eff} (K)	log g (cm s ⁻²)	v _{mic} (km s ⁻¹)	[Fe/H] (dex)
HIP 3540	NLTT 2478	F8	7.0	6185 ± 28	4.22 ± 0.06	1.13 ± 0.17	0.15 ± 0.07
HIP 5110	NLTT 3598	K2V	8.7	4715 ± 23	4.78 ± 0.07	0.49 ± 0.29	-0.07 ± 0.05
HIP 6130	G1 56.3	K1V	8.0	5288 ± 12	4.70 ± 0.02	0.77 ± 0.10	-0.07 ± 0.05
HIP 6431	NLTT 4568	K5	9.5	4926 ± 34	4.66 ± 0.09	0.52 ± 0.34	0.21 ± 0.07
HIP 6456	NLTT 4599	K0IV	7.9	5281 ± 23	4.48 ± 0.06	0.81 ± 0.19	0.42 ± 0.05
HIP 9094	G1 81.1	G5	6.4	5298 ± 9	3.94 ± 0.03	1.01 ± 0.05	0.04 ± 0.03
HIP 11565	G1 100	K4V	8.8	4594 ± 37	4.84 ± 0.09	0.50 ± 0.60	-0.06 ± 0.07
HIP 11572	BD +22353B	K0	9.2	5105 ± 22	4.53 ± 0.06	0.49 ± 0.31	0.03 ± 0.05
HIP 12114	G1 105	K3V	5.8	4832 ± 24	4.72 ± 0.04	0.12 ± 0.26	-0.09 ± 0.04
HIP 21710	G1 173.1	K3V	9.2	4836 ± 65	4.62 ± 0.13	0.17 ± 0.51	-0.02 ± 0.11
HIP 26907	NLTT 15511	K1V	8.6	5079 ± 19	4.61 ± 0.05	0.55 ± 0.29	0.10 ± 0.06
HIP 27253	NLTT 15601	G4V	6.0	5588 ± 20	3.86 ± 0.06	1.23 ± 0.08	0.33 ± 0.05
HIP 28671	NLTT 15974	G0V	9.3	5761 ± 46	4.74 ± 0.11	2.03 ± 0.37	-1.05 ± 0.07
HIP 32984	G1 250	K3V	6.6	4760 ± 46	4.79 ± 0.13	0.41 ± 0.41	0.09 ± 0.07
HIP 40035	G1 297.2	F7V	5.5	6310 ± 42	4.27 ± 0.07	1.57 ± 0.15	-0.06 ± 0.04
HIP 62471	HIP 62471B	K4/K5V	8.9	4743 ± 122	4.69 ± 0.37	1.08 ± 0.59	-0.33 ± 0.12
HIP 83591	G1 654	K5V	7.7	4666 ± 46	4.43 ± 0.38	0.28 ± 1.10	-0.58 ± 0.16
HIP 116906	NLTT 57675	G5	7.7	5760 ± 11	4.36 ± 0.03	1.05 ± 0.05	-0.02 ± 0.03
HD 24916	HD 24916B	K4V	8.1	4635 ± 43	4.91 ± 0.17	0.40 ± 0.42	0.06 ± 0.07

how this smoothing reduces the spectral resolution we measured the ratio $\lambda/(\delta\lambda)$ on several lines in a ThAr spectra after and before the smoothing finding that it goes from ~ 115000 to ~ 1000 -2000. While it is true that smoothing and resampling the data might destroy information, it also reduces the impact of high-frequency distortion in the data, and previous works have found better results at lower resolution (Muñoz Bermejo et al. 2013). Finally, all the spectra were set to a common flux scale. In order to do this, we consider the spectral flux at the R band centred at 609 nm with only 2 nm width to avoid the inclusion of strong molecular bands. We use one of the stellar spectra as reference and perform a linear fit between the “reference” and “problem” flux.

Then, a flux matrix, $F(n, j)$, was obtained where j indexes the stars (including both the training and the problem datasets) and n is the index corresponding to the wavelength bin. Finally, PCs were computed using the available routines in the scikit-learn python package (Pedregosa et al. 2011).

Our next step is to use the training dataset (that is, the M dwarfs in binary systems around an FGK primary star) to find a relationship between the PCs and the stellar abundances. While some authors have explored the possibility of using a large number of PCs (e.g. Xiang et al. 2017), our training dataset is composed of only 19 stars, so the use of a large number of PCs lead us to a reduced number of degrees of freedom. For example, a fit of the stellar abundance as a liner combination of the PCs using 17 PCs would leave us with only one degree of freedom. In order to avoid over-fitting, the use of sparse Bayesian learning algorithms have been proposed in the literature (e.g. Muñoz Bermejo et al. 2013), like the automatic relevance determination regression (ARDR).

In brief, the target value is expected to be a linear combination of the features,

each coefficient w_i is drawn from a Gaussian distribution centred at zero and a standard deviation α_i so that:

$$p(\mathbf{w}|\alpha) = \mathcal{N}(w|0, A^{-1}) \quad (2)$$

with $A = \text{diag}(\alpha_1 \dots \alpha_p)$. The aim of sparse Bayesian’s fitting is to use the available data to compute the posterior distribution for the vector of weights \mathbf{w} and the noise variance, σ^2 . ARDR is based on defining the inverse variances of these Gaussian distributions, α , as variables, and to infer their values as well so if the α_i parameter of the i -th feature tends to infinity, then its weight is very likely close to zero and is therefore pruned. In this way the solution that contains the least number of non-zero elements in \mathbf{w} is favoured. In this way, over-fitting is avoided.

Bayesian inference proceeds by applying the Bayes’s rule to compute the posterior distribution over all unknowns given the data \mathbf{x} :

$$P(\mathbf{w}, \alpha, \sigma^2 | \mathbf{x}) = \frac{P(\mathbf{x}|\mathbf{w}, \alpha, \sigma^2)P(\mathbf{w}, \alpha, \sigma^2)}{P(\mathbf{x})} \quad (3)$$

where the data, \mathbf{x} , are in our case the PCs and the stellar abundances, $P(\mathbf{x}|\mathbf{w}, \alpha, \sigma^2)$ is the likelihood function and gives a measure of how well the model fits the data, and $P(\mathbf{w}, \alpha, \sigma^2)$ is the prior distribution for the parameters.

The posterior in Eqn. 3 cannot be computed directly. It is common to decompose it, as:

$$P(\mathbf{w}, \alpha, \sigma^2 | \mathbf{x}) = P(\mathbf{w}|\mathbf{x}, \alpha, \sigma^2)P(\alpha, \sigma^2 | \mathbf{x}) \quad (4)$$

where the first term in Eqn. 4 is the posterior over the weights which can be computed analytically. Therefore, the optimisation of the evidence or the learning process reduces to the maximisation of:

$$P(\alpha, \sigma^2 | \mathbf{x}) \propto P(\mathbf{x}|\alpha, \sigma^2)P(\alpha)P(\sigma^2) \quad (5)$$

$$y(\mathbf{x}, \mathbf{w}) = \sum_{i=1}^p w_i x_i \quad (1)$$

Table 2. Derived abundances and associated uncertainties ([X/H] in dex) for the primaries FGK stars.

Star	[C/H]	[O/H]	[Na/H]	[Mg/H]	[Al/H]	[Si/H]	[Ca/H]	[Sc/H]	[Ti/H]	[V/H]	[Cr/H]	[Mn/H]	[Co/H]	[Ni/H]	[Zn/H]
HIP 3540	0.08	-0.01	0.20	0.08	0.12	0.13	0.07	0.29	0.16	0.09	0.00	0.10	0.32		
	0.15	0.05	0.06	0.05	0.09	0.08	0.06	0.10	0.07	0.09	0.23	0.05	0.09		
HIP 5110	-0.09	-0.21	-0.27	-0.11	-0.11	-0.26	-0.20	-0.09	0.10	-0.09	-0.12	-0.07	-0.13	-0.07	
	0.15	0.04	0.06	0.04	0.11	0.08	0.06	0.06	0.06	0.08	0.06	0.05	0.11		
HIP 6130	-0.15	-0.15	-0.08	-0.03	-0.10	-0.12	-0.05	-0.03	-0.07	-0.06	-0.09	-0.12	-0.12	-0.14	
	0.17	0.04	0.07	0.04	0.03	0.07	0.07	0.05	0.06	0.08	0.06	0.05	0.10		
HIP 6431	0.16	0.15	0.01	0.26	0.14	-0.03	0.13	0.24	0.37	0.17	0.32	0.22	0.16	0.19	
	0.12	0.05	0.06	0.04	0.09	0.08	0.05	0.08	0.05	0.06	0.06	0.05	0.09		
HIP 6456	0.38	0.22	0.61	0.49	0.58	0.44	0.27	0.43	0.43	0.55	0.43	0.78	0.50	0.48	0.90
	0.15	0.05	0.04	0.06	0.08	0.04	0.08	0.05	0.06	0.06	0.11	0.06	0.05	0.09	
HIP 9094	-0.01	-0.06	-0.02	0.16	0.13	0.08	0.03	0.02	0.04	0.03	0.05	0.15	0.02	0.01	0.19
	0.12	0.07	0.04	0.06	0.04	0.03	0.07	0.07	0.05	0.06	0.08	0.06	0.05	0.26	
HIP 11565	-0.18	-0.21	-0.37	-0.16	-0.16	-0.41	-0.41	-0.21	-0.09	0.18	-0.13	-0.24	-0.09	-0.21	0.01
	0.20	0.05	0.06	0.04	0.07	0.15	0.10	0.06	0.06	0.06	0.08	0.08	0.05	0.30	
HIP 11572	-0.04	0.18	0.09	0.21	0.10	-0.03	0.09	0.14	0.11	-0.02	0.05	0.08	0.02	0.23	
	0.20	0.27	0.06	0.04	0.04	0.08	0.05	0.05	0.06	0.06	0.08	0.07	0.05	0.11	
HIP 12114	-0.16	0.01	-0.05	-0.13	0.10	-0.03	-0.16	-0.05	0.08	0.21	-0.08	-0.06	-0.01	-0.09	-0.08
	0.20	0.10	0.05	0.06	0.03	0.04	0.08	0.08	0.06	0.07	0.06	0.06	0.05	0.13	
HIP 21710	-0.14	-0.06	-0.14	-0.06	-0.10	-0.23	-0.23	-0.07	0.07	0.20	-0.04	-0.08	0.01	-0.15	-0.09
	0.20	0.05	0.06	0.04	0.03	0.12	0.13	0.06	0.07	0.08	0.08	0.06	0.06	0.09	
HIP 26907	0.08	0.10	0.05	0.07	0.20	0.10	-0.02	-0.03	0.16	0.18	0.05	0.17	0.10	0.05	0.00
	0.15	0.2	0.04	0.06	0.03	0.04	0.08	0.10	0.05	0.06	0.06	0.08	0.06	0.05	0.15
HIP 27253	0.26	0.35	0.48	0.34	0.41	0.36	0.23	0.38	0.29	0.34	0.33	0.58	0.35	0.36	0.29
	0.10	0.10	0.09	0.11	0.04	0.03	0.07	0.08	0.05	0.06	0.09	0.06	0.05	0.11	
HIP 28671	-1.12	-1.27	-0.68	-0.67	-0.96	-0.84	-0.70	-0.67	-0.67	-1.13	-0.85	-0.01	-0.88	-1.07	
	0.15	0.05	0.06	0.05	0.07	0.24	0.08	0.18	0.10	0.16	0.05	0.11	0.09		
HIP 32984	0.07	-0.05	-0.20	-0.01	0.03	-0.09	-0.08	0.06	0.26	0.05	0.06	0.05	0.02	0.04	
	0.18	0.04	0.06	0.04	0.13	0.08	0.06	0.06	0.07	0.09	0.06	0.05	0.09		
HIP 40035	-0.08	0.03	-0.06	0.00	-0.13	-0.22	-0.09	-0.05	-0.11	-0.18	-0.09	-0.11	-0.11	-0.33	
	0.10	0.09	0.06	0.07	0.09	0.08	0.06	0.07	0.07	0.08	0.05	0.05	0.09		
HIP 62471	-0.60	-0.19	-0.59	-0.13	-0.28	-0.36	-0.56	-0.03	0.18	-0.08	-0.41	-0.30	-0.42	0.00	
	0.20	0.09	0.06	0.07	0.11	0.15	0.10	0.06	0.06	0.09	0.10	0.10	0.05	0.09	
HIP 83591	-0.22	-0.46	-0.03	-0.61	-0.46	-0.71	0.05	0.32	-0.33	-0.70	-0.39	-0.64	-0.80		
	0.07	0.13	0.04	0.12	0.16	0.08	0.07	0.06	0.06	0.09	0.08	0.06	0.09		
HIP 11690	-0.04	-0.02	0.01	0.09	0.06	0.00	-0.01	-0.04	-0.02	-0.02	-0.01	-0.05	-0.03	-0.05	
	0.10	0.10	0.04	0.06	0.03	0.03	0.07	0.08	0.05	0.05	0.06	0.06	0.05	0.12	
HD 24916	0.04	0.06	-0.20	-0.27	-0.03	0.02	-0.37	-0.10	0.00	0.31	0.04	0.01	0.06	-0.03	0.08
	0.20	0.07	0.07	0.06	0.04	0.18	0.10	0.06	0.06	0.09	0.06	0.06	0.05	0.13	

with respect to α and σ^2 . All the ARDR analysis was done with the SCIKIT-LEARN python package (Pedregosa et al. 2011) where the α and σ^2 hyper-parameters are assumed to follow a Gamma distribution. More details about the Bayesian's inference and the ARDR technique can be found in MacKay (1992); Tipping (2001) as well as on the SCIKIT-LEARN tutorials.

Initially, all the 19 training stars and a total of 17 PCs were used. Stellar abundances were computed in this way for our sample of M dwarfs. The derived M dwarfs metallicities were compared with a sample of nearby solar-type FGK stars coming from our previous works (Maldonado et al. 2015b). This sample was selected as comparison since the stars were analysed using similar spectra and the same methodology than the abundances of the FGK primaries of our training M dwarfs¹⁰. We found that the derived M dwarfs metallicities were shifted towards higher values when compared with the metallicities of the nearby FGK stars. This could be related to the fact that most of our training stars have metallicities larger than -0.10 dex, while only three training stars have metallicities below this value. We will discuss this issue with more detail in Sect. 3.6. To overcome this difficulty we performed a series of simulations in which 17 out of the 19 stars in the training dataset were randomly selected as effectively training stars. For each simulation we compared the metallicity distribution derived for our M dwarfs with the known metallicity distribution of the nearby solar-type FGK stars by using a two-sample Kolmogorov-Smirnov test (hereafter KS test). We selected as the “optimal” training dataset the one that provides the most similar metallicity distribution to the one of the FGK stars. We note that to force the metallicity distribution of M dwarfs to be similar to the one of nearby FGK stars is a common practice and has been used before to derive empirical calibrations for M dwarfs metallicities (e.g. Johnson & Apps 2009; Schlaufman & Laughlin 2010). It is also worth noticing that instead of using all the stars included in Maldonado et al. (2015b) we restricted the comparison to FGK stars within ~ 70 pc (as our training stars are located within this distance) and with galactic-spatial velocity components (U, V, W) similar to the ones of the training data set. In this way we ensure that the comparison is not biased by stars located at different distances or belonging to different kinematic populations. Further, the star NLTT15601 was discarded from the training dataset as its PCs deviate in a clear way from the values of the rest of the stars in the training dataset. We note that this star is the one with the lowest S/N among the whole training dataset.

The final number of training stars used in the computations amounts to 16 while the number of PCs is 14. In this way we use the maximum number of PCs while letting one degree of freedom. Figure 2 shows the comparison of the abundances derived for the training stars using our PCA technique with the abundances derived from the primaries, while the standard deviation of the differences for each element are shown in Table 3. We also show the number of training stars and PCs used as well as the residual mean square (RMS), the root-mean squared error (RMSE) and the coefficient of determination (R^2), (see e.g. Appendix in Rojas-Ayala et al. 2012). We note that for Ti, and Cr, whose abundances can be derived from lines of the neutral atom as well as from lines from the single ionised atom we consider the abundances derived from lines of the neutral atom as these are more abundant than the single ionised lines. On the contrary for Sc, abundances from lines of the single ionised atom were considered as they are more abundant. In general, we find that

Table 3. Standard deviation of the differences, residual mean square, mean squared error, and coefficient of determination between the PCA-derived abundances of the training stars and those measured in the corresponding primaries.

[X/H]	n _{training}	n(PCs)	σ	RMS	RMSE	R^2
Fe	16	14	0.04	0.03	0.00	0.99
C	15	13	0.03	0.03	0.00	0.99
Na	16	14	0.05	0.05	0.00	0.98
Mg	16	14	0.12	0.11	0.01	0.86
Al	13	11	0.05	0.05	0.00	0.93
Si	16	14	0.07	0.07	0.00	0.93
Ca	16	14	0.12	0.11	0.01	0.83
ScII	16	14	0.05	0.05	0.00	0.98
TiI	16	14	0.06	0.06	0.00	0.94
V	16	14	0.12	0.12	0.01	0.79
CrI	16	14	0.04	0.04	0.00	0.99
Mn	16	14	0.07	0.06	0.00	0.97
Co	16	14	0.02	0.02	0.00	0.99
Ni	16	14	0.05	0.05	0.00	0.97
Zn	16	14	0.09	0.08	0.01	0.96

the differences between our derived abundances and those measured in the FGK primaries have standard deviation lower than ~ 0.10 dex, the RMS and RMSE values are close to zero and R^2 close to one as expected when a model fit is useful for prediction. Slightly higher dispersions are found for elements like Mg, Ca and V for which we note that their abundances are more difficult to measure even in solar-type stars. Indeed, for some stars we were not able to derive the abundances of C, and Al. Therefore, for these elements we were forced to use less training stars and a lower number of PCs. As far as oxygen abundances are concerned, we were able to measure the FGK primaries' abundances in only six stars and the methodology (using four PCs) fails to derive reliable values. We will discuss the effect on the results of the number of training stars and PCs used in the next subsection.

The derived abundances for our sample of M dwarfs are given in Table A.4.

3.4. Validation of the methodology I: Comparison with FGK stars

As mentioned we applied the PCA plus ARDR methodology to our sample of “problem” M dwarfs described in Sect. 2. Unfortunately, we do not have a sample of M dwarfs with known abundances determined from spectroscopy to validate our methodology. Some efforts have been done to apply the spectral synthesis methods to M dwarfs but, to the very best of our understanding, they are mainly focused on a small number of stars and mainly analyse strong atomic lines at wavelengths redder than the HARPS/HARPS-N spectral coverage (e.g. Woolf & Wallerstein 2005; Bean et al. 2006; Abia, C. et al. 2020). Abundance analysis of M dwarfs in the near infrared has also been performed but on a small number of stars (e.g. Önehag et al. 2012; Souto et al. 2017).

Therefore, we need to find alternative ways of testing the reliability of our methods. As a first step to validate our methodology we compare the [X/H] vs [Fe/H] trends derived from our M dwarfs with those known for FGK stars, as it is reasonable to expect similar trends for both types of stars. As before, the abundance for the FGK stars came from our previous works (Maldonado et al. 2015b), although we now use the full dataset. The corresponding plots are shown in Figure 3, where FGK stars

¹⁰ With the only exception of the carbon abundances that in Maldonado et al. (2015b) were derived from atomic lines.

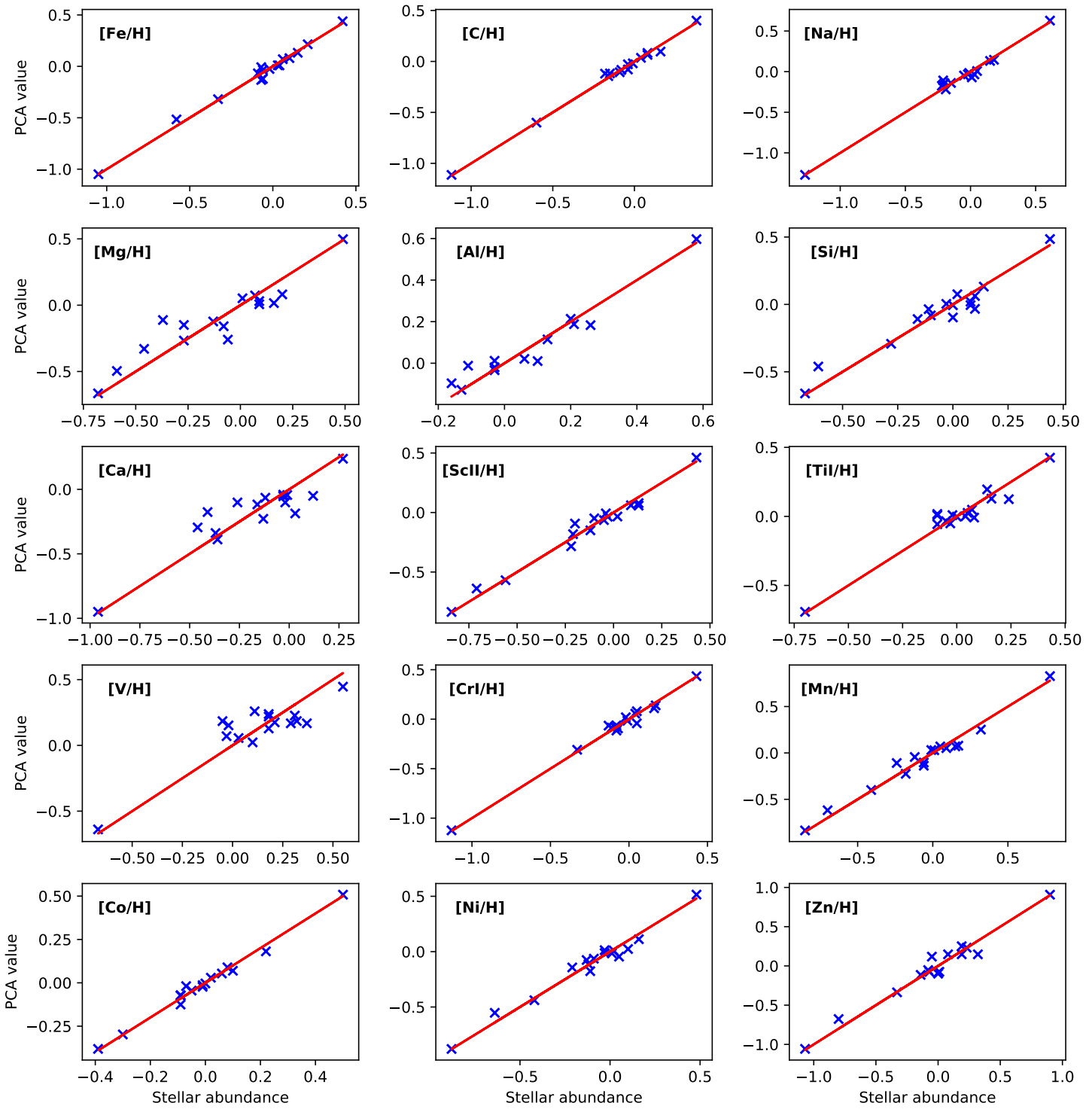


Fig. 2. Stellar abundances, $[X/H]$, derived for the M dwarfs included in the training dataset using our PCA/Bayes technique versus the abundances measured in the corresponding primary stars. The red line denotes the one-to-one relationship.

are shown as blue plus symbols, the M dwarf training dataset as green circles, and the “problem” M stars as red crosses. Several conclusions can be drawn from this figure:

i) A good agreement between FGK and M stars is found for the abundances of C, Na, Si, Ti, Cr, Mn, and Ni although some outliers can be seen specially at low and high abundance values.

ii) The $[X/H]$ versus $[Fe/H]$ relationship shows a larger spread when the abundances of Al and Zn are considered, having the M dwarfs slightly lower Zn abundances. We note that for

these elements, even for solar-type stars, their abundances are based on a relatively few number of lines.

iii) For V and Ca the general tendency for FGK and M dwarfs are slightly different. For Mg and Sc, the tendency is similar but M dwarfs seem to have lower abundances. The opposite happens for Co, with M dwarfs having higher abundances.

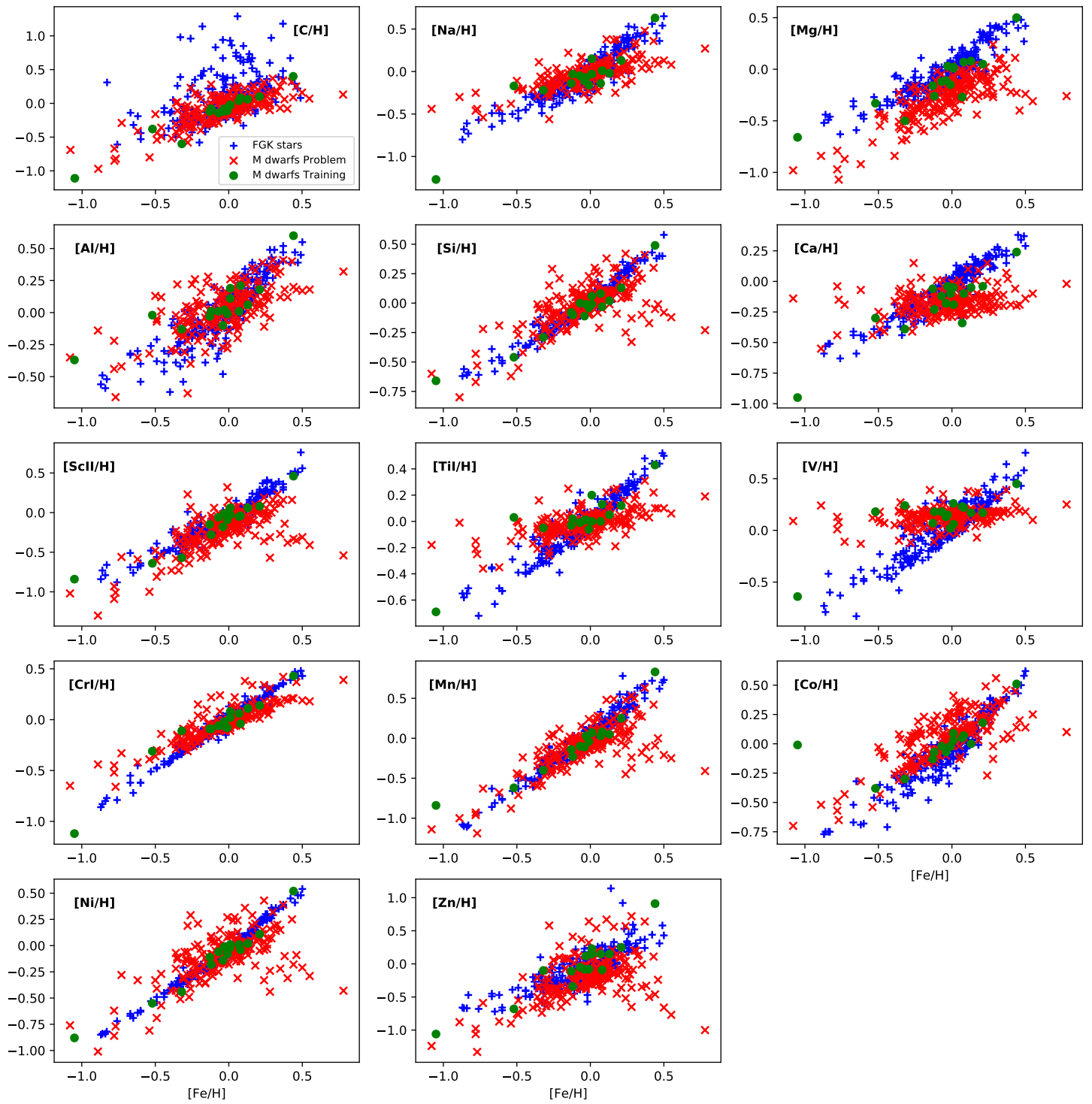


Fig. 3. $[X/H]$ versus $[Fe/H]$ plots for FGK stars (blue plus symbols), the M dwarf training stars (green circles) and our sample of “problem” M stars (red crosses).

3.5. Validation of the methodology II: Cross-validation with FGK stars

While PCA and Bayesian methods have been already used to determine stellar parameters and abundances, it is clear that the small number of training stars used in this work might raise some doubts on the applicability of these techniques. In other words, we need to be sure that sparse Bayesian methods do effectively

avoid over-fitting and can be safely applied even with a small number of training stars.

Therefore, we performed a cross-validation of the technique using it to derive the stellar abundances of a sample of FGK stars with HARPS/HARPS-N spectra. We use a total of 37 HARPS spectra from our previous works. Giant stars were excluded and only stars with measured abundances for all elements were considered.

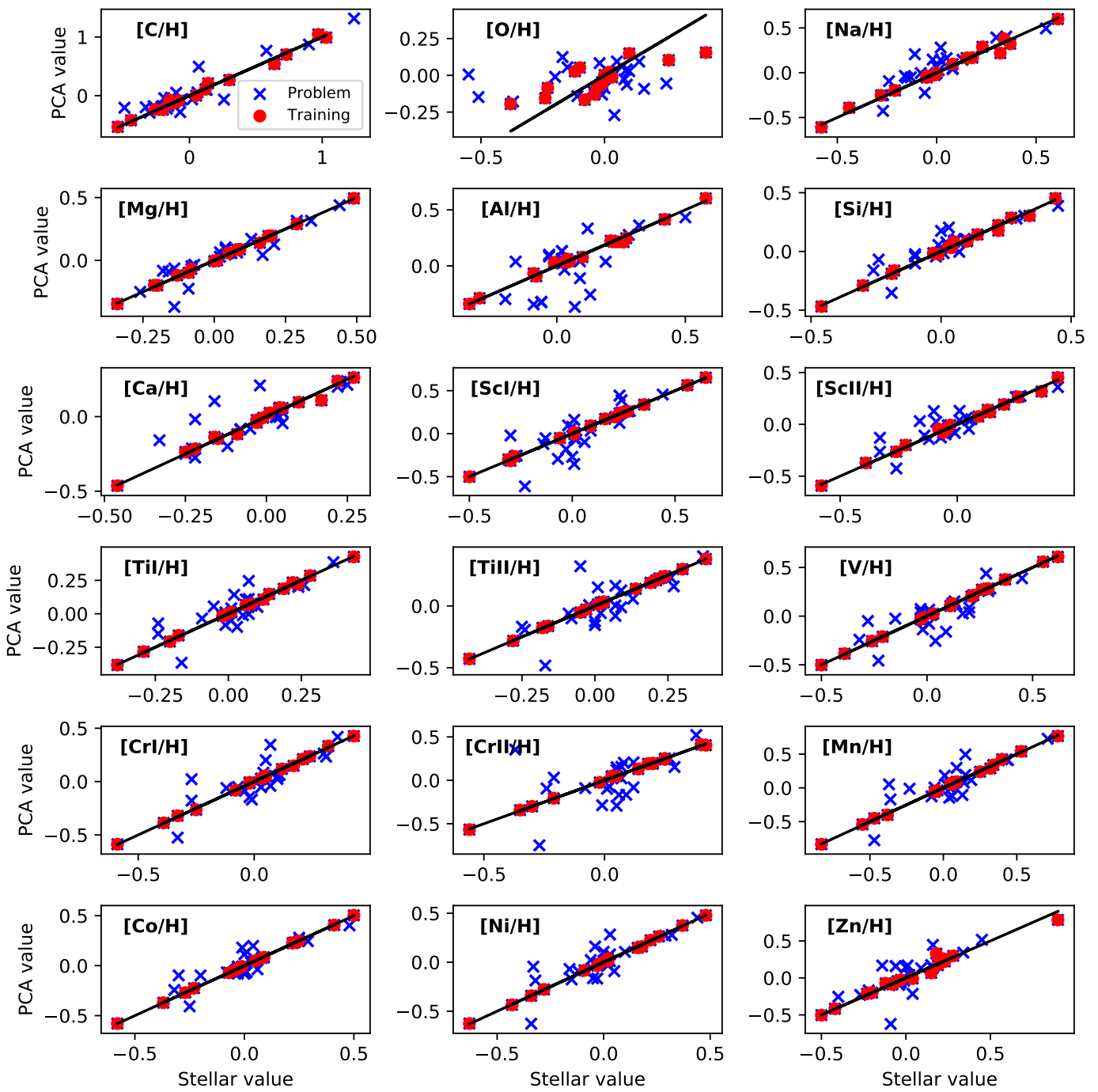


Fig. 4. PCA-derived abundances versus stellar abundances for our sample of FGK stars with HARPS/HARPS-N spectra from one of the performed simulations. The training dataset is shown in red circles while problem stars are shown in blue crosses.

A total of 100 simulations were performed. In each simulation 16 stars were randomly selected as the training dataset and exactly the same procedure used for the M dwarfs was applied. In particular, we note that we keep the number of PCs used to 14 (as in the M dwarfs case).

Figure 4 shows the results for one of the simulations, where the abundances derived from the PCA methodology are compared with the measured abundances for both the training (red circles) and problem stars (blue crosses).

We consider the standard deviation of the differences between the stellar abundances and the PCA-derived values as a measure of the goodness of the technique. For each simula-

tion and for each element, we compute the standard deviation of the differences between the PCA/Bayes derived abundances and those derived from a curve-of-growth approach from measured EWs of selected lines in the stellar spectra (as described in Sect. 3.1). We plot the distributions of the 100 standard deviations from the 100 simulation in Figure 5. Excluding some outliers, for most elements, the agreement between the PCA-abundances and those measured in the usual way is better than 0.10/0.15 dex. An agreement between 0.10 and 0.20 dex is found for some elements like Na, Mn, and Zn, whose abundances are based only on a few number of lines.

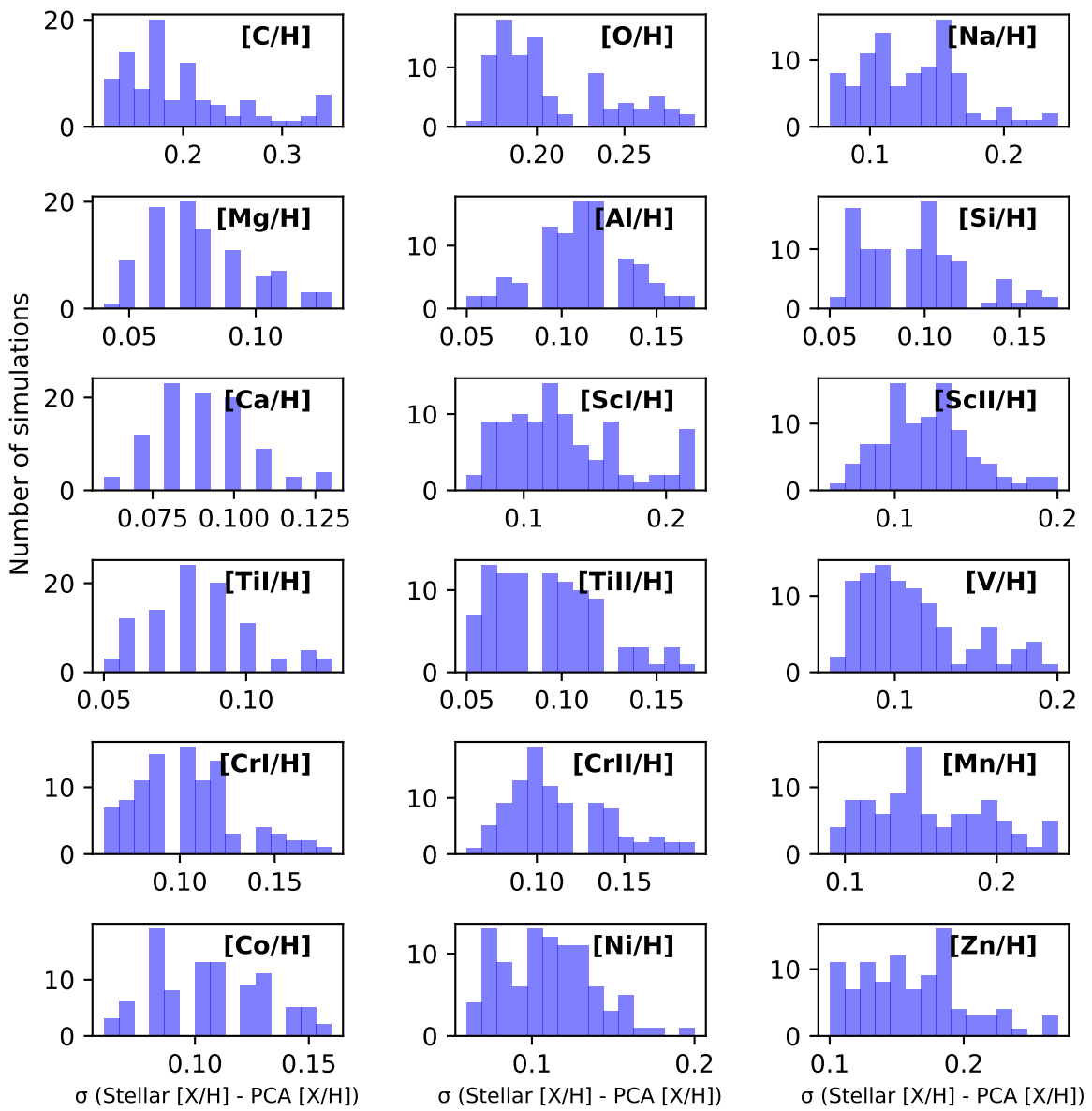


Fig. 5. Histograms of the obtained standard deviations of the differences between the PCA-derived abundances and the measured stellar abundances for our sample of FGK stars with HARPS-N spectra. The histograms show the results from 100 simulations. Outliers are excluded from the plot.

Our results show that the PCA-Bayesian fit technique can provide reliable results even if a low number of stars (as it is our case) is considered in the training dataset. Certainly, a larger number of M dwarfs in the training dataset, especially at low-abundance values would be desirable. We will discuss about this possibility in Sect. 6.

3.6. On the metallicity scale of M dwarfs. Comparison with previous works.

We compare the metallicity values derived from the new PCA technique with those previously reported in the literature. Values for the comparison include: those values computed by us using our previous msdlines technique (see Sect. 2, MSDL); the metallicities provided by Rojas-Ayala et al. (2012, hereafter RA12) which are derived from spectral indexes in the near infrared domain; the values by Önehag et al. (2012, hereafter ON12) which

perform spectral synthesis in the infrared J band; those derived by Neves et al. (2013, NE13) using a technique based on pseudo-equivalent widths of spectral features measured in optical high-resolution spectra; the values by Gaidos et al. (2014, GA14) computed from metal-sensitive atomic and molecular features; the work by Newton et al. (2014, NE14) derived from spectral lines and indexes in moderate-resolution near infrared spectra; Woolf & Wallerstein (2020, WW20) which perform spectral synthesis in the spectral range 5700 - 10000Å; Souto et al. (2020, SO20) which perform spectral synthesis on APOGEE spectra in the H band; and Passegger et al. (2019) which derive stellar parameters from high-resolution spectra by performing spectral synthesis in both the visible wavelength range (PA19-V) and the near infrared (PA19-N).

The comparison for iron abundance is shown in Figure 6 while Table 4 shows the main statistics of the comparisons. The agreement is in all cases overall good with RMSE values lower

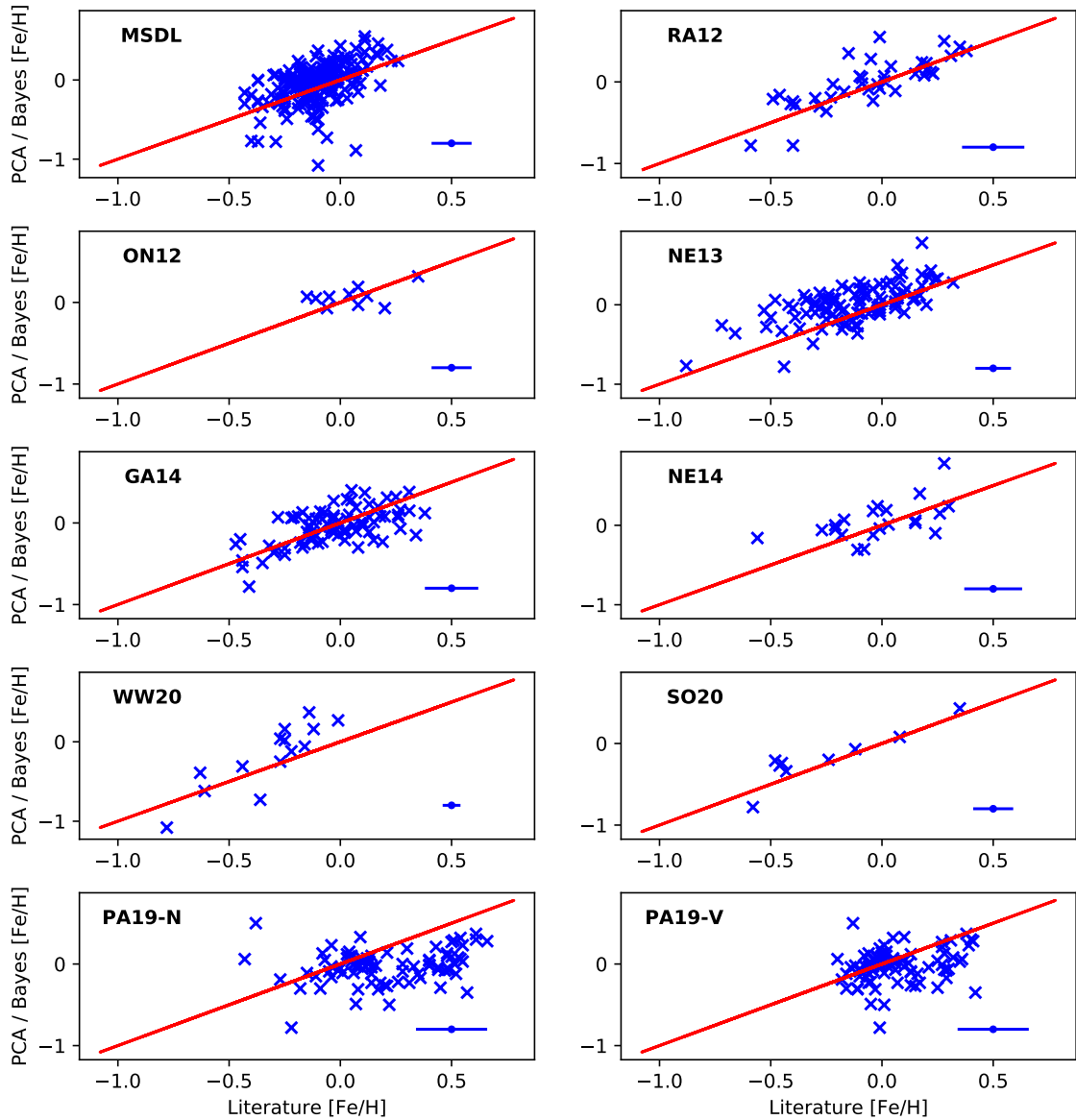


Fig. 6. Comparison between the iron abundances derived in this work and those previously reported in the literature. The red line denotes the one-to-one relationship.

than 0.10 dex (that is, the typical uncertainties reported in M dwarf abundances).

As an additional test, in Fig. 7 we show the empirical cumulative distribution function (ECDF) of the derived metallicities compared to the metallicities of FGK stars. We also show the results if all the 19 training stars are considered as well as the ECDF obtained using the msdlines metallicities and the NE12 calibration. Several conclusions can be drawn from this figure:

i) Metallicity values derived from photometry (we recall that the msdlines method was calibrated using NE12 due to the lack of high-resolution spectroscopic observations of M dwarfs in binary systems around solar-type stars) provide a ECDF shifted towards lower metallicities in comparison with FGK stars for metallicity values higher than -0.20 dex.

ii) If no selection of the training dataset is performed, PCA-Bayes derived metallicities are shifted towards higher values when compared with FGK stars. As mentioned before, this is likely a dataset shift from selection bias as most of our training stars have metallicities higher than +0.00 dex. Although several

methods are available to deal with this problem (e.g. density ratio estimator) they have provided unsuccessful results, probably due to our reduced number of training stars.

iii) Our finally adopted metallicity values for M dwarfs do reproduce the metallicity behaviour of nearby solar-type stars. A KS test between our derived M dwarf metallicities and the FGK metallicities returns the values $D=0.04$, $p\text{-value}=0.99$, with $n_{\text{eff}}=112.5$, meaning that both samples show statistically identical metallicity distributions.

As a final test we checked whether our derived metallicities show any correlation with the stellar effective temperatures and masses finding no significant correlation between these quantities. For metallicity and temperature the Spearman's rank ρ is -0.0959 ± 0.0696 with a z -score = -0.578 ± 0.422 , while for metallicity and stellar mass we obtain $\rho = 0.0548 \pm 0.0700$ and z -score = 0.329 ± 0.422 . The statistical tests were performed by a bootstrap Monte Carlo (MC) simulation plus a Gaussian random

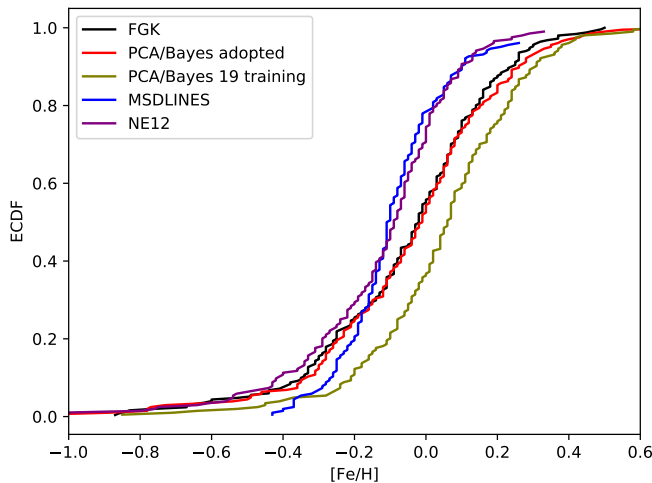


Fig. 7. [Fe/H] empirical cumulative distribution function for the derived metallicities with those obtained with other methods. See text for details.

shift of each data-point within its error bars (Curran 2014)¹¹. This result is expected as we derive these quantities using independent methodologies. Note that, unlike photometric calibrations, our PCA/Bayes metallicities are not based on stellar evolution models.

As far as other abundances besides iron are considered, only few elemental abundances for few stars are available in the literature. WW20 also compute abundances of Ti, while SO20 derive abundances of C. The corresponding comparisons are shown in Figure 8. It is clear that our derived Ti abundances are higher than those previously reported and there seems to be an offset between our derived abundances and those reported in WW20. The reason for this offset is not clear, given the good agreement between WW20 and our results for the iron abundance. For carbon, SO20 abundances are higher but the agreement is overall good and there seems to be a linear relationship between our abundances and those given in SO20. Finally, Souto et al. (2018, SO18) derived abundances of several elements (namely Fe, C, Mg, Al, Ca, and Ti) from near infrared spectra for the star Gl 447.

3.7. Stellar abundance and kinematics

Stars of the thin and thick disc populations are known to differ in terms of age, chemical composition, spatial distribution, and kinematics. Thin disc stars rotate faster than the local standard of rest and show solar α -element abundances. On the other hand, the thick disc is enriched in α elements and lags the local standard of rest (e.g. Reddy et al. 2003, 2006; Bensby et al. 2014). Most of our targets have a kinematics compatible with the thin disc population. If we consider the metallicity values derived from our PCA/Bayes analysis, we note that the mean metallicity of these stars is +0.01 dex. On the other hand, for the stars possible members of the thick disc population our new technique gives a mean metallicity of -0.39 dex. As it is common in the literature we consider Mg, Si, Ca, and Ti as α elements. Whilst thin disc stars in our sample show a mean $[\alpha/\text{Fe}]$ value of -0.11 dex, thick discs have larger α abundances with a mean value of +0.10 dex.

Table 4. Standard deviation of the differences, residual mean square, mean squared error, and coefficient of determination between the PCA-derived abundances of the training stars and those provided in previous works. Note that for SO18 we compare the abundances of six different species for one single star.

[X/H]	n _{stars}	σ	RMS	RMSE	R ²
MSDL	Fe	196	0.22	0.23	0.05
RA12	Fe	38	0.19	0.19	0.42
ON12	Fe	10	0.14	0.14	0.02
NE13	Fe	100	0.19	0.24	0.06
GA14	Fe	81	0.19	0.19	0.10
NE14	Fe	21	0.22	0.22	-0.12
WW20	Fe	14	0.25	0.28	-0.72
SO20	Fe	9	0.14	0.15	0.72
PA19-N	Fe	84	0.28	0.36	-1.17
PA19-V	Fe	85	0.23	0.24	-1.31
WW20	Ti	14	0.15	0.31	-1.90
SO20	C	9	0.14	0.19	-0.15
SO18		6	0.13	0.15	-3.40

This can also be seen in Fig. 9 where we show the Toomre diagram of the observed stars. Stars are plotted with different colours and symbols according to their metallicities (left) and $[\alpha/\text{Fe}]$ abundances (right). The dashed lines indicate values of constant total velocities. The figure shows that low-metallicity stars span a much larger range of total velocities than the metal-rich stars. On the other hand, stars with higher $[\alpha/\text{Fe}]$ abundances show larger total velocities. We conclude that our derived abundances reproduce the known kinematic trends from the different stellar populations.

3.8. Stellar abundances and activity.

In cool stars with convective outer-layers chromospheric activity and rotation are linked by the stellar dynamo (e.g. Kraft 1967; Noyes et al. 1984; Montesinos et al. 2001) and both (activity and rotation) are known to decrease with time as a star loses angular momentum with stellar winds via magnetic braking (Weber & Davis 1967; Jianke & Collier Cameron 1993). On the other hand, stellar metallicity reflects the enrichment history of the interstellar medium (e.g. Timmes et al. 1995) and for a given spectral type young stars are expected to show higher metallicity values. In addition, stars with a greater metallicity may be more active because their convection zones tend to be deeper than those of less-metallic stars with the same parameters and because the chromospheric emission in metal spectral lines may be enhanced (cf. Karoff et al. 2018). We caution that this result has been observed in only one solar twin star so similar analysis on other stars are needed to test it. In particular it is unclear whether it would also hold for low-mass stars, and specially for fully convective late-M dwarfs.

We tested whether this is the case. Activity indexes in the main optical indicators, Ca II H & K, Balmer lines (from H α to H ϵ), Na I D₁ D₂ and He I D₃ were computed following the bandpasses defined in Maldonado et al. (2019a). Figure 10 shows the mean Ca II (left) and H α (right) activity indexes values of the stars divided into three metallicity bins as a function of the spectral type. When considering the calcium index the figure clearly shows a tendency of higher levels of activity at higher metallicities for a given spectral type, which suggests that more active stars have higher metallicities. For H α , the tendency is even more clear. Similar results are obtained for the other activity indexes

¹¹ <https://github.com/PACurran/MCSpearman/>

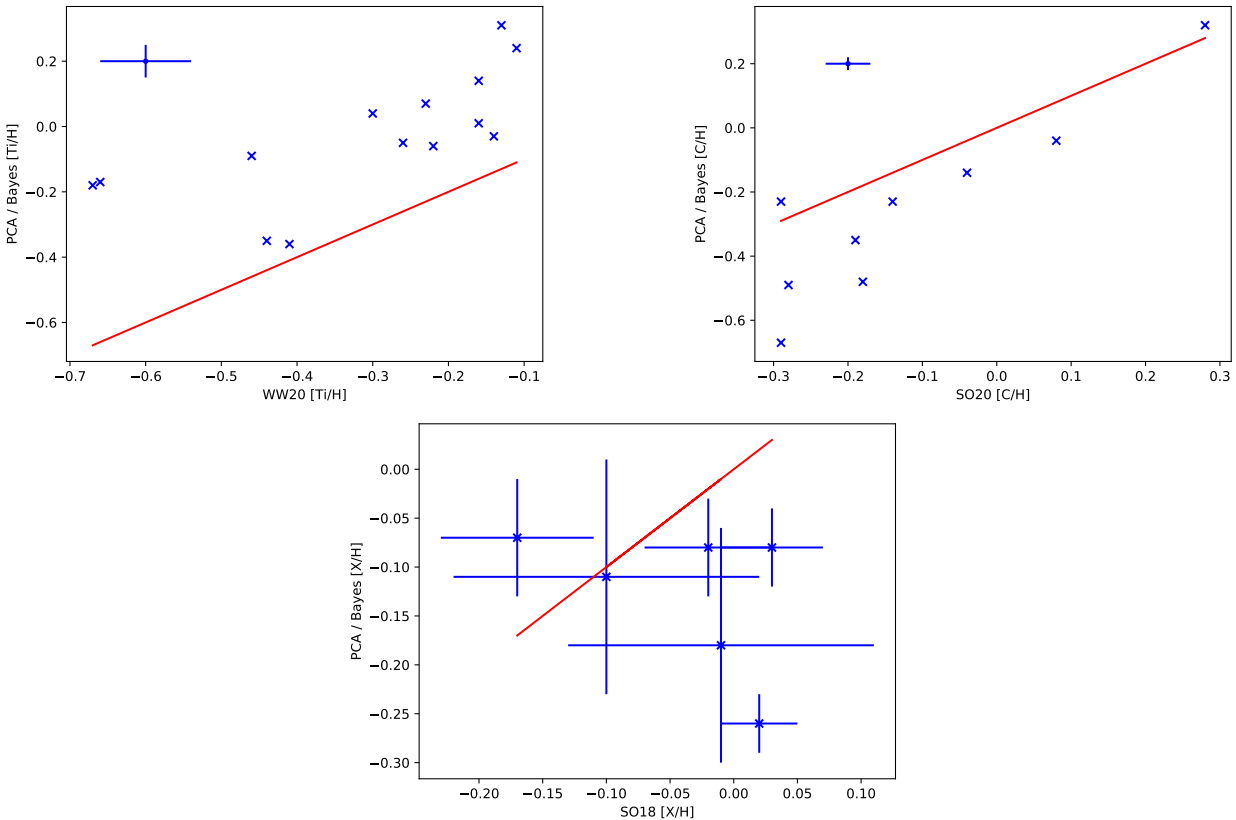


Fig. 8. Comparison between our derived PCA/Bayes abundances and those reported by WW20 (Ti, top left panel), SO20 (C, top right panel), and SO18 (Fe, C, Mg, Al, Ca, and Ti for the star Gl 447, bottom panel). The red line denotes the one-to-one relationship.

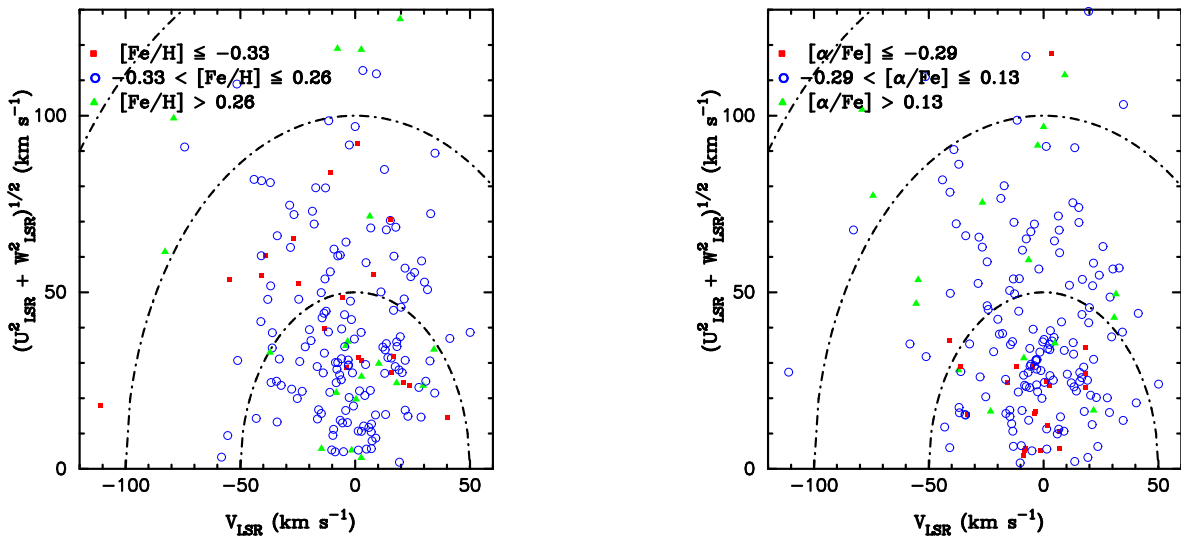


Fig. 9. Toomre diagram for the stars analysed in this work. Stars are shown with different colours and symbols according to their iron abundances (left) and [α/Fe] abundances (right). Intervals in [Fe/H] and [α/Fe] were selected to show the stars in the 10 and 90 quartiles of the distribution.

(not shown). Our conclusion is that our derived abundances reproduce the expected trends with stellar activity.

4. Completeness of the planet host sample

Our aim is to understand planet formation and evolution as a function of the main stellar properties. It is therefore fundamental to select stars for which planets of a given mass and period can be detected in a uniform way. In order to estimate the de-

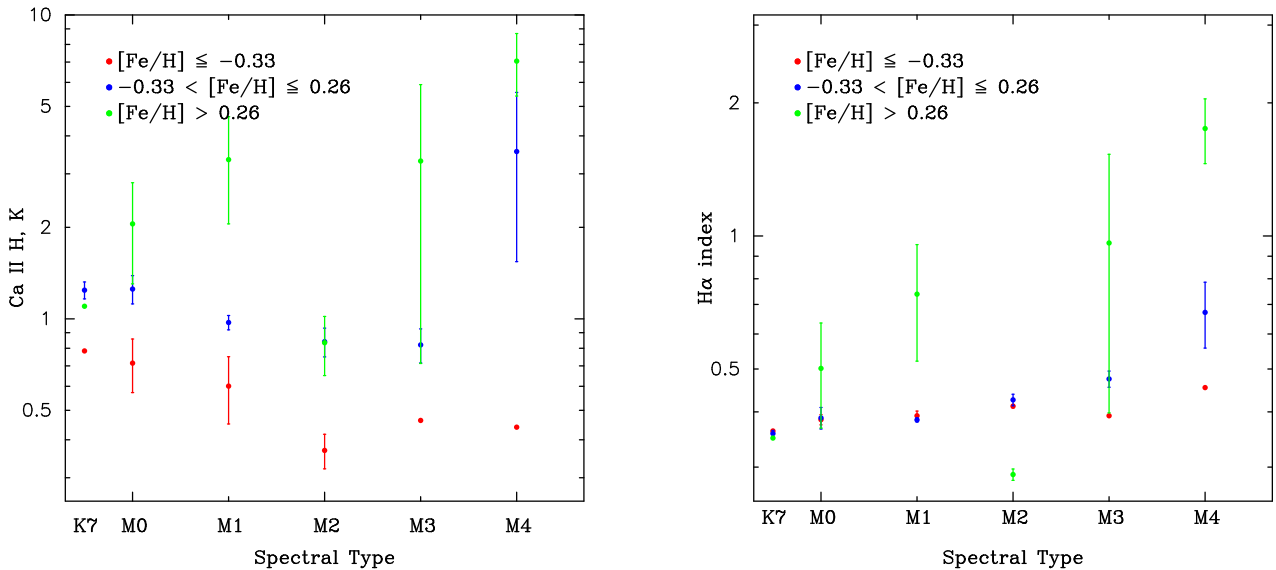


Fig. 10. Ca II H & K (left), and H α (right) activity indexes as a function of the spectral sub-type. Mean values for stars into three bins of metallicity ranges are shown with different colours.

tectability limits of our planet hosts, we proceeded as in Maldonado et al. (2019b). For each star we collected all the available HARPS and HARPS-N data. We are aware that for many stars there should be radial velocities measured with other instruments. However, given that radial velocity time series are usually non available for non-planet detections, we decided to focus only on HARPS and HARPS-N data. This is certainly a “conservative” approach, as it might overestimate the detection limits for some periods. However, it is a robust and homogeneous method and allows us to obtain an efficient determination of the detection limits. More detailed detection limits around samples of M dwarfs, in particular for the stars included in the HADES survey will be addressed in forthcoming works.

For each star, radial velocities were computed from the available data using the TERRA pipeline (Anglada-Escudé & Butler 2012), which provides a better radial velocity accuracy when applied to M dwarfs (Perger et al. 2017). For those stars with known planets, we used the code *rvalin*¹² (Wright & Howard 2009) to subtract the contribution of the planets to the radial velocity by using a multiplanet Keplerian fit with the planetary periods fixed to the published values.

We then computed the expected radial velocity semi-amplitude due to the presence of different types of planets by sampling in logarithmic space the planetary mass-period space. In particular, planetary masses from 0.005 to 80 M_{Jup} and orbital periods from one to 10⁴ days were considered. Circular orbits were considered as it has been shown that planet detection’s limits are not strongly dependent on the eccentricity (Endl et al. 2002; Cumming & Dragomir 2010). For each planet, the expected radial velocities were computed keeping the same time as in the original observations. Several realisations of the radial velocity were performed, each one corresponding to a different phase offset. Following previous works (Galland et al. 2005; Lagrange et al. 2012; Meunier et al. 2012) a planet is considered to be detectable around a given star if the root mean square (rms) of the planet’s expected radial velocity is larger than the rms of the

residuals of the stellar radial velocity (that is, after subtracting the signals of the already known planets) in each of the simulated phases.

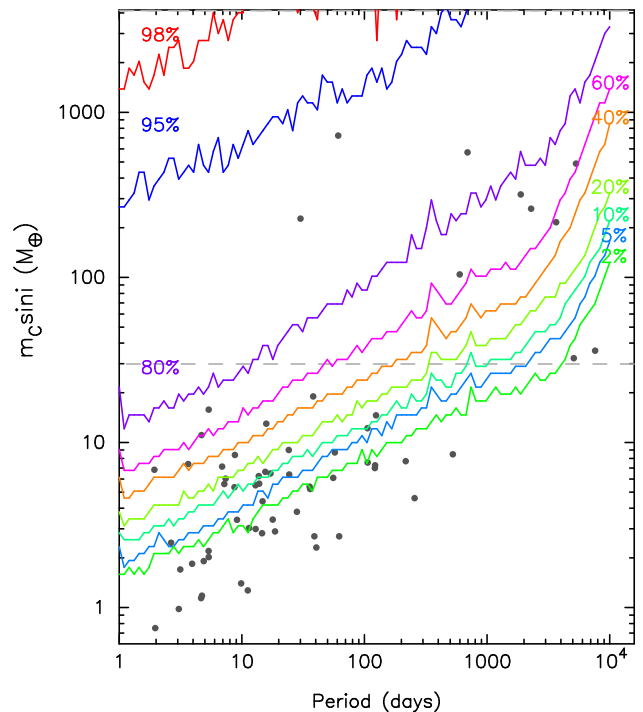


Fig. 11. Minimum mass versus planetary period diagram. Substellar companions known around M dwarfs are shown in grey circles. Detection probability curves are superimposed with different colours. The horizontal dashed line indicates the standard mass loci of low-mass planets, and gas-giant planet companions.

The derived detection probability curves are shown in Figure 11. The curves show for each period the percentage of stars from our sample for which planets with corresponding minimum mass can be detected. The results show that for ∼ 80% of the

¹² <http://exoplanets.org/code/>

stars in our sample, low-mass planets within a 10 days period might be detected. Gaseous planets more massive than $100 M_{\oplus}$ and $\sim 200 M_{\oplus}$ with periods within 100 and 1000 days, respectively can also be excluded for $\sim 80\%$ of the stars. It can be seen that several known planets are actually located under the 2% probability curve. This is not surprising. As mentioned before our approach is quite conservative.

5. Results

Our sample is composed of a total of 204 stars with homogeneous mass and metallicity measurements. Five stars host at least one giant planet (hereafter giant host subsample), while 29 stars harbour at least one low-mass planet (hereafter low-mass host subsample). Two stars namely GJ 15A and GJ 433 host one (two) low-mass planets plus an additional planet somehow in the boundary between low-mass and giant (minimum masses 36 and $32 M_{\oplus}$, respectively). These two stars were considered in the low-mass planet subsample. On the other hand, GJ 832 and GJ 876 harbour simultaneously low-mass companions as well as planets more massive than $200 M_{\oplus}$ so we add these stars to the giant host subsample. As seen before, given the available data, it is unlikely that stars in the low-mass host and comparison subsamples host a non-detected gas-giant planet at short periods (with the data at hand they should have been already detected). However, we cannot rule out the possibility that stars in the comparison subsample host non-detected low-mass planets. In the following, unless otherwise noticed, we consider the stellar metallicity values derived with the PCA/Bayes technique.

5.1. Biases

Before we proceed further in the comparison between the different subsamples, an exploration of the possible sources of bias that could mimic metallicity differences is called for. We therefore compared the different subsamples in terms of distance, age, and kinematics, which are the parameters most likely to affect the metal content of a star. The comparison is given in Table 5, while Figure 12 shows the corresponding cumulative distribution functions for the distance (left), age (centre), and the Toomre diagram (right).

The comparison shows that while there seems to be no differences in terms of age or kinematics between planet hosts and the comparison stars, stars with planets tend to be systematically located at shorter distances. Note that typical uncertainties in the stellar age is around 4 Gyr, while errors in the distance are around 0.03 pc. A KS test confirms that there are no differences in terms of age ($D = 0.24$, p -value = 0.18, $n_{\text{eff}} = 18.94$ for comparison/low-mass hosts; and $D = 0.36$, p -value = 0.43, $n_{\text{eff}} = 5.75$ for comparison/giant hosts) while low-mass planet hosts are located at shorter distances ($D = 0.41$, p -value = 0.0002, $n_{\text{eff}} = 26.1$ for comparison/low-mass hosts; and $D = 0.28$, p -value = 0.59, $n_{\text{eff}} = 6.7$ for comparison/giant hosts). This trend could reflect a bias in the exoplanet surveys, as closer stars are usually brighter and thus higher signal-to-noise observations can be obtained with shorter integration times. Therefore, closer and brighter stars can be observed with a more dense temporal cadence and higher signal-to-noise values thus favouring the detection of planets.

5.2. Metallicity distribution

The cumulative distribution function of the metallicity for the different samples analysed in this work is presented in Fig. 13, left panel. For guidance some statistical diagnostics are also given in Table 6. The figure shows a tendency of giant hosts to show high metallicities although their cumulative distribution does not look very different from those of the comparison sample. On the other hand the low-mass hosts also show a similar metallicity distribution than the comparison sample. A KS test shows that there are no statistically significant differences between the metallicity distribution of the three subsamples ($D = 0.21$, p -value = 0.16, $n_{\text{eff}} = 26.1$ for comparison/low-mass hosts; and $D = 0.25$, p -value = 0.70, $n_{\text{eff}} = 6.7$ for comparison/giant hosts).

Figure 13 shows that M dwarfs with gas-giant planets might have high metallicity values (suggesting that the gas-giant planet-metallicity correlation found on FGK stars might also hold for M dwarfs) although the trend needs statistical confirmation. On the other hand, stars with low-mass planets do not show the metal-rich signature. These results seem in line with previous works (Bonfils et al. 2007; Johnson & Apps 2009; Schlaufman & Laughlin 2010; Rojas-Ayala et al. 2012; Terrien et al. 2012; Neves et al. 2013).

Figure 14, left panel, shows the fraction of gas-giant planets (light orange) and low-mass planets (light blue) as a function of the stellar metallicity. The errors in the frequency of each bin are calculated using the binomial distribution,

$$P(f_p, n, N) = \frac{N!}{n!(N-n)!} f_p^n (1-f_p)^{N-n} \quad (6)$$

where $P(f_p, n, N)$ is the probability of n detections given a sample of size N when the true planetary companion frequency is f_p . Given that the probability distribution is not symmetric about its maximum, a common practice is to report the range in planetary fraction that delimits the 68.2% of the integrated probability function, which is equivalent to the 1σ limits for a Gaussian distribution (e.g. Burgasser et al. 2003; Endl et al. 2006; Sozzetti et al. 2009; Neves et al. 2013).

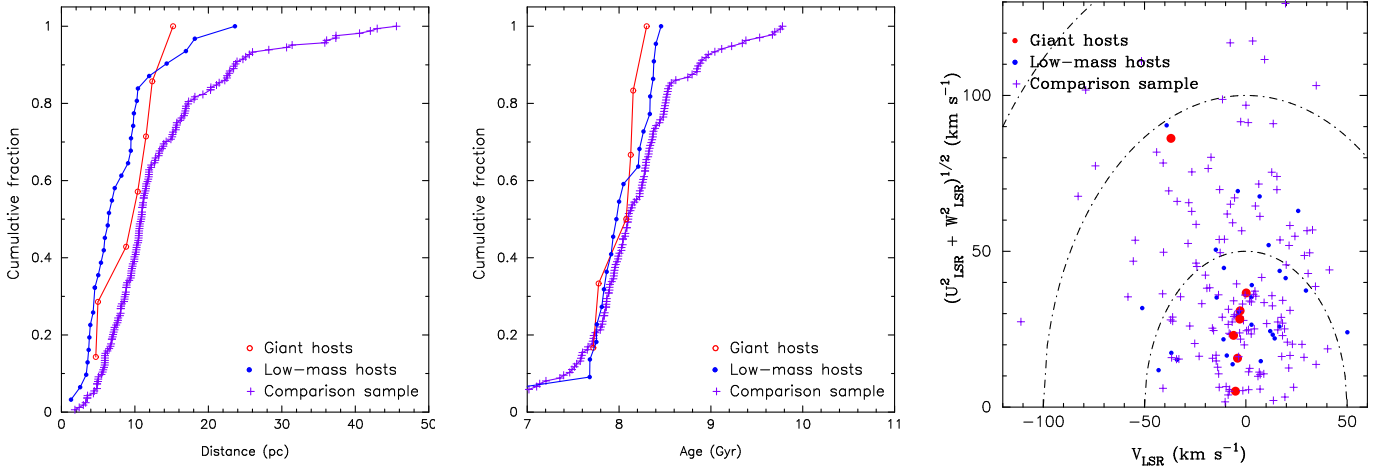
The fraction of stars with planets was fitted to a function with the functional form $f = C 10^{\alpha[Fe/H]}$, following previous works (e.g. Fischer & Valenti 2005; Udry & Santos 2007), although other functional forms have been discussed in the literature (e.g. Mortier et al. 2013). Our analysis provides $C = 0.20 \pm 0.03$, $\alpha = -0.12 \pm 0.16$ for the low-mass planets hosts; and $C = 0.04 \pm 0.02$, $\alpha = 0.98 \pm 0.87$ for the giant hosts.

Two conclusions can be drawn from this analysis. First, the frequency of low-mass planets does not seem to be a function of the stellar metallicity. Furthermore, as the α value is negative there might be an anti correlation, that is, a decreasing fraction of planet frequency with increasing stellar metallicity. This result seems to be in line with previous analysis of samples of M dwarfs (Neves et al. 2013). Second, gas-giant planets show a planet-metallicity correlation with an α value compatible within errors with the values found for FGK stars, ~ 1.7 (e.g. Fischer & Valenti 2005). However, our value of α is lower than previous values found in samples of M dwarfs, $\alpha \sim 1.26-2.94$, (Neves et al. 2013). Nevertheless, we caution that the uncertainty in α is high, and we have not taken into account a possible dependence of the planet fraction on the stellar mass. We address these issues in the following sections.

Table 5. Comparison between the properties of the different samples analysed in this work.

Comparison			Giant hosts			Low-mass hosts			
	Range	Mean	Median	Range	Mean	Median	Range	Mean	Median
Distance (pc)	1.83/45.60	13.24	10.90	4.68/15.20	9.70	10.38	1.30/23.62	7.94	6.47
Age (Gyr)	0.65/9.78	8.00	8.10	7.72/8.30	8.03	8.13	6.40/8.46	7.98	8.00
D/TD [†] (%)	77 (D); 4 (TD); 17 (R); 2 (H)			86 (D); 14 (R)			80 (D); 3.3 (TD); 13.3 (R); 3.3 (H)		

Notes. [†] D: thin disc, TD: thick disc, R: transition, H: halo

**Fig. 12.** Cumulative distribution function for the distance (left), age (centre), and Toomre diagram (right) for the stars analysed in this work.**Table 6.** [Fe/H] statistics of the stellar samples.

Sample	Mean	Median	Deviation	Min	Max	N
Comparison	-0.04	+0.00	0.27	-1.08	0.78	166
Low-mass	-0.07	-0.06	0.18	-0.77	0.20	31
Giants	0.09	0.08	0.21	-0.23	0.44	7

5.3. Mass distribution

Planet occurrence is also known to show a dependence on the stellar mass (Lawson et al. 2003; Lovis & Mayor 2007; Johnson et al. 2007, 2010a). Figure 13, right panel, shows the cumulative distribution function of the stellar mass for the samples analysed in this work. The figure shows a hint of planet hosts to be less massive than the comparison stars although this could be an observational bias, as planets are easier to find around less massive stars. Some statistical diagnostics are also provided in Table 7. The results from a KS tests provide $D = 0.20$, $p\text{-value} = 0.19$, $n_{\text{eff}} = 26.1$ for comparison/low-mass hosts; and $D = 0.26$, $p\text{-value} = 0.69$, $n_{\text{eff}} = 6.7$ for comparison/giant hosts.

Figure 14, right panel, shows the fraction of gas-giant planets (light orange) and low-mass planets (light blue) as a function of the stellar mass. The fraction of stars with planets was fitted to a power-law function $f = CM_{\star}^{\alpha}$ as previous works have shown that planet occurrence rises monotonically with the stellar mass (Johnson et al. 2010a). The derived values are $C = 0.06 \pm 0.06$, $\alpha = 0.94 \pm 1.23$ for the gas-giant planets hosts; and $C = 0.18 \pm 0.05$, $\alpha = -0.41 \pm 0.25$ for the low-mass planets hosts.

Our results show that gas-giant planet occurrence increases with the stellar mass in line with previous findings (Johnson et al. 2010a; Montet et al. 2014), while the frequency of low-mass planets tends to decrease as we move towards more massive stars. This last fact might be an observational bias due to the fact that small planets are easier to detect around less-massive stars. However, we note that a similar trend, that is, a higher fre-

quency of planets towards less massive stars has been found in the KEPLER data (Hardegree-Ullman et al. 2019).

5.4. Simultaneous fit to stellar mass and metallicity

Finally, we test the planet frequency as a function of the stellar mass and metallicity simultaneously. For this purpose we follow a Bayesian approach, discussed at length in Johnson et al. (2010a); Mortier et al. (2013) and Montet et al. (2014).

In brief, we fit the planetary frequency as a function of the mass and metallicity through the following relationship:

$$f(M, F) = CM^{\alpha}10^{\beta F} \quad (7)$$

where M is the stellar mass, F is the stellar metallicity and $X = (C, \alpha, \beta)$ are the parameters to be optimised. Each star represents a Bernoulli trial and the probability of finding a planet at a given mass and metallicity is given by the binomial distribution. For a total of T stars, the probability of a detection around a star i (of H total detections) is given by $f(M_i, F_i)$, while the probability of a non-detection around a star j is $1 - f(M_j, F_j)$. The probability of a specific model X , considering our data d , is given by the Bayes' theorem:

$$P(X|d) \propto P(X) \prod_i^H f(M_i, F_i) \times \prod_j^{T-H} [1 - f(M_j, F_j)] \quad (8)$$

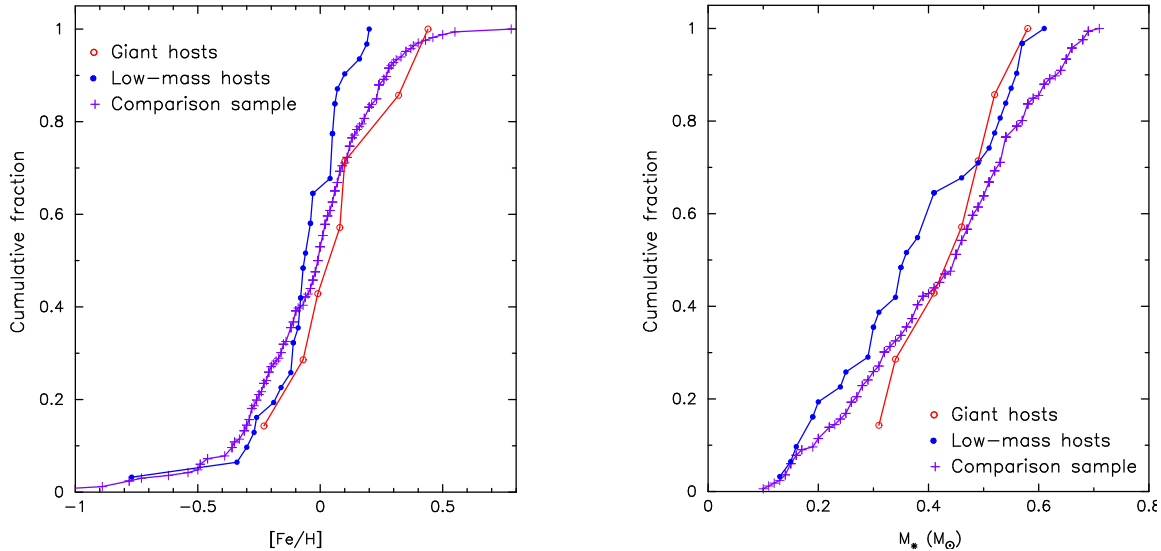


Fig. 13. [Fe/H] (left) and stellar mass (right) cumulative distributions for the different samples studied in this work.

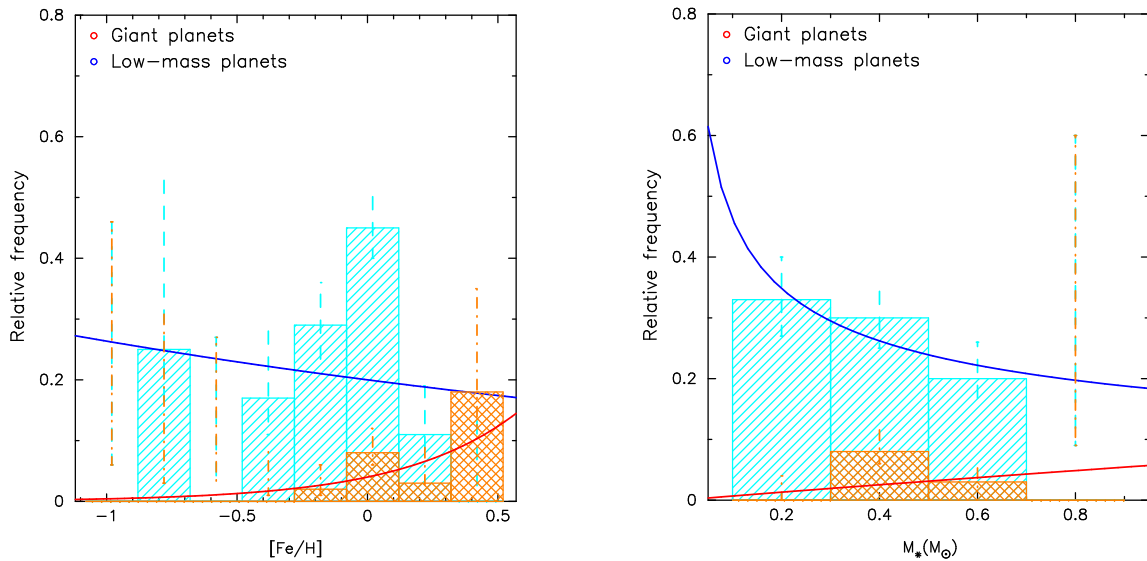


Fig. 14. Fraction of gas-giant planets (light orange) and low-mass planets (light blue) as a function of the stellar [Fe/H] (left) and stellar mass (right). The best bin fitting are shown in red for gas-giant planets and in blue for low-mass planets.

Table 7. Stellar mass statistics of the stellar samples.

Sample	Mean	Median	Deviation	Min	Max	N
Comparison	0.43	0.45	0.16	0.10	0.71	166
Low-mass	0.38	0.36	0.14	0.13	0.61	31
Giants	0.44	0.46	0.09	0.31	0.58	7

Each star's mass and metallicity is considered to be a Gaussian distribution with means (M_i, F_i) and standard deviations ($\sigma_{M,i}, \sigma_{F,i}$), so the predicted planet fraction for the i -th star is:

$$\mathcal{L} \equiv \log P(X/d) \propto \sum_i^H \log f(M_i, F_i) + \sum_j^{T-H} \log[1 - f(M_j, F_j)] + \log P(X) \quad (10)$$

$$f(M_i, F_i) = \iint p_{obs}(M_i, F_i)f(M, F)dMdf \quad (9)$$

The marginal log likelihood is finally obtained by taking logarithms in Eqn. 7:

Our results are shown in Table 8 where the median values and their corresponding 68.2% confidence interval are provided while Fig. 15 shows the marginal posterior probability distribution functions for the model parameters for the gas-giant planets (left) and for low-mass planets (right). Uniformly distribution priors were chosen for the parameters.

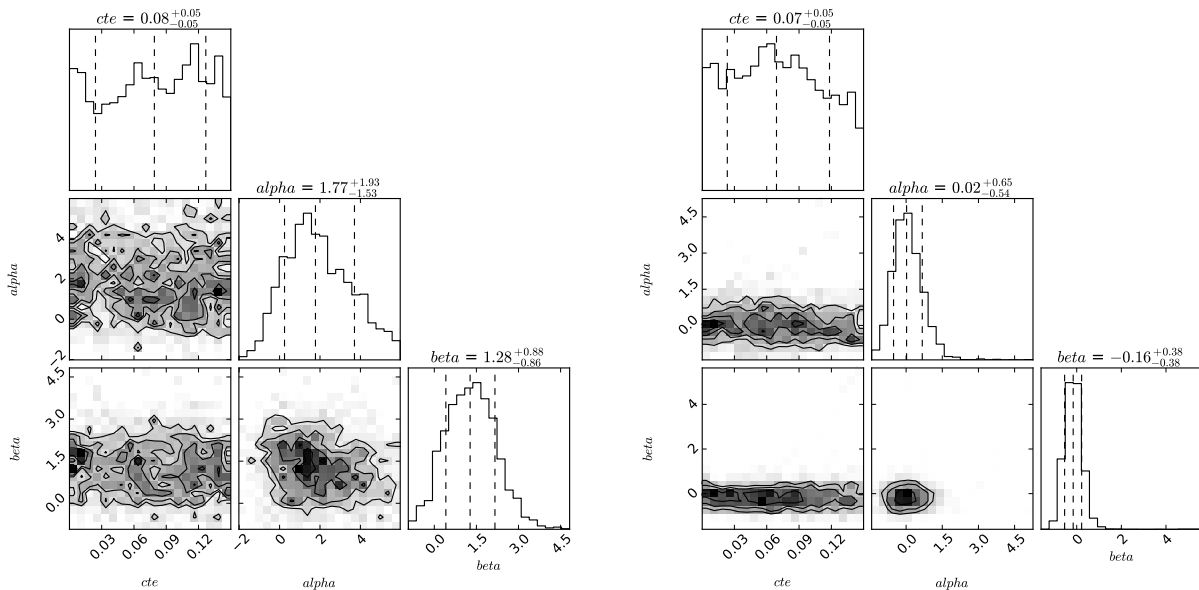


Fig. 15. Marginal posterior probability distribution functions of the fit to Eqn. 7 for gas-giant planets (left), and for low-mass planets (right). The metallicity values used in this analysis are those derived with the PCA/Bayes technique developed in this work.

Table 8. Parameters of the Bayesian fit.

Gas-giant hosts			
Parameter	Uniform prior	Value	68.2% confidence interval
C	(0.00, 0.15)	0.08	(+0.05, -0.05)
α	(-3.0, 6.0)	1.77	(+1.93, -1.53)
β	(-1.0, 9.0)	1.28	(+0.88, -0.86)
Low-mass hosts			
Parameter	Uniform prior	Value	68.2% confidence interval
C	(0.00, 0.15)	0.07	(+0.05, -0.05)
α	(-3.0, 5.0)	0.02	(+0.65, -0.54)
β	(-3.0, 6.0)	-0.16	(+0.38, -0.38)

Table 9 shows a comparison between the results from this work and those previously reported in the literature. Our results are consistent with a planet-metallicity correlation for gas-giant planets. We find that the dependence of the gas-giant planet frequency on the stellar metallicity, $\beta = 1.28$, is lower but compatible within errors with what is known for FGK stars, that is the frequency of gas-giant planets goes as $\sim 10^{2[\text{Fe}/\text{H}]}$. In particular we note that our result is fully compatible with the findings of Johnson et al. (2010a), based on an analysis of FGKM stars including intermediate-mass subgiants. Our result, however, suggests a weaker gas-giant planet-metallicity correlation than recent works focused on M dwarfs that found a dependency on the metallicity with β values between 2 and 4 (Neves et al. 2013; Montet et al. 2014). We also find a stronger dependence of the gas-giant planet frequency on the stellar mass, $\alpha = 1.77$, than recent works. That is, we find a slightly weaker gas-giant planet-metallicity correlation in M dwarfs, but a stronger planet-stellar mass, so it is possible that lower metallicities environments can be compensated by a higher stellar (and therefore disc) mass to allow gas-giant planet formation to occur. This is consistent with the view that the mass of solids in protoplanetary discs is the main factor controlling the formation of planets and can be explained in the framework of core-accretion models (e.g. Pollack et al. 1996; Ida & Lin 2004; Mordasini et al. 2009, 2012).

Regarding low-mass planets, their frequency does not seem to depend on the stellar mass (in disagreement with what we found in the bin fitting). We confirm that the frequency of low-mass planets does not depend on, or might show an anti-correlation with, increasing stellar metallicity.

Since the value of β derived by us is lower than the values obtained by other works focused on M dwarfs, we repeated our analysis using, this time, the metallicities obtained by the msd-lines code. The results are $C = 0.07^{+0.05}_{-0.05}$, $\alpha = 1.65^{+2.45}_{-2.12}$, and $\beta = 3.94^{+2.57}_{-2.21}$ for the gas-giant hosts, and $C = 0.09^{+0.05}_{-0.06}$, $\alpha = 0.22^{+0.69}_{-0.59}$, and $\beta = -1.13^{+1.02}_{-0.99}$ when considering the low-mass planet hosts subsample. The corresponding posterior distributions are shown in Figure 16. It can be seen that the values of the parameter α obtained using the msdlines metallicities are similar to the one obtained by the PCA/Bayes values for the low-mass planet sample. On the contrary, the value of β differs. The value obtained by using the PCA/Bayes metallicities is compatible with a rather flat dependency of the low-mass planet frequency on the stellar metallicity. However, the value obtained when using the msd-lines metallicities ($\beta = -1.13$) might indicate an anti-correlation.

On the other hand, for the gas-giant sample we obtain a similar mass dependency but, clearly, a stronger correlation between the planet occurrence and the stellar metallicity. This is in line with the works of Neves et al. (2013); Montet et al. (2014) who discussed that M dwarfs should show a stronger giant planet-metallicity correlation than their FGK counterparts, given their smaller protoplanetary disc's masses. We caution that the posterior distributions of the parameters α , and β are very broad and their associated uncertainties very high. This could be related to the small size of the giant-hosts subsample.

Given that the msdlines metallicities are shifted towards lower values when compared with the nearby FGK stars (see Fig. 7) we speculate whether the very high β values found in previous works ($\sim 3, 4$) and with our msdlines metallicities may be related to the use of a photometric scale. However, further analysis should be done to clarify this issue.

Table 9. Comparison with previous works.

	[Fe/H] parameter	M_\star parameter	Stellar sample	Notes
FV05	2.0		FGK	
US07	2.04		FGK	[Fe/H] > 0.00
	0.00			[Fe/H] < 0.00
JO10	$1.2_{-1.4}^{+1.0}$	$1.0_{-1.30}^{+0.70}$	FGKM	
NE13	2.94 ± 1.03		M	giant hosts
	-0.41 ± 0.77		M	low-mass hosts
M014	3.8 ± 1.2	$0.8_{-0.9}^{+1.1}$	M	
This work	$1.28_{-0.86}^{+0.88}$	$1.77_{-1.53}^{+1.93}$	M	giant hosts
(PCA/Bayes)	-0.16 ± 0.38	$0.02_{-0.54}^{+0.65}$	M	low-mass hosts
This work (msdlines)	$3.94_{-2.21}^{+2.57}$	$1.65_{-2.12}^{+2.45}$	M	giant hosts
	$-1.13_{-0.99}^{+1.02}$	$0.22_{-0.59}^{+0.69}$	M	low-mass hosts

Notes. FV05: Fischer & Valenti (2005), US07: Udry & Santos (2007), JO10: Johnson et al. (2010a), NE13: Neves et al. (2013), MO14: Montet et al. (2014).

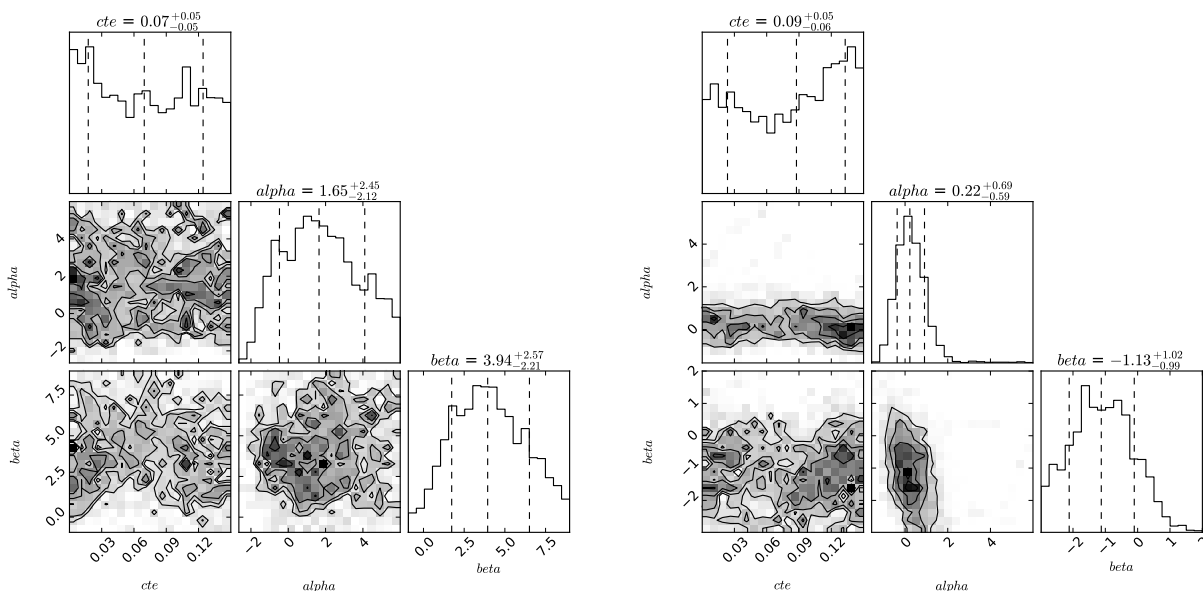


Fig. 16. Marginal posterior probability distribution functions of the fit to Eqn. 7 for gas-giant planets (left), and for low-mass planets (right). The metallicity values used in this analysis are those derived with the msdlines code.

5.5. Other chemical signatures

To try to disclose differences in the abundances of other chemical elements besides iron, we show in Fig. 17 the cumulative distribution of the abundances [X/H] of the comparison, the low-mass hosts, and the giant hosts subsamples. Some statistic diagnostics are shown in Table 10, where the results of a KS test for each element are also listed.

Similar behaviour between planet and non-planet hosts is found in all elements, both for gas-giant and low-mass planets. However, a small hint of higher abundances of Ti, Na, Mg, and Al can be seen for gas-giant planet hosts. Slightly lower abundances of Co for low-mass planet hosts can also be seen. Since these trends are not statistically significant we conclude that our results are similar to what is found in FGK stars where planet hosts have been shown to have indiscernible abundances from stars without planets (e.g. Bodaghee et al. 2003; Ecuivillon et al. 2006; Gonzalez 2006; Gilli et al. 2006; da Silva et al. 2011; Adibekyan et al. 2012b). We included the α abundance in our analysis as Adibekyan et al. (2012a,b) showed that stars with planets at low-metallicity values tend to belong to the thick disc

and show high α values, but besides the general trend of higher α abundances in less-metallic stars discussed in Sect. 3.7, no differences in α abundances between planet and non-planet hosts were found. It is important to note that chemical differences between planet and non-planet hosts, when claimed, are rather modest. For instance, a depletion of only ~ 0.08 dex on refractory relative to volatile elements have been found in the Sun and other solar analogues (e.g. Meléndez et al. 2009; Ramírez et al. 2009). In Table 3 we list the standard deviation of the differences between the PCA-derived abundances and those measured in the corresponding primaries for our training dataset. These values can be considered as a lower limit of the uncertainties derived. It is clear that we are still far from achieving the precision that can be obtained in the abundance analysis of FGK stars, so small chemical differences beyond the limits of our precision can still be present in our sample.

Table 10. Comparison between the elemental abundances of the different subsamples.

Ion	Comparison		Giant hosts		Low-mass hosts		K-S test comparison/giants		K-S test comparison/low-mass	
	Mean	σ	Mean	σ	Mean	σ	D	p-value	D	p-value
C	-0.03	0.22	0.04	0.08	-0.13	0.22	0.38	0.22	0.25	0.06
Na	-0.03	0.17	0.08	0.10	-0.06	0.12	0.44	0.10	0.24	0.07
Mg	-0.25	0.21	-0.06	0.18	-0.24	0.22	0.44	0.10	0.12	0.80
Al	0.05	0.18	0.18	0.13	-0.01	0.17	0.48	0.06	0.19	0.28
Si	0.02	0.19	0.06	0.10	-0.05	0.15	0.25	0.74	0.28	0.03
Ca	-0.16	0.10	-0.17	0.05	-0.20	0.08	0.22	0.85	0.22	0.14
Sc	-0.17	0.26	-0.01	0.18	-0.17	0.24	0.35	0.30	0.15	0.58
Ti	-0.01	0.10	0.05	0.06	-0.02	0.07	0.51	0.04	0.18	0.35
V	0.14	0.09	0.18	0.04	0.14	0.06	0.38	0.24	0.14	0.63
Cr	-0.03	0.18	0.05	0.11	-0.05	0.14	0.31	0.47	0.25	0.06
Mn	-0.07	0.28	-0.05	0.16	-0.11	0.26	0.22	0.85	0.18	0.35
Co	0.08	0.21	0.13	0.14	-0.03	0.18	0.24	0.77	0.30	0.01
Ni	-0.06	0.23	0.00	0.11	-0.12	0.20	0.27	0.66	0.23	0.10
Zn	-0.22	0.34	-0.15	0.19	-0.17	0.29	0.19	0.95	0.13	0.71
X_a	-0.07	0.20	-0.11	0.19	-0.08	0.10	0.25	0.73	0.20	0.23

6. Conclusions

M dwarfs are considered promising targets in the search for small, rocky, potentially habitable planets. They also constitute valuable tools to understand planet formation as a function of the stellar mass. However the analysis of their optical spectra has proven to be a difficult task. In this work we develop a technique to derive stellar abundances of M dwarfs from the same optical, high-resolution spectra that are used in exoplanet searches, that is, without the necessity of relying on additional infrared observations or atmospheric models.

Our methodology is based on the use of principal component analysis and Bayesian regression methods. The procedure is trained with spectra of M dwarfs orbiting around an FGK primary. We found the agreement between the abundances derived from our method and those measured in the FGK primary to be better than 0.10 dex in most of the cases. While it is true that these dispersions should be regarded as lower limits of the uncertainties of our technique, we believe that it is encouraging to see that they are of the same order of magnitude than the dispersion found in the individual abundances of FGK stars when measured from different lines of the same ion. A cross-validation of the technique performed on FGK stellar spectra shows that in spite of the small training sample used, the methodology seems to give reliable abundances.

Since we are lacking a suitable comparison sample, we are forced to compare our derived abundances for M dwarfs with the known trends for FGK stars. We find similar $[X/H]$ vs. $[Fe/H]$ trends for M dwarfs and FGK stars in most of the ions. We also show that our PCA/Bayes metallicities reproduce the metallicity scale of nearby FGK stars. On the contrary, metallicity values derived from photometry provide a ECDF distribution shifted towards lower metallicities values in comparison with FGK stars. Nevertheless, we recognise that the methodology can be improved by observing more training stars. This is specially evident at low-metallicities. Further observations of M dwarfs in the near infrared domain will help us to validate our techniques.

To the very best of our knowledge, we performed for the first time a detailed chemical analysis of several elements for a large sample of M dwarfs with and without gas-giant and low-mass planets. We note that while it is unlikely that giant planets may be hidden in the sample, we can not discard the possibility that there are more non-detected low-mass planets in the different subsamples analysed in this work. A comparison of the proper-

ties of the different subsamples reveals no differences in age or kinematics between planet and non-planet hosts. We find planet hosts to be located at lower distances than the comparison sample. This, likely, reveals the fact that closer stars are brighter and easier to observe at higher S/N.

Regarding the dependency of the planetary fraction on the stellar metallicity and mass, our results confirm previous works. That is, gas-giant planet hosts show a planet-metallicity correlation as well as a dependence with the stellar mass. We note, however, that our PCA/Bayes metallicities predict a weaker planet metallicity correlation and a stronger mass-dependency than photometric values for giant-planet hosts. On the other hand the frequency of low-mass planets is not a function of the stellar metallicity, although a weak anti-correlation might be present. We also find an anti-correlation between the frequency of low-mass planets and the stellar mass in line with recent results from the KEPLER mission. However, we caution that this anti-correlation was found only in the bin fitting analysis, but not in the Bayesian fit. For other elements besides iron, we do not find differences in the abundance distributions of stars with and without planets. These results are in line with what is known from the chemical analysis of solar-type stars and can be explained within the framework of core-accretion models.

We finally note that the homogeneous determination of stellar abundances of M dwarfs might be of interest for many other studies dealing with the local properties of the Galaxy, for example the study of stars in clusters and other stellar associations. Our codes are public available¹³, so the whole community can benefit from them.

Acknowledgements. This research was supported by the Italian Ministry of Education, University, and Research through the PREMALE WOW 2013 research project under grant *Ricerca di pianeti intorno a stelle di piccola massa*. J.M. acknowledges support from the Accordo Attuativo ASI-INAF n. 2018.22.HH.O, *Partecipazione alla fase B1 della missione Ariel* (ref. G. Micela). M.P., I.R., J.C.M, and E.H acknowledge support from the Spanish Ministry of Science and Innovation and the European Regional Development Fund through grant PGC2018-098153-B-C33, as well as the support of the Generalitat de Catalunya/CERCA programme. J.I.G.H. acknowledges financial support from Spanish Ministry of Science and Innovation (MICINN) under the 2013 Ramón y Cajal program RYC-2013-14875. A.S.M. acknowledges financial support from the Spanish MICINN under the 2019 Juan de la Cierva Programme. B.T.P. acknowledges Fundación La Caixa for the financial support received in the form of a Ph.D. contract. J.I.G.H., R.R., A.S.M., B.T.P. acknowledge financial support from the Spanish MICINN AYA2017-

¹³ https://github.com/jesús-maldonado/prado/mdwarfs_abundances

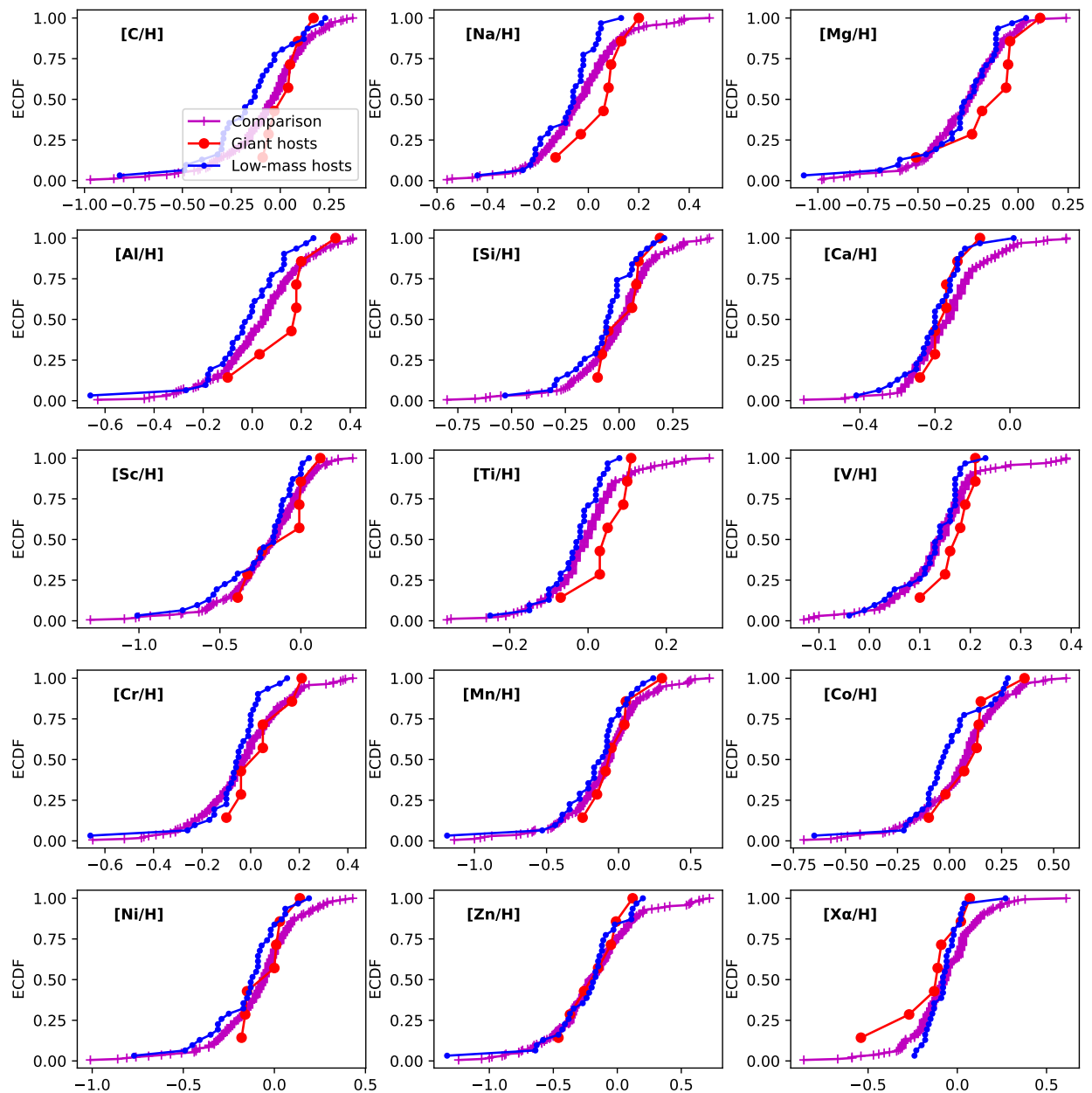


Fig. 17. [X/H] cumulative fraction of low-mass hosts (blue), gas-giant hosts (red), and comparison M dwarfs (purple).

86389-P. This research has made use of the NASA Exoplanet Archive, which is operated by the California Institute of Technology, under contract with the National Aeronautics and Space Administration under the Exoplanet Exploration Program. This work has made use of data from the European Space Agency (ESA) mission *Gaia* (<https://www.cosmos.esa.int/gaia>), processed by the *Gaia* Data Processing and Analysis Consortium (DPAC, <https://www.cosmos.esa.int/web/gaia/dpac/consortium>). Funding for the DPAC has been provided by national institutions, in particular the institutions participating in the *Gaia* Multilateral Agreement. Additional data collected at the European Southern Observatory and Telescopio Nazionale Galileo under programme ID GAPS, 082.C-0718(B), 072.C-0488(E), 183.C-0437(A), 180.C-0886(A), 198.C-0838(A), 0101.C-0516(A), 1102.C-0339(A), 183.C-0972(A), 096.C-0460(A), 082.C-0718(A), 191.C-0505(A), 096.C-0499(A), 191.C-0873, 191.C-0873(A), 088.C-0662(B), 089.C-0497(A), 090.C-0395(A), 087.C-0831(A), 093.C-0409(A), 60.A-9036(A), 192.C-0224(G), 192.C-0224(H), 192.C-0224(C), CAT14B_162, CAT16A_99, 198.C-0873(A), CAT17A_95, CAT14A_43, OPT16A_11, CAT16A_134, 092.C-0721(A), 0100.C-0097(A), 0101.C-0379(A), 0102.C-0558(A), CAT13B_170, CAT14A_128, 185.D-0056(A), 185.D-0056(B), 185.D-0056(K), 076.C-0155(A), 086.C-0284(A), 089.C-0732(A), 090.C-0421(A), 0101.D-0494(A), 192.C-0224(B), 099.C-0205(A), 085.C-0019(A), 495.L-0963(A), 097.C-0390(B), 099.C-0798(A),

0100.C-0487(A), 0101.D-0494(B), 095.C-0718(A), 077.C-0364(E), 097.C-0864(B), 099.C-0880(A), 075.C-0202(A), 192.C-0224, 098.C-0739(A), 60.A-9709(G), 060.A-9709(G), 074.C-0364(A), 078.C-0044(A), 097.C-0561(A), 075.D-0614(A), have been used. We sincerely appreciate the careful reading of the manuscript and the constructive comments of the anonymous referee.

References

- Abia, C., Tabernero, H. M., Korotin, S. A., et al. 2020, A&A, 642, A227
- Adibekyan, V. Z., Delgado Mena, E., Sousa, S. G., et al. 2012a, A&A, 547, A36
- Adibekyan, V. Z., González Hernández, J. I., Delgado Mena, E., et al. 2014, A&A, 564, L15
- Adibekyan, V. Z., Santos, N. C., Sousa, S. G., et al. 2012b, A&A, 543, A89
- Affer, L., Micela, G., Damasso, M., et al. 2016, A&A, 593, A117
- Anglada-Escudé, G. & Butler, R. P. 2012, ApJS, 200, 15
- Antoniadis-Karnavas, A., Sousa, S. G., Delgado-Mena, E., et al. 2020, A&A, 636, A9
- Baratella, M., D’Orazi, V., Biazzo, K., et al. 2020, A&A, 640, A123
- Bean, J. L., Benedict, G. F., & Endl, M. 2006, ApJ, 653, L65

- Bensby, T., Feltzing, S., & Lundström, I. 2003, A&A, 410, 527
- Bensby, T., Feltzing, S., Lundström, I., & Ilyin, I. 2005, A&A, 433, 185
- Bensby, T., Feltzing, S., & Oey, M. S. 2014, A&A, 562, A71
- Bertone, E., Buzzoni, A., Chávez, M., & Rodríguez-Merino, L. H. 2008, A&A, 485, 823
- Bodaghee, A., Santos, N. C., Israelian, G., & Mayor, M. 2003, A&A, 404, 715
- Bonfils, X., Delfosse, X., Udry, S., et al. 2013, A&A, 549, A109
- Bonfils, X., Mayor, M., Delfosse, X., et al. 2007, A&A, 474, 293
- Buchhave, L. A., Latham, D. W., Johansen, A., et al. 2012, Nature, 486, 375
- Burgasser, A. J., Kirkpatrick, J. D., Reid, I. N., et al. 2003, ApJ, 586, 512
- Butler, R. P., Johnson, J. A., Marcy, G. W., et al. 2006, PASP, 118, 1685
- Carpenter, J. M. 2001, AJ, 121, 2851
- Cosentino, R., Lovis, C., Pepe, F., et al. 2012, Society of Photo-Optical Instrumentation Engineers (SPIE) Conference Series, Vol. 8446, Harps-N: the new planet hunter at TNG, 84461V
- Courcol, B., Bouchy, F., & Deleuil, M. 2016, MNRAS, 461, 1841
- Cumming, A., Butler, R. P., Marcy, G. W., et al. 2008, PASP, 120, 531
- Cumming, A., & Dragomir, D. 2010, MNRAS, 401, 1029
- Curran, P. A. 2014, arXiv e-prints, arXiv:1411.3816
- Cutri, R. M., Skrutskie, M. F., van Dyk, S., et al. 2003, VizieR Online Data Catalog, II/246
- da Silva, R., Milone, A. C., & Reddy, B. E. 2011, A&A, 526, A71
- Dressing, C. D. & Charbonneau, D. 2013, ApJ, 767, 95
- Ecuvillon, A., Israelian, G., Santos, N. C., et al. 2006, A&A, 445, 633
- Endl, M., Cochran, W. D., Kürster, M., et al. 2006, ApJ, 649, 436
- Endl, M., Cochran, W. D., Tull, R. G., & MacQueen, P. J. 2003, AJ, 126, 3099
- Endl, M., Kürster, M., Els, S., et al. 2002, A&A, 392, 671
- Fischer, D. A. & Valenti, J. 2005, ApJ, 622, 1102
- Francis, P. J. & Wills, B. J. 1999, Astronomical Society of the Pacific Conference Series, Vol. 162, Introduction to Principal Components Analysis, ed. G. Fernand & J. Baldwin, 363
- Gaia Collaboration, Brown, A. G. A., Vallenari, A., et al. 2018, A&A, 616, A1
- Gaidos, E., Mann, A. W., Lépine, S., et al. 2014, MNRAS, 443, 2561
- Galland, F., Lagrange, A. M., Udry, S., et al. 2005, A&A, 443, 337
- Ghezzi, L., Cunha, K., Smith, V. V., et al. 2010, ApJ, 720, 1290
- Ghezzi, L., Dutra-Ferreira, L., Lorenzo-Oliveira, D., et al. 2014, AJ, 148, 105
- Gilli, G., Israelian, G., Ecuvillon, A., Santos, N. C., & Mayor, M. 2006, A&A, 449, 723
- Giribaldi, R. E., Porto de Mello, G. F., Lorenzo-Oliveira, D., Amôres, E. B., & Ubaldo-Melo, M. L. 2019, A&A, 629, A33
- Gonzalez, G. 1997, MNRAS, 285, 403
- Gonzalez, G. 2006, PASP, 118, 1494
- González Hernández, J. I., Delgado-Mena, E., Sousa, S. G., et al. 2013, A&A, 552, A6
- González Hernández, J. I., Israeli, G., Santos, N. C., et al. 2010, ApJ, 720, 1592
- Hardegree-Ullman, K. K., Cushing, M. C., Muirhead, P. S., & Christiansen, J. L. 2019, AJ, 158, 75
- Henry, T. J. & McCarthy, Donald W., J. 1993, AJ, 106, 773
- Howard, A. W., Marcy, G. W., Bryson, S. T., et al. 2012, ApJS, 201, 15
- Hubickyj, O., Bodenheimer, P., & Lissauer, J. J. 2005, Icarus, 179, 415
- Ida, S. & Lin, D. N. C. 2004, ApJ, 616, 567
- Jianke, L. & Collier Cameron, A. 1993, MNRAS, 261, 766
- Johnson, D. R. H. & Soderblom, D. R. 1987, AJ, 93, 864
- Johnson, J. A., Aller, K. M., Howard, A. W., & Crepp, J. R. 2010a, PASP, 122, 905
- Johnson, J. A. & Apps, K. 2009, ApJ, 699, 933
- Johnson, J. A., Butler, R. P., Marcy, G. W., et al. 2007, ApJ, 670, 833
- Johnson, J. A., Howard, A. W., Marcy, G. W., et al. 2010b, PASP, 122, 149
- Karoff, C., Metcalfe, T. S., Santos, Á. R. G., et al. 2018, ApJ, 852, 46
- Kim, Y.-C., Demarque, P., Yi, S. K., & Alexander, D. R. 2002, ApJS, 143, 499
- Kraft, R. P. 1967, ApJ, 150, 551
- Kurucz, R. 1993a, ATLAS9 Stellar Atmosphere Programs and 2 km/s grid. Kurucz CD-ROM No. 13. Cambridge, Mass.: Smithsonian Astrophysical Observatory, 1993., 13
- Kurucz, R. 1993b, SYNTHE Spectrum Synthesis Programs and Line Data. Kurucz CD-ROM No. 18. Cambridge, 18
- Lagrange, A. M., De Bondt, K., Meunier, N., et al. 2012, A&A, 542, A18
- Laws, C., Gonzalez, G., Walker, K. M., et al. 2003, AJ, 125, 2664
- Lovis, C. & Mayor, M. 2007, A&A, 472, 657
- MacKay, D. J. C. 1992, Neural computation, 4, 415
- Maldonado, J. 2012, PhD thesis, Universidad Autónoma de Madrid
- Maldonado, J., Affer, L., Micela, G., et al. 2015a, A&A, 577, A132
- Maldonado, J., Eiroa, C., Villaver, E., Montesinos, B., & Mora, A. 2015b, A&A, 579, A20
- Maldonado, J., Phillips, D. F., Dumusque, X., et al. 2019a, A&A, 627, A118
- Maldonado, J. & Villaver, E. 2016, A&A, 588, A98
- Maldonado, J., Villaver, E., Eiroa, C., & Micela, G. 2019b, A&A, 624, A94
- Mann, A. W., Brewer, J. M., Gaidos, E., Lépine, S., & Hilton, E. J. 2013a, AJ, 145, 52
- Mann, A. W., Gaidos, E., & Ansdell, M. 2013b, ApJ, 779, 188
- Masseron, T., Plez, B., Van Eck, S., et al. 2014, A&A, 571, A47
- Mayor, M., Marmier, M., Lovis, C., et al. 2011, arXiv e-prints, arXiv:1109.2497
- Mayor, M., Pepe, F., Queloz, D., et al. 2003, The Messenger, 114, 20
- Mayor, M., & Queloz, D. 1995, Nature, 378, 355
- Meléndez, J., Asplund, M., Gustafsson, B., & Yong, D. 2009, ApJ, 704, L66
- Meunier, N., Lagrange, A. M., & De Bondt, K. 2012, A&A, 545, A87
- Montes, D., González-Peinado, R., Tabernero, H. M., et al. 2018, MNRAS, 479, 1332
- Montes, D., López-Santiago, J., Gálvez, M. C., et al. 2001, MNRAS, 328, 45
- Montesinos, B., Thomas, J. H., Ventura, P., & Mazzitelli, I. 2001, MNRAS, 326, 877
- Montet, B. T., Crepp, J. R., Johnson, J. A., Howard, A. W., & Marcy, G. W. 2014, ApJ, 781, 28
- Mordasini, C., Alibert, Y., & Benz, W. 2009, A&A, 501, 1139
- Mordasini, C., Alibert, Y., Benz, W., Klahr, H., & Henning, T. 2012, A&A, 541, A97
- Mortier, A., Santos, N. C., Sousa, S., et al. 2013, A&A, 551, A112
- Muñoz Bermejo, J., Asensio Ramos, A., & Allende Prieto, C. 2013, A&A, 553, A95
- Mulders, G. D., Pascucci, I., & Apai, D. 2015a, ApJ, 798, 112
- Mulders, G. D., Pascucci, I., & Apai, D. 2015b, ApJ, 814, 130
- Neves, V., Bonfils, X., Santos, N. C., et al. 2012, A&A, 538, A25
- Neves, V., Bonfils, X., Santos, N. C., et al. 2013, A&A, 551, A36
- Neves, V., Bonfils, X., Santos, N. C., et al. 2014, A&A, 568, A121
- Newton, E. R., Charbonneau, D., Irwin, J., et al. 2014, AJ, 147, 20
- Noyes, R. W., Hartmann, L. W., Baliunas, S. L., Duncan, D. K., & Vaughan, A. H. 1984, ApJ, 279, 763
- Önehag, A., Heiter, U., Gustafsson, B., et al. 2012, A&A, 542, A33
- Passegger, V. M., Reiners, A., Jeffers, S. V., et al. 2018, A&A, 615, A6
- Passegger, V. M., Schweitzer, A., Shulyak, D., et al. 2019, A&A, 627, A161
- Pedregosa, F., Varoquaux, G., Gramfort, A., et al. 2011, Journal of Machine Learning Research, 12, 2825
- Perger, M., García-Piquer, A., Ribas, I., et al. 2017, A&A, 598, A26
- Perryman, M. 2018, The Exoplanet Handbook
- Pinamonti, M., Sozzetti, A., Giacobbe, P., et al. 2019, A&A, 625, A126
- Pollack, J. B., Hubickyj, O., Bodenheimer, P., et al. 1996, Icarus, 124, 62
- Quirrenbach, A., Amado, P. J., Ribas, I., et al. 2018, in Society of Photo-Optical Instrumentation Engineers (SPIE) Conference Series, Vol. 10702, Ground-based and Airborne Instrumentation for Astronomy VII, 107020W
- Ramírez, I., Meléndez, J., & Asplund, M. 2009, A&A, 508, L17
- Ramírez, I., Meléndez, J., Bean, J., et al. 2014, A&A, 572, A48
- Rauscher, E. & Marcy, G. W. 2006, PASP, 118, 617
- Reddy, B. E., Lambert, D. L., & Allende Prieto, C. 2006, MNRAS, 367, 1329
- Reddy, B. E., Tomkin, J., Lambert, D. L., & Allende Prieto, C. 2003, MNRAS, 340, 304
- Rojas-Ayala, B., Covey, K. R., Muirhead, P. S., & Lloyd, J. P. 2012, ApJ, 748, 93
- Santos, N. C., Israeli, G., & Mayor, M. 2004, A&A, 415, 1153
- Schlaufman, K. C. & Laughlin, G. 2010, A&A, 519, A105
- Schweitzer, A., Passegger, V. M., Cifuentes, C., et al. 2019, A&A, 625, A68
- Sinclair, J. A., Helling, C., & Greaves, J. S. 2010, MNRAS, 409, L49
- Sneden, C. A. 1973, PhD thesis, THE UNIVERSITY OF TEXAS AT AUSTIN.
- Soubiran, C., Jasniewicz, G., Chemin, L., et al. 2018, A&A, 616, A7
- Sousa, S. G., Santos, N. C., Adibekyan, V., Delgado-Mena, E., & Israeli, G. 2015, A&A, 577, A67
- Sousa, S. G., Santos, N. C., Israeli, G., Mayor, M., & Monteiro, M. J. P. F. G. 2007, A&A, 469, 783
- Sousa, S. G., Santos, N. C., Israeli, G., Mayor, M., & Udry, S. 2011, A&A, 533, A141
- Sousa, S. G., Santos, N. C., Mayor, M., et al. 2008, A&A, 487, 373
- Souto, D., Cunha, K., García-Hernández, D. A., et al. 2017, ApJ, 835, 239
- Souto, D., Cunha, K., Smith, V. V., et al. 2020, ApJ, 890, 133
- Souto, D., Unterborn, C. T., Smith, V. V., et al. 2018, ApJ, 860, L15
- Sozzetti, A., Torres, G., Latham, D. W., et al. 2009, ApJ, 697, 544
- Spada, F., Demarque, P., Kim, Y. C., & Sills, A. 2013, ApJ, 776, 87
- Takeda, Y., Ohkubo, M., & Sadakane, K. 2002a, PASJ, 54, 451
- Takeda, Y., Ohkubo, M., Sato, B., Kambe, E., & Sadakane, K. 2005, PASJ, 57, 27
- Takeda, Y., Sato, B., Kambe, E., Sadakane, K., & Ohkubo, M. 2002b, PASJ, 54, 1041
- Terrien, R. C., Mahadevan, S., Bender, C. F., et al. 2012, ApJ, 747, L38
- Timmes, F. X., Woosley, S. E., & Weaver, T. A. 1995, ApJS, 98, 617
- Tipping, M. E. 2001, J. Mach. Learn. Res., 1, 211–244
- Udry, S. & Santos, N. C. 2007, ARA&A, 45, 397
- Weber, E. J. & Davis, Leverett, J. 1967, ApJ, 148, 217
- Wolszczan, A. & Frail, D. A. 1992, Nature, 355, 145
- Woolf, V. M. & Wallerstein, G. 2005, MNRAS, 356, 963
- Woolf, V. M. & Wallerstein, G. 2020, MNRAS, 494, 2718
- Wright, J. T. & Howard, A. W. 2009, ApJS, 182, 205
- Xiang, M. S., Liu, X. W., Shi, J. R., et al. 2017, MNRAS, 464, 3657
- Yi, S., Demarque, P., Kim, Y.-C., et al. 2001, ApJS, 136, 417

Appendix A: Additional tables

Table A.1. Basic properties of the stars considered in this work.

Star	T _{eff} (K)	SptType	[Fe/H] (dex)	M _★ (M _⊙)	R _★ (R _⊙)	log(g) (cm s ⁻²)	log(L _★ /L _⊙)	Age (Gyr)
GJ 2	3709 ± 68	M1.0	-0.14 ± 0.09	0.50 ± 0.05	0.49 ± 0.05	4.76 ± 0.04	-1.385 ± 0.087	8.28 ± 4.11
GJ 1	3478 ± 68	M2.5	-0.26 ± 0.09	0.33 ± 0.07	0.33 ± 0.06	4.91 ± 0.06	-1.833 ± 0.169	8.27 ± 4.11
GJ 1002	3378 ± 69	M4.0	-0.25 ± 0.10	0.22 ± 0.10	0.24 ± 0.09	5.01 ± 0.10	-2.176 ± 0.344	
GJ 3014	3692 ± 69	M1.5	-0.19 ± 0.09	0.48 ± 0.05	0.47 ± 0.05	4.79 ± 0.04	-1.437 ± 0.090	8.22 ± 4.10
GJ 12	3387 ± 68	M3.0	-0.29 ± 0.09	0.22 ± 0.10	0.24 ± 0.09	5.01 ± 0.09	-2.180 ± 0.327	7.20 ± 4.23
GJ 16	3679 ± 68	M1.5	-0.16 ± 0.09	0.48 ± 0.05	0.47 ± 0.05	4.78 ± 0.04	-1.434 ± 0.089	8.23 ± 4.10
GJ 15A	3610 ± 68	M1.0	-0.35 ± 0.09	0.38 ± 0.05	0.38 ± 0.05	4.87 ± 0.04	-1.659 ± 0.112	
GJ 15B	3386 ± 68	M3.0	-0.43 ± 0.09	0.16 ± 0.10	0.19 ± 0.09	5.06 ± 0.09	-2.387 ± 0.416	
GJ 1009	3662 ± 68	M2.0	0.01 ± 0.09	0.54 ± 0.05	0.53 ± 0.05	4.73 ± 0.04	-1.350 ± 0.082	8.08 ± 4.13
GJ 21	3762 ± 68	M0.5	-0.11 ± 0.09	0.54 ± 0.05	0.53 ± 0.05	4.73 ± 0.04	-1.303 ± 0.086	8.29 ± 4.07
GJ 26	3507 ± 68	M2.5	-0.15 ± 0.09	0.39 ± 0.06	0.39 ± 0.06	4.85 ± 0.06	-1.677 ± 0.132	7.95 ± 4.22
GJ 27.1	3750 ± 68	M1.0	-0.09 ± 0.09	0.54 ± 0.05	0.53 ± 0.05	4.73 ± 0.04	-1.306 ± 0.085	8.27 ± 4.08
LHS 1134	3304 ± 71	M4.0	-0.16 ± 0.09	0.14 ± 0.14	0.16 ± 0.13	5.09 ± 0.13	-2.551 ± 0.681	8.07 ± 4.12
GJ 47	3517 ± 68	M2.0	-0.26 ± 0.09	0.36 ± 0.06	0.36 ± 0.06	4.89 ± 0.05	-1.746 ± 0.139	
GJ 49	3711 ± 68	M1.5	-0.03 ± 0.09	0.55 ± 0.05	0.53 ± 0.05	4.73 ± 0.04	-1.318 ± 0.081	8.34 ± 4.07
GJ 1030	3652 ± 68	M2.0	-0.06 ± 0.09	0.51 ± 0.05	0.50 ± 0.05	4.76 ± 0.04	-1.403 ± 0.086	8.49 ± 4.06
GJ 54.1	3295 ± 68	M4.0	-0.24 ± 0.09	0.13 ± 0.02	0.12 ± 0.13	5.14 ± 0.13	-2.824 ± 0.914	
NLTT 4188	3810 ± 69	M0.5	-0.06 ± 0.09	0.59 ± 0.06	0.57 ± 0.05	4.70 ± 0.05	-1.213 ± 0.088	8.22 ± 4.09
L 707-74	3418 ± 68	M3.0	-0.23 ± 0.09	0.28 ± 0.09	0.29 ± 0.08	4.96 ± 0.08	-1.982 ± 0.236	7.10 ± 4.26
GJ 70	3498 ± 68	M2.5	-0.21 ± 0.09	0.36 ± 0.07	0.37 ± 0.06	4.88 ± 0.06	-1.745 ± 0.145	7.86 ± 4.21
GJ 3117	3566 ± 68	M2.5	-0.06 ± 0.09	0.47 ± 0.06	0.46 ± 0.05	4.79 ± 0.05	-1.515 ± 0.101	8.17 ± 4.15
GJ 83.1	3346 ± 69	M4.0	0.02 ± 0.09	0.28 ± 0.12	0.29 ± 0.11	4.96 ± 0.11	-2.023 ± 0.317	
GJ 3126	3491 ± 68	M3.0	-0.02 ± 0.09	0.43 ± 0.07	0.43 ± 0.06	4.82 ± 0.06	-1.613 ± 0.128	7.94 ± 4.23
GJ 87	3568 ± 68	M2.0	-0.11 ± 0.09	0.45 ± 0.06	0.44 ± 0.05	4.81 ± 0.05	-1.546 ± 0.104	8.37 ± 4.02
GJ 105B	3289 ± 69	M4.0	-0.04 ± 0.09	0.15 ± 0.14	0.18 ± 0.13	5.08 ± 0.14	-2.478 ± 0.639	7.58 ± 4.25
LP 993-115	3359 ± 68	M3.5	0.26 ± 0.10	0.39 ± 0.11	0.39 ± 0.10	4.87 ± 0.10	-1.758 ± 0.226	7.52 ± 4.22
GJ 3186	3768 ± 68	M1.0	-0.14 ± 0.09	0.53 ± 0.05	0.52 ± 0.05	4.74 ± 0.05	-1.313 ± 0.088	8.57 ± 4.03
GJ 119A	3776 ± 69	M1.0	-0.08 ± 0.09	0.56 ± 0.05	0.54 ± 0.05	4.72 ± 0.05	-1.268 ± 0.086	8.55 ± 4.03
GJ 119B	3490 ± 68	M3.0	0.03 ± 0.09	0.45 ± 0.07	0.44 ± 0.06	4.81 ± 0.06	-1.581 ± 0.124	9.34 ± 3.81
LHS 1481	3393 ± 68	M2.5	-0.37 ± 0.09	0.20 ± 0.10	0.22 ± 0.09	5.03 ± 0.09	-2.260 ± 0.353	3.04 ± 3.09
IP 771-96	3389 ± 68	M3.0	-0.25 ± 0.09	0.24 ± 0.10	0.25 ± 0.09	5.00 ± 0.09	-2.123 ± 0.306	7.87 ± 4.23
IHS 1513	3413 ± 68	M3.5	-0.28 ± 0.10	0.26 ± 0.09	0.27 ± 0.08	4.98 ± 0.08	-2.056 ± 0.266	7.40 ± 4.27
TYC 1795-941-1 [†]	3761 ± 68	M0.0	-0.09 ± 0.09	0.31 ± 0.10	0.31 ± 0.09	4.94 ± 0.09	-1.929 ± 0.240	
GJ 1057	3394 ± 68	M4.0	-0.11 ± 0.09	0.52 ± 0.05	0.51 ± 0.05	4.75 ± 0.04	-1.355 ± 0.085	
NLTT 10614	3719 ± 69	M1.0	-0.18 ± 0.09	0.32 ± 0.08	0.33 ± 0.07	4.92 ± 0.07	-1.873 ± 0.198	7.65 ± 4.24
GJ 145	3437 ± 68	M3.0	-0.12 ± 0.09	0.66 ± 0.06	0.63 ± 0.05	4.63 ± 0.05	-1.119 ± 0.081	9.67 ± 3.78
TYC 3720-426-1	3813 ± 69	M1.5	-0.03 ± 0.09	0.56 ± 0.05	0.55 ± 0.05	4.71 ± 0.04	-1.277 ± 0.082	8.90 ± 3.95
GJ 150.1B	3725 ± 68	M1.0	-0.12 ± 0.09	0.52 ± 0.05	0.51 ± 0.05	4.75 ± 0.04	-1.354 ± 0.086	8.33 ± 4.08
GJ 1065	3331 ± 69	M3.5	-0.25 ± 0.09	0.15 ± 0.12	0.17 ± 0.11	5.08 ± 0.11	-2.476 ± 0.555	
GJ 156 [†]	3864 ± 70	M0.0	-0.68 ± 0.10	0.66 ± 0.11	0.63 ± 0.15	-1.060 ± 0.148		
GJ 156.1	3746 ± 68	M1.5	-0.03 ± 0.09	0.56 ± 0.05	0.55 ± 0.05	4.71 ± 0.04	-1.277 ± 0.082	8.90 ± 3.95
GJ 162	3759 ± 68	M0.5	-0.19 ± 0.09	0.51 ± 0.05	0.50 ± 0.05	4.76 ± 0.04	-1.354 ± 0.090	8.32 ± 4.07
GJ 1068	3294 ± 67	M3.5	-0.37 ± 0.09	0.12 ± 0.02	0.07 ± 0.12	5.18 ± 0.13	-3.255 ± 1.493	

Table A.1. Continued.

Star	T _{eff} (K)	SpType	[Fe/H] (dex)	M _★ (M _⊙)	R _★ (R _⊙)	log(g) (cm s ⁻²)	log(L _★ /L _⊙)	Age (Gyr)
GJ 166C	3331 ± 67	M4.5	0.11 ± 0.09	0.29 ± 0.12	0.30 ± 0.11	4.96 ± 0.11	-2.005 ± 0.317	1.79 ± 2.13
GJ 169 [†]	3901 ± 71	M0.0	0.68 ± 0.10	0.66 ± 0.11	4.63 ± 0.15	-1.044 ± 0.148		
GJ 173	3610 ± 68	M2.0	-0.15 ± 0.09	0.46 ± 0.05	0.45 ± 0.05	4.80 ± 0.04	-1.513 ± 0.096	8.08 ± 4.15
GJ 176	3612 ± 68	M2.0	0.04 ± 0.09	0.53 ± 0.05	0.52 ± 0.05	4.74 ± 0.04	-1.393 ± 0.085	8.00 ± 4.15
GJ 179	3381 ± 68	M3.5	0.05 ± 0.09	0.34 ± 0.10	0.35 ± 0.09	4.91 ± 0.09	-1.851 ± 0.230	7.78 ± 4.20
GJ 180	3536 ± 68	M2.0	-0.17 ± 0.09	0.41 ± 0.06	0.40 ± 0.05	4.84 ± 0.05	-1.640 ± 0.120	7.84 ± 4.25
GJ 1074	3779 ± 69	M0.5	-0.13 ± 0.09	0.54 ± 0.05	0.53 ± 0.05	4.73 ± 0.05	-1.292 ± 0.089	8.37 ± 4.06
LHS 1723	3268 ± 70	M4.0	-0.19 ± 0.09	0.15 ± 0.02	0.09 ± 0.14	5.17 ± 0.15	-3.128 ± 1.466	
LHS 1731	3401 ± 68	M3.0	-0.22 ± 0.09	0.26 ± 0.09	0.28 ± 0.08	4.97 ± 0.09	-2.035 ± 0.265	7.59 ± 4.24
GJ 184	3744 ± 69	M0.5	-0.10 ± 0.09	0.53 ± 0.05	0.52 ± 0.05	4.74 ± 0.04	-1.319 ± 0.085	8.48 ± 4.03
GJ 191	3571 ± 68	M0.0	-0.40 ± 0.09	0.34 ± 0.06	0.34 ± 0.05	4.90 ± 0.05	-1.764 ± 0.130	
GJ 203	3325 ± 69	M3.5	-0.22 ± 0.09	0.15 ± 0.13	0.18 ± 0.11	5.08 ± 0.12	-2.474 ± 0.565	7.36 ± 4.21
GJ 205	3799 ± 68	M1.5	0.00 ± 0.09	0.60 ± 0.06	0.58 ± 0.05	4.68 ± 0.05	-1.196 ± 0.084	8.48 ± 4.03
GJ 3352	3822 ± 69	M0.5	-0.13 ± 0.09	0.57 ± 0.06	0.55 ± 0.06	4.71 ± 0.05	-1.234 ± 0.093	8.52 ± 4.03
GJ 3356	3394 ± 68	M3.5	-0.01 ± 0.09	0.34 ± 0.10	0.34 ± 0.09	4.91 ± 0.09	-1.857 ± 0.222	7.80 ± 4.21
GJ 208	3860 ± 70	M0.0	0.05 ± 0.09	0.66 ± 0.07	0.64 ± 0.06	4.63 ± 0.06	-1.088 ± 0.091	9.38 ± 3.84
GJ 213	3264 ± 69	M4.0	-0.10 ± 0.09	0.19 ± 0.04	0.11 ± 0.14	5.15 ± 0.15	-2.919 ± 1.141	7.14 ± 4.00
GJ 229	3782 ± 68	M1.0	-0.06 ± 0.09	0.57 ± 0.05	0.55 ± 0.05	4.71 ± 0.05	-1.249 ± 0.085	8.34 ± 4.07
TYC 3379-1077-1	3921 ± 71	K7.5	-0.02 ± 0.09	0.69 ± 0.08	0.67 ± 0.08	4.60 ± 0.07	-1.023 ± 0.108	9.12 ± 3.90
TYC 743-1836-1	3909 ± 70	M0.0	-0.09 ± 0.09	0.65 ± 0.08	0.63 ± 0.08	4.64 ± 0.07	-1.076 ± 0.108	8.80 ± 3.96
HIP 31293	3450 ± 68	M3.0	-0.07 ± 0.09	0.38 ± 0.08	0.38 ± 0.07	4.87 ± 0.07	-1.742 ± 0.165	8.03 ± 4.15
HIP 31292	3450 ± 68	M3.0	-0.07 ± 0.09	0.38 ± 0.08	0.38 ± 0.07	4.87 ± 0.07	-1.742 ± 0.165	7.46 ± 4.26
G 108-21	3421 ± 68	M3.5	0.09 ± 0.09	0.41 ± 0.09	0.41 ± 0.08	4.85 ± 0.08	-1.696 ± 0.171	7.96 ± 4.15
Gl 250B	3566 ± 68	M2.5	-0.11 ± 0.09	0.45 ± 0.06	0.44 ± 0.05	4.81 ± 0.05	-1.549 ± 0.104	7.94 ± 4.25
GJ 272	3773 ± 68	M1.0	-0.12 ± 0.09	0.54 ± 0.05	0.53 ± 0.05	4.73 ± 0.05	-1.295 ± 0.087	8.32 ± 4.06
GJ 273	3315 ± 69	M4.0	-0.04 ± 0.09	0.20 ± 0.13	0.22 ± 0.12	5.03 ± 0.12	-2.274 ± 0.465	7.75 ± 4.22
GJ 1097	3423 ± 68	M3.0	-0.01 ± 0.09	0.37 ± 0.09	0.37 ± 0.08	4.88 ± 0.08	-1.767 ± 0.184	7.92 ± 4.16
StKM 1-650	3897 ± 70	M0.0	-0.10 ± 0.09	0.63 ± 0.08	0.62 ± 0.07	4.65 ± 0.07	-1.101 ± 0.105	8.88 ± 3.94
LHS 1935	3403 ± 68	M3.0	-0.19 ± 0.09	0.28 ± 0.09	0.29 ± 0.08	4.96 ± 0.09	-1.996 ± 0.253	7.59 ± 4.26
Gl 285 [†]	3481 ± 67	M4.0	0.30 ± 0.06	0.30 ± 0.06	0.49 ± 0.18	-1.926 ± 0.177		
Gl 299 [†]	3245 ± 68	M4.0	-0.43 ± 0.09	0.13 ± 0.02	0.17 ± 0.03	5.09 ± 0.15	-2.542 ± 0.158	
Gl 300	3315 ± 69	M4.0	0.06 ± 0.09	0.24 ± 0.13	0.26 ± 0.12	5.00 ± 0.12	-2.146 ± 0.403	6.91 ± 4.22
Gl 2066	3559 ± 68	M2.0	-0.10 ± 0.09	0.45 ± 0.06	0.44 ± 0.05	4.81 ± 0.05	-1.552 ± 0.105	7.99 ± 4.24
Gl 317	3398 ± 68	M3.5	0.18 ± 0.09	0.41 ± 0.09	0.41 ± 0.09	4.84 ± 0.09	-1.694 ± 0.183	8.15 ± 4.10
NLTT 21156	3623 ± 68	M2.0	-0.04 ± 0.09	0.50 ± 0.05	0.49 ± 0.05	4.76 ± 0.04	-1.426 ± 0.088	
Gl 1123	3349 ± 70	M4.0	0.07 ± 0.09	0.30 ± 0.12	0.31 ± 0.10	4.94 ± 0.11	-1.958 ± 0.294	
Gl 341	3798 ± 69	M0.5	-0.16 ± 0.09	0.54 ± 0.06	0.53 ± 0.05	4.73 ± 0.05	-1.284 ± 0.092	8.29 ± 4.07
Gl 1125	3391 ± 68	M3.5	-0.11 ± 0.09	0.29 ± 0.10	0.30 ± 0.09	4.95 ± 0.09	-1.961 ± 0.252	7.71 ± 4.25
Gl 357	3461 ± 68	M2.5	-0.14 ± 0.09	0.36 ± 0.08	0.36 ± 0.07	4.89 ± 0.07	-1.773 ± 0.165	7.81 ± 4.25
Gl 358	3423 ± 68	M3.0	0.10 ± 0.09	0.41 ± 0.09	0.41 ± 0.08	4.84 ± 0.08	-1.683 ± 0.167	8.19 ± 4.14
Gl 361	3619 ± 68	M2.0	-0.13 ± 0.09	0.47 ± 0.05	0.46 ± 0.05	4.79 ± 0.04	-1.488 ± 0.094	8.04 ± 4.15
Gl 367	3558 ± 68	M2.5	-0.07 ± 0.09	0.46 ± 0.06	0.45 ± 0.05	4.80 ± 0.05	-1.533 ± 0.103	8.26 ± 4.09
Gl 1129	3345 ± 69	M4.0	-0.06 ± 0.09	0.25 ± 0.12	0.26 ± 0.11	4.99 ± 0.11	-2.117 ± 0.353	7.54 ± 4.24

Table A.1. Continued.

Star	T _{eff} (K)	SpType	[Fe/H] (dex)	M _★ (M _⊙)	R _★ (R _⊙)	log(g) (cm s ⁻²)	log(L _★ /L _⊙)	Age (Gyr)
GJ 382	3660 ± 68	M2.0	0.02 ± 0.09	0.54 ± 0.05	0.53 ± 0.05	4.73 ± 0.04	-1.348 ± 0.081	8.14 ± 4.13
GJ 388	3427 ± 68	M3.5	0.11 ± 0.10	0.42 ± 0.09	0.42 ± 0.08	4.83 ± 0.08	-1.665 ± 0.164	8.03 ± 4.13
GJ 390	3713 ± 68	M1.5	-0.06 ± 0.09	0.54 ± 0.05	0.52 ± 0.05	4.74 ± 0.04	-1.332 ± 0.083	8.33 ± 4.08
GJ 393	3549 ± 68	M2.0	-0.14 ± 0.09	0.43 ± 0.06	0.42 ± 0.05	4.83 ± 0.05	-1.595 ± 0.112	7.90 ± 4.25
GJ 399	3542 ± 68	M2.5	-0.05 ± 0.09	0.46 ± 0.06	0.45 ± 0.05	4.80 ± 0.05	-1.545 ± 0.107	8.12 ± 4.22
LHS 288 [†]	3297 ± 68	M4.0	0.10 ± 0.01	0.14 ± 0.02	5.10 ± 0.16	-2.683 ± 0.129		
GJ 402	3344 ± 69	M3.5	-0.07 ± 0.09	0.24 ± 0.12	0.26 ± 0.11	5.00 ± 0.11	-2.132 ± 0.360	6.89 ± 4.17
GJ 406	3419 ± 70	M4.0	0.23 ± 0.10	0.46 ± 0.09	0.45 ± 0.08	4.80 ± 0.08	-1.601 ± 0.160	
GJ 408	3461 ± 68	M2.5	-0.21 ± 0.09	0.33 ± 0.08	0.34 ± 0.07	4.91 ± 0.07	-1.833 ± 0.177	7.86 ± 4.23
GJ 410	3839 ± 70	M0.0	-0.05 ± 0.10	0.61 ± 0.06	0.59 ± 0.06	4.68 ± 0.06	-1.168 ± 0.095	8.30 ± 4.07
GJ 411	3517 ± 68	M2.0	-0.28 ± 0.09	0.35 ± 0.06	0.36 ± 0.06	4.89 ± 0.05	-1.762 ± 0.142	7.91 ± 4.20
GJ 412A	3634 ± 68	M0.5	-0.37 ± 0.09	0.38 ± 0.05	0.38 ± 0.05	4.87 ± 0.04	-1.640 ± 0.109	
GJ 413.1	3574 ± 68	M2.0	-0.10 ± 0.09	0.46 ± 0.05	0.45 ± 0.05	4.80 ± 0.05	-1.530 ± 0.101	8.00 ± 4.25
GJ 414B	3668 ± 68	M2.0	-0.07 ± 0.09	0.51 ± 0.05	0.50 ± 0.05	4.75 ± 0.04	-1.391 ± 0.085	8.51 ± 4.04
GJ 3649	3706 ± 68	M1.5	-0.11 ± 0.09	0.51 ± 0.05	0.50 ± 0.05	4.76 ± 0.04	-1.371 ± 0.085	8.10 ± 4.14
GJ 433	3625 ± 68	M2.0	-0.15 ± 0.09	0.46 ± 0.05	0.46 ± 0.05	4.80 ± 0.04	-1.494 ± 0.094	8.05 ± 4.14
GJ 436	3489 ± 68	M3.0	-0.06 ± 0.09	0.41 ± 0.07	0.41 ± 0.06	4.84 ± 0.06	-1.647 ± 0.134	7.94 ± 4.21
GJ 438	3645 ± 68	M1.0	-0.25 ± 0.09	0.43 ± 0.05	0.43 ± 0.05	4.82 ± 0.04	-1.536 ± 0.098	7.80 ± 4.27
GJ 447 [†]	3279 ± 69	M4.0	-0.20 ± 0.09	0.16 ± 0.02	0.19 ± 0.03	5.07 ± 0.14	-2.427 ± 0.142	
GJ 450	3649 ± 68	M1.5	-0.22 ± 0.09	0.45 ± 0.05	0.44 ± 0.05	4.81 ± 0.04	-1.511 ± 0.095	7.90 ± 4.22
GJ 3708	3444 ± 68	M3.0	-0.11 ± 0.09	0.35 ± 0.08	0.36 ± 0.07	4.89 ± 0.07	-1.791 ± 0.177	7.82 ± 4.24
GJ 9404	3891 ± 70	M0.5	-0.13 ± 0.09	0.62 ± 0.07	0.60 ± 0.07	4.67 ± 0.07	-1.127 ± 0.106	8.85 ± 3.94
GJ 465	3408 ± 68	M2.5	-0.25 ± 0.09	0.26 ± 0.09	0.27 ± 0.08	4.97 ± 0.08	-2.041 ± 0.262	7.72 ± 4.26
GJ 476	3486 ± 68	M3.0	-0.10 ± 0.09	0.40 ± 0.07	0.40 ± 0.06	4.85 ± 0.06	-1.682 ± 0.140	8.53 ± 3.98
GJ 479	3496 ± 68	M3.0	0.03 ± 0.09	0.45 ± 0.07	0.45 ± 0.06	4.80 ± 0.06	-1.569 ± 0.121	7.89 ± 4.19
LHS 337 [†]	3257 ± 67	M4.0	-0.31 ± 0.09	0.14 ± 0.02	0.18 ± 0.03	5.08 ± 0.15	-2.486 ± 0.149	
GJ 480.1	3353 ± 68	M3.0	-0.30 ± 0.09	0.17 ± 0.11	0.19 ± 0.10	5.06 ± 0.10	-2.393 ± 0.467	0.65 ± 0.09
GJ 486	3309 ± 69	M4.0	-0.01 ± 0.09	0.20 ± 0.13	0.22 ± 0.12	5.03 ± 0.13	-2.277 ± 0.475	7.84 ± 4.19
GJ 488	3925 ± 66	M0.0	-0.03 ± 0.10	0.69 ± 0.08	0.67 ± 0.08	4.60 ± 0.07	-1.021 ± 0.105	9.70 ± 3.78
GJ 494 [†]	3721 ± 71	M1.5	0.58 ± 0.09	0.57 ± 0.09	4.70 ± 0.15	-1.253 ± 0.141		
GJ 9440	3719 ± 68	M1.5	-0.11 ± 0.09	0.52 ± 0.05	0.51 ± 0.05	4.75 ± 0.04	-1.355 ± 0.085	8.45 ± 4.03
GJ 514	3730 ± 68	M1.0	-0.14 ± 0.09	0.51 ± 0.05	0.50 ± 0.05	4.76 ± 0.04	-1.360 ± 0.087	8.25 ± 4.11
GJ 521A	3609 ± 68	M1.5	-0.12 ± 0.09	0.47 ± 0.05	0.46 ± 0.05	4.79 ± 0.04	-1.495 ± 0.095	8.75 ± 3.98
GJ 526	3604 ± 68	M2.0	-0.09 ± 0.09	0.48 ± 0.05	0.47 ± 0.05	4.79 ± 0.04	-1.481 ± 0.094	8.39 ± 4.04
GJ 3804	3342 ± 69	M3.5	-0.02 ± 0.09	0.26 ± 0.12	0.27 ± 0.11	4.98 ± 0.11	-2.087 ± 0.343	7.89 ± 4.19
GJ 536	3679 ± 68	M1.5	-0.08 ± 0.09	0.51 ± 0.05	0.50 ± 0.05	4.75 ± 0.04	-1.384 ± 0.085	8.46 ± 4.06
GJ 3822	3832 ± 69	M0.5	-0.12 ± 0.09	0.58 ± 0.06	0.56 ± 0.06	4.70 ± 0.05	-1.215 ± 0.094	8.50 ± 4.03
GJ 548A	3908 ± 70	M0.0	-0.10 ± 0.09	0.64 ± 0.08	0.63 ± 0.07	4.64 ± 0.07	-1.083 ± 0.108	8.95 ± 3.92
GJ 552	3603 ± 68	M2.0	-0.11 ± 0.09	0.47 ± 0.05	0.46 ± 0.05	4.79 ± 0.04	-1.497 ± 0.095	8.25 ± 4.05
GJ 551	3306 ± 67	M4.5	-0.04 ± 0.09	0.19 ± 0.13	0.21 ± 0.12	5.05 ± 0.12	-2.338 ± 0.499	
GJ 553.1	3352 ± 69	M3.5	-0.08 ± 0.09	0.25 ± 0.11	0.26 ± 0.10	4.99 ± 0.11	-2.101 ± 0.337	7.87 ± 4.21
GJ 555	3327 ± 69	M4.0	0.10 ± 0.09	0.28 ± 0.13	0.29 ± 0.11	4.97 ± 0.12	-2.035 ± 0.340	7.49 ± 4.23
GJ 9492	3504 ± 68	M2.0	-0.27 ± 0.09	0.35 ± 0.07	0.35 ± 0.06	4.90 ± 0.06	-1.782 ± 0.150	7.95 ± 4.19

Table A.1. Continued.

Star	T _{eff} (K)	SpType	[Fe/H] (dex)	M _★ (M _⊙)	R _★ (R _⊙)	log(g) (cm s ⁻²)	log(L _★ /L _⊙)	Age (Gyr)
GJ 569A	3596 ± 68	M2.0	-0.03 ± 0.09	0.49 ± 0.05	0.48 ± 0.05	4.77 ± 0.05	-1.454 ± 0.092	8.04 ± 4.19
GJ 570B	3754 ± 69	M1.0	0.08 ± 0.10	0.61 ± 0.05	0.59 ± 0.05	4.67 ± 0.05	-1.209 ± 0.081	8.53 ± 4.04
GJ 581	3417 ± 68	M3.0	-0.18 ± 0.09	0.30 ± 0.09	0.31 ± 0.08	4.94 ± 0.08	-1.935 ± 0.225	7.68 ± 4.28
GJ 588	3525 ± 68	M3.0	0.10 ± 0.09	0.50 ± 0.06	0.49 ± 0.06	4.76 ± 0.05	-1.475 ± 0.103	8.11 ± 4.23
GJ 606	3662 ± 68	M1.5	-0.15 ± 0.09	0.48 ± 0.05	0.47 ± 0.05	4.78 ± 0.04	-1.448 ± 0.090	8.07 ± 4.11
GJ 3942	3860 ± 69	M0.0	-0.08 ± 0.09	0.61 ± 0.07	0.60 ± 0.06	4.67 ± 0.06	-1.152 ± 0.096	8.37 ± 4.05
GJ 618A	3455 ± 68	M3.0	-0.08 ± 0.09	0.38 ± 0.08	0.38 ± 0.07	4.87 ± 0.07	-1.739 ± 0.162	7.84 ± 4.19
GJ 625	3512 ± 68	M2.0	-0.40 ± 0.09	0.30 ± 0.06	0.31 ± 0.06	4.94 ± 0.06	-1.883 ± 0.164	
GJ 628	3336 ± 69	M3.5	-0.02 ± 0.09	0.25 ± 0.12	0.26 ± 0.11	4.99 ± 0.11	-2.120 ± 0.364	7.76 ± 4.21
GJ 643	3306 ± 68	M3.5	-0.23 ± 0.09	0.11 ± 0.13	0.14 ± 0.12	5.11 ± 0.13	-2.666 ± 0.743	5.93 ± 3.80
GJ 649	3735 ± 68	M1.0	-0.14 ± 0.09	0.52 ± 0.05	0.50 ± 0.05	4.75 ± 0.04	-1.353 ± 0.087	8.30 ± 4.09
GJ 3997	3761 ± 69	M0.0	-0.25 ± 0.09	0.49 ± 0.05	0.48 ± 0.05	4.78 ± 0.04	-1.388 ± 0.094	7.99 ± 4.15
GJ 3998	3726 ± 68	M1.0	-0.13 ± 0.09	0.52 ± 0.05	0.50 ± 0.05	4.75 ± 0.04	-1.358 ± 0.086	8.38 ± 4.06
GJ 2128	3522 ± 68	M2.5	-0.26 ± 0.09	0.36 ± 0.06	0.37 ± 0.06	4.88 ± 0.05	-1.735 ± 0.136	7.73 ± 4.25
GJ 667C	3693 ± 68	M1.0	0.06 ± 0.10	0.57 ± 0.05	0.56 ± 0.05	4.70 ± 0.04	-1.288 ± 0.082	
GJ 671	3442 ± 68	M2.5	-0.24 ± 0.09	0.30 ± 0.08	0.31 ± 0.07	4.94 ± 0.07	-1.914 ± 0.204	7.86 ± 4.20
GJ 674	3462 ± 68	M2.5	-0.16 ± 0.09	0.35 ± 0.07	0.36 ± 0.07	4.89 ± 0.07	-1.785 ± 0.166	7.68 ± 4.23
GJ 678.1A	3831 ± 69	M0.0	-0.11 ± 0.09	0.58 ± 0.06	0.56 ± 0.06	4.70 ± 0.05	-1.211 ± 0.093	8.10 ± 4.11
GJ 680	3578 ± 68	M2.0	-0.15 ± 0.09	0.44 ± 0.05	0.43 ± 0.05	4.82 ± 0.05	-1.559 ± 0.104	8.09 ± 4.19
GJ 685	3813 ± 69	M0.5	-0.12 ± 0.09	0.56 ± 0.06	0.55 ± 0.05	4.71 ± 0.05	-1.241 ± 0.091	8.40 ± 4.06
GJ 687	3390 ± 68	M3.5	-0.06 ± 0.09	0.31 ± 0.10	0.32 ± 0.09	4.93 ± 0.09	-1.918 ± 0.241	8.21 ± 4.13
GJ 682	3349 ± 69	M4.0	0.05 ± 0.09	0.29 ± 0.12	0.30 ± 0.10	4.95 ± 0.11	-1.979 ± 0.298	6.40 ± 4.30
GJ 686	3656 ± 68	M1.0	-0.32 ± 0.09	0.41 ± 0.05	0.41 ± 0.05	4.84 ± 0.04	-1.572 ± 0.102	7.97 ± 4.18
GJ 694.2	3848 ± 69	M0.5	-0.19 ± 0.09	0.56 ± 0.06	0.55 ± 0.06	4.72 ± 0.06	-1.228 ± 0.100	8.49 ± 4.04
GJ 693	3391 ± 68	M3.0	-0.18 ± 0.09	0.27 ± 0.10	0.28 ± 0.09	4.97 ± 0.09	-2.032 ± 0.273	7.60 ± 4.25
GJ 699 [†]	3260 ± 68	M3.5	-0.37 ± 0.10	0.15 ± 0.02	0.18 ± 0.03	5.08 ± 0.15	-2.484 ± 0.149	
GJ 701	3683 ± 68	M1.0	-0.18 ± 0.09	0.48 ± 0.05	0.47 ± 0.05	4.79 ± 0.04	-1.441 ± 0.090	7.90 ± 4.17
GJ 1224	3371 ± 66	M4.0	-0.01 ± 0.09	0.31 ± 0.10	0.31 ± 0.09	4.94 ± 0.09	-1.941 ± 0.255	
GJ 4057	3876 ± 69	M0.0	-0.19 ± 0.09	0.58 ± 0.07	0.57 ± 0.07	4.70 ± 0.06	-1.184 ± 0.105	8.51 ± 4.03
GJ 720A	3837 ± 69	M0.5	-0.11 ± 0.09	0.58 ± 0.06	0.57 ± 0.06	4.70 ± 0.05	-1.202 ± 0.094	8.85 ± 3.95
G J 141-29	3417 ± 68	M4.0	0.07 ± 0.09	0.39 ± 0.09	0.39 ± 0.08	4.86 ± 0.08	-1.722 ± 0.178	
GJ 725A	3374 ± 68	M3.0	-0.25 ± 0.09	0.22 ± 0.10	0.23 ± 0.09	5.01 ± 0.10	-2.195 ± 0.348	7.98 ± 4.20
GJ 725B	3291 ± 69	M3.5	-0.27 ± 0.09	0.23 ± 0.05	0.10 ± 0.13	5.15 ± 0.13	-2.962 ± 1.099	7.86 ± 4.20
GJ 729	3364 ± 67	M3.5	0.05 ± 0.10	0.32 ± 0.11	0.32 ± 0.10	4.93 ± 0.10	-1.917 ± 0.261	
GJ 731	3845 ± 69	M0.0	-0.16 ± 0.09	0.57 ± 0.06	0.56 ± 0.06	4.71 ± 0.06	-1.216 ± 0.098	8.28 ± 4.09
GJ 740	3840 ± 69	M0.5	-0.13 ± 0.09	0.58 ± 0.06	0.56 ± 0.06	4.70 ± 0.05	-1.207 ± 0.096	8.62 ± 4.01
GJ 4092	3888 ± 70	M0.5	-0.01 ± 0.09	0.66 ± 0.07	0.64 ± 0.07	4.63 ± 0.06	-1.073 ± 0.099	9.23 ± 3.87
GJ 1232	3342 ± 69	M4.0	-0.11 ± 0.09	0.22 ± 0.12	0.24 ± 0.11	5.01 ± 0.11	-2.191 ± 0.386	
GJ 752A	3538 ± 68	M3.0	0.05 ± 0.09	0.49 ± 0.06	0.48 ± 0.05	4.77 ± 0.05	-1.487 ± 0.102	8.22 ± 4.16
GJ 754	3263 ± 67	M4.0	-0.16 ± 0.09	0.16 ± 0.02	0.09 ± 0.14	5.17 ± 0.15	-3.125 ± 1.424	
GJ 1236	3373 ± 68	M3.0	-0.37 ± 0.09	0.17 ± 0.10	0.19 ± 0.09	5.06 ± 0.10	-2.368 ± 0.425	7.02 ± 4.04
GJ 9689	3836 ± 69	M0.5	-0.10 ± 0.09	0.59 ± 0.06	0.57 ± 0.06	4.69 ± 0.05	-1.198 ± 0.093	8.86 ± 3.94
GJ 793	3458 ± 68	M3.0	-0.18 ± 0.09	0.34 ± 0.08	0.35 ± 0.07	4.90 ± 0.07	-1.814 ± 0.174	7.82 ± 4.24
GJ 1256	3351 ± 69	M4.0	-0.02 ± 0.09	0.27 ± 0.11	0.28 ± 0.10	4.97 ± 0.11	-2.041 ± 0.317	

Table A.1. Continued.

Star	T _{eff} (K)	SpType	[Fe/H] (dex)	M _★ (M _⊙)	R _★ (R _⊙)	log(g) (cm s ⁻²)	log(L _★ /L _⊙)	Age (Gyr)
GJ 803 [†]	3755 ± 69	M1.0	0.69 ± 0.10	0.67 ± 0.11	4.62 ± 0.15	-1.097 ± 0.146		
LHS 3583	3436 ± 68	M3.0	-0.19 ± 0.09	0.32 ± 0.08	4.93 ± 0.07	-1.886 ± 0.201	7.71 ± 4.28	
LP 816-60	3311 ± 69	M4.0	-0.04 ± 0.09	0.20 ± 0.13	5.04 ± 0.12	-2.297 ± 0.482	5.08 ± 3.95	
GJ 821	3519 ± 68	M1.5	-0.36 ± 0.09	0.32 ± 0.06	4.92 ± 0.05	-1.829 ± 0.152	7.84 ± 4.21	
BPM 96441	3942 ± 71	M0.0	-0.01 ± 0.09	0.71 ± 0.09	4.58 ± 0.08	-0.982 ± 0.112	8.36 ± 4.04	
TYC 2710-691-1	3867 ± 71	K7.5	0.02 ± 0.09	0.65 ± 0.07	4.63 ± 0.06	-1.092 ± 0.094	9.78 ± 3.76	
TYC 2703-706-1	3822 ± 70	M0.5	0.17 ± 0.09	0.68 ± 0.06	4.61 ± 0.05	-1.084 ± 0.081	9.04 ± 3.93	
GJ 4196	3666 ± 68	M1.0	0.07 ± 0.10	0.56 ± 0.05	4.71 ± 0.04	-1.313 ± 0.082	9.53 ± 3.81	
GJ 832	3584 ± 68	M2.0	-0.11 ± 0.09	0.46 ± 0.05	4.45 ± 0.05	4.80 ± 0.05	-1.522 ± 0.099	8.08 ± 4.19
NLTT 52021	3687 ± 68	M2.0	-0.12 ± 0.09	0.50 ± 0.05	0.49 ± 0.05	4.77 ± 0.04	-1.400 ± 0.086	8.52 ± 4.02
GJ 846	3863 ± 69	M0.0	-0.07 ± 0.09	0.62 ± 0.07	0.60 ± 0.06	4.67 ± 0.06	-1.141 ± 0.097	8.44 ± 4.06
LHS 3746	3323 ± 68	M3.5	-0.18 ± 0.09	0.16 ± 0.13	0.19 ± 0.11	5.07 ± 0.12	-2.416 ± 0.528	
GJ 849	3476 ± 68	M3.5	0.17 ± 0.09	0.49 ± 0.07	0.48 ± 0.06	4.77 ± 0.06	-1.517 ± 0.120	8.13 ± 4.19
NLTT 53166	3868 ± 69	K7.5	-0.10 ± 0.09	0.61 ± 0.07	0.59 ± 0.06	4.67 ± 0.06	-1.149 ± 0.099	8.09 ± 4.13
GJ 1265	3346 ± 68	M4.0	-0.20 ± 0.09	0.19 ± 0.12	0.21 ± 0.10	5.04 ± 0.11	-2.290 ± 0.425	
LHS 3799	3489 ± 68	M4.0	0.21 ± 0.09	0.52 ± 0.07	0.51 ± 0.06	4.75 ± 0.06	-1.468 ± 0.110	
2MASSJ22 [*]	3895 ± 71	K7.5	-0.16 ± 0.09	0.61 ± 0.08	0.60 ± 0.07	4.67 ± 0.07	-1.135 ± 0.110	8.97 ± 3.91
GJ 9793	3892 ± 68	M0.0	-0.03 ± 0.09	0.66 ± 0.07	0.64 ± 0.07	4.63 ± 0.06	-1.076 ± 0.099	9.76 ± 3.77
GJ 873	3396 ± 70	M4.0	0.11 ± 0.10	0.38 ± 0.10	0.39 ± 0.09	4.87 ± 0.09	-1.752 ± 0.203	7.66 ± 4.22
GJ 876	3356 ± 69	M4.0	0.07 ± 0.09	0.31 ± 0.11	0.32 ± 0.10	4.93 ± 0.10	-1.928 ± 0.274	7.72 ± 4.23
GJ 877	3434 ± 68	M3.0	-0.05 ± 0.09	0.37 ± 0.08	0.37 ± 0.07	4.88 ± 0.07	-1.769 ± 0.178	8.14 ± 4.15
GJ 4306	3769 ± 68	M1.0	-0.14 ± 0.09	0.53 ± 0.05	0.52 ± 0.05	4.74 ± 0.05	-1.312 ± 0.088	8.34 ± 4.06
GJ 880	3741 ± 68	M1.5	0.02 ± 0.09	0.58 ± 0.05	0.56 ± 0.05	4.70 ± 0.04	-1.256 ± 0.080	8.35 ± 4.05
GJ 884 [†]	3832 ± 69	M0.0	0.64 ± 0.10	0.62 ± 0.10	4.66 ± 0.15	-1.129 ± 0.144		
GJ 887	3712 ± 68	M1.0	-0.17 ± 0.09	0.49 ± 0.05	0.48 ± 0.05	4.77 ± 0.04	-1.399 ± 0.088	8.04 ± 4.13
GJ 891	3575 ± 68	M2.0	-0.20 ± 0.09	0.42 ± 0.05	0.41 ± 0.05	4.83 ± 0.05	-1.599 ± 0.108	7.74 ± 4.28
LHS 543	3339 ± 69	M4.0	0.16 ± 0.09	0.32 ± 0.12	0.33 ± 0.11	4.93 ± 0.11	-1.918 ± 0.285	7.96 ± 4.16
GJ 895	3754 ± 68	M1.0	-0.11 ± 0.09	0.54 ± 0.05	0.52 ± 0.05	4.74 ± 0.04	-1.312 ± 0.086	8.38 ± 4.05
GJ 908	3553 ± 68	M1.5	-0.29 ± 0.09	0.37 ± 0.06	0.37 ± 0.05	4.88 ± 0.05	-1.703 ± 0.125	8.29 ± 4.10
LTT 9759	3578 ± 68	M2.5	0.11 ± 0.09	0.54 ± 0.05	0.52 ± 0.05	4.73 ± 0.05	-1.394 ± 0.088	8.26 ± 4.08
GJ 911	3887 ± 69	K7.5	-0.04 ± 0.09	0.65 ± 0.07	0.63 ± 0.07	4.64 ± 0.06	-1.089 ± 0.100	8.40 ± 4.07

Notes. * 2MASS J22353504+3712131; [†] evolutionary parameters computed from photometry.

Table A.2. Kinematic data for the observed stars.

Star	π (mas)	μ_α (mas yr $^{-1}$)	μ_δ (mas yr $^{-1}$)	V_{rad} (km s $^{-1}$)	U (km s $^{-1}$)	V (km s $^{-1}$)	W (km s $^{-1}$)	Notes
GJ 2	86.9567 ± 0.0407	870.753 ± 0.057	-151.267 ± 0.036	-0.23 ± 0.0013	-38.96 ± 0.02	-23.28 ± 0.01	-16.18 ± 0.01	D
Gl 1	230.1331 ± 0.0600	5633.374 ± 0.170	-2334.794 ± 0.075	25.53 ± 0.0030	-74.51 ± 0.02	-97.38 ± 0.03	-37.35 ± 0.00	TD
GJ 1002	206.2134 ± 0.1281	-811.480 ± 0.206	-1892.905 ± 0.125	-33.70 ± 3.8000	38.14 ± 0.07	-39.17 ± 1.44	19.72 ± 3.52	D
GJ 3014	51.9505 ± 0.0270	250.623 ± 0.051	184.890 ± 0.048	-15.61 ± 0.0028	-11.69 ± 0.01	-29.24 ± 0.01	7.72 ± 0.01	D
Gl 12	81.8711 ± 0.0866	618.003 ± 0.163	329.319 ± 0.139	51.21 ± 0.0036	-51.03 ± 0.04	26.66 ± 0.01	-30.85 ± 0.01	TR
GJ 16	59.5952 ± 0.0950	2.385 ± 0.185	-29.318 ± 0.084	-15.10 ± 0.4000	4.04 ± 0.08	-10.41 ± 0.23	10.43 ± 0.31	D
GJ 15A	280.6902 ± 0.0429	2891.525 ± 0.061	411.903 ± 0.034	11.82 ± 0.007	-49.15 ± 0.01	-12.04 ± 0.00	-3.45 ± 0.00	D
GJ 15B	280.7866 ± 0.0519	2863.284 ± 0.069	336.529 ± 0.039	11.00 ± 0.007	-48.04 ± 0.01	-12.78 ± 0.00	-4.31 ± 0.00	D
GJ 1009	55.3900 ± 0.0379	63.303 ± 0.073	-193.889 ± 0.058	16.93 ± 0.2100	56.64 ± 0.03	-17.22 ± 0.01	-16.22 ± 0.21	D
GJ 21	61.8444 ± 0.0250	-136.999 ± 0.045	-146.205 ± 0.038	-2.97 ± 0.0019	10.74 ± 0.01	4.50 ± 0.00	-10.44 ± 0.01	D
GJ 26	78.9551 ± 0.0355	1558.504 ± 0.076	26.829 ± 0.057	-0.50 ± 0.0010	-79.98 ± 0.04	-48.52 ± 0.02	-2.90 ± 0.00	D
GJ 27.1	42.3328 ± 0.0456	482.467 ± 0.107	-220.759 ± 0.102	12.32 ± 0.0019	-31.50 ± 0.04	-51.40 ± 0.06	-6.91 ± 0.01	D
LHS 1134	97.7275 ± 0.0819	-488.556 ± 0.068	-582.327 ± 0.098	-150.43 ± 52.8840	11.08 ± 8.21	18.00 ± 10.12	153.43 ± 51.25	H
Gl 47	95.0899 ± 0.0372	362.568 ± 0.049	-811.628 ± 0.051	7.57 ± 0.0017	-19.91 ± 0.01	-5.59 ± 0.01	-39.92 ± 0.02	D
Gl 49	101.4650 ± 0.0335	731.135 ± 0.041	90.690 ± 0.048	-5.97 ± 0.0011	-24.73 ± 0.01	-23.99 ± 0.01	5.77 ± 0.00	D
Gl 1030	44.9593 ± 0.0458	-108.209 ± 0.095	-251.270 ± 0.080	16.04 ± 0.2200	12.88 ± 0.10	-1.69 ± 0.12	30.34 ± 0.16	D
Gl 54.1	269.3628 ± 0.0785	1205.176 ± 0.170	637.758 ± 0.120	28.09 ± 0.1000	-28.23 ± 0.02	-0.36 ± 0.01	-23.83 ± 0.10	D
NLTT 4188	39.0922 ± 0.0418	379.482 ± 0.065	-199.286 ± 0.064	7.19 ± 0.4100	-42.63 ± 0.24	-23.19 ± 0.33	-19.94 ± 0.03	D
L 707-74	63.6479 ± 0.0497	-12.215 ± 0.096	331.305 ± 0.048	-0.79 ± 0.0035	-12.72 ± 0.01	20.08 ± 0.02	6.74 ± 0.01	D
Gl 70	88.3392 ± 0.0453	-422.187 ± 0.090	-765.210 ± 0.076	-25.90 ± 0.0016	47.80 ± 0.02	-23.80 ± 0.01	-4.37 ± 0.01	D
GJ 3117	57.7647 ± 0.0299	237.744 ± 0.037	-193.600 ± 0.043	-13.32 ± 0.4600	-9.35 ± 0.29	-24.33 ± 0.36	-11.46 ± 0.02	D
GJ 83.1	223.6349 ± 0.1066	1096.565 ± 0.171	-1772.865 ± 0.153	-28.31 ± 0.1920	13.13 ± 0.11	-50.74 ± 0.07	2.74 ± 0.14	D
Gl 3126	84.0271 ± 0.0588	-258.314 ± 0.118	-94.539 ± 0.109	-84.10 ± 0.0014	64.06 ± 0.01	-55.39 ± 0.01	-11.90 ± 0.01	TR
Gl 87	95.1619 ± 0.0413	-1762.475 ± 0.073	-1852.764 ± 0.067	-2.56 ± 0.0070	104.59 ± 0.05	-11.98 ± 0.01	-71.77 ± 0.03	TD
Gl 105B	138.4637 ± 0.0886	1801.837 ± 0.147	1449.914 ± 0.132	26.27 ± 0.0017	-77.01 ± 0.04	0.73 ± 0.01	32.06 ± 0.03	TR
LP 993-115	90.1616 ± 0.0554	31.859 ± 0.085	-387.965 ± 0.094	28.33 ± 0.0023	11.64 ± 0.01	-26.25 ± 0.01	-19.92 ± 0.00	D
Gl 3186	42.6652 ± 0.0407	5.450 ± 0.079	-231.392 ± 0.076	-11.54 ± 0.2600	12.38 ± 0.20	-21.35 ± 0.10	-13.62 ± 0.13	D
GJ 119A	49.2824 ± 0.0383	727.627 ± 0.076	-455.066 ± 0.085	76.20 ± 0.2500	-110.89 ± 0.20	-14.55 ± 0.17	-10.66 ± 0.02	TR
GJ 119B	49.2873 ± 0.0430	710.482 ± 0.082	-455.942 ± 0.102	70.50 ± 10.0000	-105.57 ± 7.66	-17.14 ± 6.41	-11.17 ± 0.56	TR
LHS 1481	86.8162 ± 0.1176	274.051 ± 0.114	539.370 ± 0.147	100.74 ± 0.0033	-80.05 ± 0.04	-1.06 ± 0.02	-69.51 ± 0.02	TD
LP 771-96	145.5466 ± 0.0800	-369.196 ± 0.140	-268.510 ± 0.147					
LHS 1513	44.3268 ± 0.0296	831.977 ± 0.042	-263.567 ± 0.058					
TYC 1795-941-1	27.6986 ± 0.2625	-22.339 ± 0.496	-83.748 ± 0.360	-22.18 ± 2.5300	21.74 ± 2.12	-14.99 ± 0.95	-3.86 ± 1.03	D
Gl 1057	116.1536 ± 0.0882	1741.859 ± 0.168	86.017 ± 0.151	26.00 ± 4.0000	-58.75 ± 2.91	-43.13 ± 0.24	20.75 ± 2.74	D
NLTT 10614								
Gl 145	91.1916 ± 0.0338	-311.440 ± 0.060	133.852 ± 0.068	22.80 ± 0.0016	-2.34 ± 0.00	1.15 ± 0.01	-28.70 ± 0.00	D
TYC 3720-426-1	27.8955 ± 0.0344	96.931 ± 0.068	-116.539 ± 0.055	-4.65 ± 0.5600	-10.32 ± 0.46	-23.32 ± 0.32	-5.91 ± 0.01	D
Gl 150.1B	58.0070 ± 0.0457	156.215 ± 0.089	-310.291 ± 0.064	34.67 ± 0.0020	-29.26 ± 0.00	-22.84 ± 0.02	-25.10 ± 0.01	D
Gl 1065	100.5599 ± 0.1050	-445.445 ± 0.152	-1371.117 ± 0.153					
Gl 156	63.7059 ± 0.0468	-5.687 ± 0.081	527.290 ± 0.073	62.65 ± 0.0017	-66.86 ± 0.02	15.60 ± 0.02	-27.40 ± 0.01	TR
GJ 156.1	44.4070 ± 0.0404	308.815 ± 0.085	-394.748 ± 0.062	-20.83 ± 0.0404	-9.73 ± 0.04	-55.49 ± 0.05	-11.06 ± 0.01	D
GJ 162	71.8130 ± 0.0431	526.942 ± 0.103	125.977 ± 0.046	34.94 ± 0.0013	-44.75 ± 0.01	-6.77 ± 0.01	21.24 ± 0.02	D
GJ 1068	140.5559 ± 0.0354	-825.179 ± 0.068	-2415.606 ± 0.087	27.00 ± 0.5000	83.41 ± 0.05	-26.13 ± 0.35	-22.37 ± 0.35	TR

Table A.2. Continued.

Star	π (mas)	μ_α (mas yr $^{-1}$)	μ_δ (mas yr $^{-1}$)	V_{rad} (km s $^{-1}$)	U (km s $^{-1}$)	V (km s $^{-1}$)	W (km s $^{-1}$)	Notes
GJ 166C	199.4552 ± 0.3204	-2250.1118 ± 1.598	-3408.280 ± 0.551	-45.00 ± 5.0000	98.67 ± 3.68	-11.24 ± 1.40	-39.82 ± 3.08	TR
GJ 169	88.9622 ± 0.0494	-66.934 ± 0.109	174.500 ± 0.076	-35.44 ± 0.0010	33.30 ± 0.00	6.76 ± 0.01	14.16 ± 0.01	D
GJ 173	89.1708 ± 0.0313	-226.991 ± 0.040	-196.108 ± 0.029	-6.76 ± 0.0008	14.63 ± 0.00	2.89 ± 0.00	-8.81 ± 0.01	D
GJ 176	105.5627 ± 0.0700	656.378 ± 0.148	-1116.502 ± 0.056	26.24 ± 0.0007	-22.79 ± 0.00	-57.69 ± 0.04	-14.97 ± 0.01	D
GJ 179	80.9036 ± 0.0606	153.425 ± 0.109	-306.106 ± 0.063	-8.71 ± 0.0025	12.92 ± 0.01	-17.60 ± 0.02	1.30 ± 0.01	D
GJ 180	83.7182 ± 0.0313	408.571 ± 0.040	-644.464 ± 0.041	-14.48 ± 0.0010	31.40 ± 0.01	-29.42 ± 0.01	15.00 ± 0.00	D
GJ 1074	47.3755 ± 0.0461	502.452 ± 0.081	-336.742 ± 0.080	17.11 ± 0.0020	-36.75 ± 0.02	-46.83 ± 0.06	20.30 ± 0.02	D
LHS 1723	186.0231 ± 0.0590	-551.722 ± 0.099	-533.936 ± 0.083	42.31 ± 0.0809	-23.34 ± 0.06	-18.00 ± 0.03	-36.12 ± 0.04	D
LHS 1731	108.3263 ± 0.0500	-228.056 ± 0.070	-444.616 ± 0.077	15.47 ± 0.0020	5.12 ± 0.01	-14.23 ± 0.00	-22.11 ± 0.01	D
GJ 184	72.1506 ± 0.0357	1302.359 ± 0.067	-1537.773 ± 0.055	65.76 ± 0.0014	-113.33 ± 0.03	-93.64 ± 0.06	15.58 ± 0.01	TD
GJ 191	254.2263 ± 0.0263	6491.474 ± 0.049	-5709.218 ± 0.051	245.23 ± 0.0040	19.84 ± 0.01	-288.05 ± 0.01	-52.52 ± 0.01	H
GJ 203	97.9790 ± 0.0952	-191.297 ± 0.136	-756.774 ± 0.111	60.61 ± 0.0028	-44.32 ± 0.01	-38.77 ± 0.03	-40.41 ± 0.03	D
GJ 205	175.4287 ± 0.0672	761.548 ± 0.119	-2092.322 ± 0.097	8.63 ± 0.0030	22.10 ± 0.01	-55.68 ± 0.02	-10.29 ± 0.01	D
GJ 3352	40.4768 ± 0.0354	-52.645 ± 0.076	-221.563 ± 0.067	-72.42 ± 0.0354	57.42 ± 0.03	-41.26 ± 0.02	-30.93 ± 0.02	TR
GJ 3356	83.8543 ± 0.0685	-118.691 ± 0.116	-396.695 ± 0.093	37.70 ± 0.5000	-30.26 ± 0.48	-22.18 ± 0.10	-23.70 ± 0.09	D
GJ 208	87.4367 ± 0.0562	-2.752 ± 0.091	-56.648 ± 0.072	21.74 ± 0.0016	-19.77 ± 0.00	-7.57 ± 0.01	-5.82 ± 0.01	D
GJ 213	172.7068 ± 0.0788	1997.706 ± 0.132	-1569.794 ± 0.108	105.88 ± 0.0018	-90.06 ± 0.01	-88.87 ± 0.03	7.99 ± 0.01	TR
GJ 229	173.6955 ± 0.0457	-135.985 ± 0.104	-719.088 ± 0.152	4.73 ± 0.0003	11.85 ± 0.01	-11.80 ± 0.00	-11.90 ± 0.00	D
TYC 3379-1077-1	26.7747 ± 0.0526	-80.145 ± 0.079	-38.968 ± 0.070	28.47 ± 0.4300	-30.59 ± 0.41	7.20 ± 0.10	-8.48 ± 0.11	D
TYC 743-1836-1	39.8711 ± 0.0474	106.085 ± 0.082	-44.410 ± 0.072					
HIP 31293	113.1206 ± 0.0271	-297.958 ± 0.050	280.641 ± 0.060	12.03 ± 0.0009	-10.36 ± 0.00	-8.60 ± 0.00	-16.05 ± 0.00	D
HIP 31292	113.1455 ± 0.0346	-328.672 ± 0.066	262.955 ± 0.069	12.20 ± 0.0500	-9.85 ± 0.01	-7.98 ± 0.04	-17.30 ± 0.02	D
G 108-21	66.3502 ± 0.0702	42.036 ± 0.097	-258.753 ± 0.089	82.52 ± 0.0021	-63.80 ± 0.01	-55.22 ± 0.02	-6.39 ± 0.01	D
Gl 250B	114.4148 ± 0.0516	-576.233 ± 0.090	-13.262 ± 0.081	-7.25 ± 0.0007	0.05 ± 0.00	13.13 ± 0.01	-21.22 ± 0.01	D
Gl 272	58.9849 ± 0.0420	-120.604 ± 0.068	-237.972 ± 0.045	-31.71 ± 0.2400	20.51 ± 0.22	-19.17 ± 0.03	-26.02 ± 0.10	D
Gl 273	262.9800 ± 1.3900	572.510 ± 1.500	-3693.510 ± 0.960	18.22 ± 0.1000	16.03 ± 0.19	-65.76 ± 0.30	-17.04 ± 0.12	TR
Gl 1097	85.3378 ± 0.0694	439.654 ± 0.193	-788.976 ± 0.155	1.45 ± 0.0012	31.35 ± 0.03	-39.17 ± 0.04	1.30 ± 0.01	D
StKM 1-650	23.2642 ± 0.0540	31.746 ± 0.072	-160.216 ± 0.063	-18.64 ± 0.5500	2.17 ± 0.44	-37.65 ± 0.22	-5.70 ± 0.26	D
LHS 1935	95.8401 ± 0.0413	456.667 ± 0.047	-475.606 ± 0.063	-28.90 ± 0.0020	42.24 ± 0.01	7.13 ± 0.01	7.99 ± 0.00	D
Gl 285	167.0186 ± 0.0592	-348.103 ± 0.109	-445.878 ± 0.064	26.50 ± 0.0052	-19.67 ± 0.00	-22.57 ± 0.00	-7.99 ± 0.01	D
Gl 299	145.4757 ± 0.5695	1078.931 ± 1.697	-5096.181 ± 0.415	14.60 ± 0.0028	68.73 ± 0.34	-152.52 ± 0.58	-32.26 ± 0.19	TD
Gl 300	123.2204 ± 0.0667	13.695 ± 0.109	-694.016 ± 0.089	6.30 ± 0.9000	16.18 ± 0.43	-17.83 ± 0.79	-13.16 ± 0.11	D
Gl 2066	111.8419 ± 0.0534	-376.316 ± 0.087	60.397 ± 0.055	62.22 ± 0.0007	-53.52 ± 0.01	-34.57 ± 0.00	8.55 ± 0.01	D
Gl 317	65.7744 ± 0.0557	-461.162 ± 0.139	805.571 ± 0.126	87.73 ± 0.1170	-94.41 ± 0.07	-51.56 ± 0.11	24.51 ± 0.03	TR
NLT T 21156		-154.900 ± 2.300	-233.200 ± 2.200	8.90 ± 0.6800				
Gl 1123	105.1290 ± 0.0444	636.467 ± 0.087	-806.638 ± 0.103	0.00 ± 0.5000	42.52 ± 0.18	18.32 ± 0.44	-1.73 ± 0.17	D
Gl 341	95.6279 ± 0.0284	-840.114 ± 0.056	182.090 ± 0.062	40.12 ± 0.0006	-29.06 ± 0.01	-42.26 ± 0.00	-28.20 ± 0.01	D
Gl 1125	100.9992 ± 0.0746	-568.699 ± 0.116	-549.788 ± 0.105	46.21 ± 0.0017	-29.59 ± 0.01	-51.25 ± 0.02	-3.47 ± 0.02	D
Gl 357	105.8830 ± 0.0569	138.694 ± 0.100	-990.311 ± 0.083	-34.56 ± 0.0010	41.09 ± 0.02	11.24 ± 0.01	-37.20 ± 0.01	TR
Gl 358	104.1538 ± 0.0387	-527.203 ± 0.062	356.825 ± 0.064	18.53 ± 0.0008	-29.20 ± 0.01	-18.14 ± 0.00	-1.12 ± 0.00	D
Gl 361	86.5522 ± 0.0430	-660.061 ± 0.077	-143.226 ± 0.076	11.50 ± 0.0009	-30.54 ± 0.01	-15.36 ± 0.01	-18.23 ± 0.01	D
Gl 367	106.2112 ± 0.0317	-462.549 ± 0.056	-582.814 ± 0.058	47.74 ± 0.0006	3.26 ± 0.00	-50.69 ± 0.00	-28.31 ± 0.01	D
Gl 1129	90.8249 ± 0.0849	-1599.951 ± 0.139	-171.719 ± 0.163	9.00 ± 0.5000	-60.21 ± 0.14	-20.15 ± 0.43	-55.71 ± 0.23	TR
Gl 382	129.7887 ± 0.0838	-152.931 ± 0.100	-243.598 ± 0.113	7.95 ± 0.0005	-2.49 ± 0.00	-12.71 ± 0.01	-2.44 ± 0.01	D

Table A.2. Continued.

Star	π (mas)	μ_α (mas yr $^{-1}$)	μ_δ (mas yr $^{-1}$)	V_{rad} (km s $^{-1}$)	U (km s $^{-1}$)	V (km s $^{-1}$)	W (km s $^{-1}$)	Notes
GJ 388	201.3683 ± 0.0679	-498.605 ± 0.119	-43.683 ± 0.103	12.44 ± 0.0006	-15.00 ± 0.00	-7.50 ± 0.00	3.52 ± 0.00	D
GJ 390	78.0003 ± 0.0982	-693.137 ± 0.176	121.370 ± 0.222	21.61 ± 0.007	-43.07 ± 0.06	-20.49 ± 0.01	-4.64 ± 0.03	D
GJ 393	142.1885 ± 0.0499	-603.003 ± 0.084	-732.075 ± 0.070	8.35 ± 0.005	-7.37 ± 0.00	-28.01 ± 0.01	-15.20 ± 0.01	D
GJ 399	64.1884 ± 0.0863	-718.366 ± 0.146	-105.176 ± 0.095	3.25 ± 0.019	-41.17 ± 0.06	-20.63 ± 0.03	-27.66 ± 0.04	D
LHS 288	206.8172 ± 0.0735	-346.435 ± 0.168	1610.336 ± 0.243	-	-	-	-	
GJ 402	143.4971 ± 0.0626	-856.291 ± 0.106	-818.845 ± 0.095	-1.10 ± 0.0020	-11.43 ± 0.01	-29.30 ± 0.01	-23.32 ± 0.01	D
GJ 406	413.1300 ± 1.2700	-3808.090 ± 0.300	-2692.610 ± 0.420	19.32 ± 0.1450	-27.94 ± 0.08	-47.63 ± 0.14	-13.70 ± 0.15	D
GJ 408	148.1283 ± 0.0569	-426.924 ± 0.080	-282.411 ± 0.078	3.16 ± 0.013	-9.39 ± 0.00	-13.23 ± 0.01	-3.87 ± 0.00	D
GJ 410	83.7765 ± 0.0573	142.849 ± 0.080	-51.955 ± 0.071	-13.90 ± 0.0013	12.71 ± 0.01	3.52 ± 0.00	-9.66 ± 0.00	D
GJ 411	392.6400 ± 0.6700	-580.270 ± 0.620	-4765.850 ± 0.640	-84.69 ± 0.1000	46.15 ± 0.05	-53.69 ± 0.10	-74.30 ± 0.09	TD
GJ 412A	206.2700 ± 1.0000	-4410.430 ± 0.780	942.930 ± 0.700	68.75 ± 0.0220	-123.19 ± 0.46	-5.34 ± 0.06	16.33 ± 0.22	TR
GJ 413.1	92.7821 ± 0.0538	-797.369 ± 0.090	-446.773 ± 0.073	-3.83 ± 0.0006	-24.16 ± 0.02	-20.08 ± 0.01	-34.77 ± 0.02	D
GJ 414B	84.1971 ± 0.0579	604.831 ± 0.081	-206.442 ± 0.075	-16.11 ± 0.3600	39.31 ± 0.13	2.27 ± 0.04	-1.88 ± 0.33	D
GJ 3649	59.9389 ± 0.0527	-21.025 ± 0.108	6.518 ± 0.095	31.80 ± 0.7300	-10.42 ± 0.20	-9.68 ± 0.22	28.50 ± 0.67	D
GJ 433	110.2908 ± 0.0444	-70.768 ± 0.053	-850.679 ± 0.034	17.99 ± 0.0006	17.11 ± 0.01	-29.01 ± 0.01	-23.14 ± 0.01	D
GJ 436	102.5015 ± 0.0936	895.047 ± 0.128	-814.030 ± 0.123	9.61 ± 0.010	50.07 ± 0.05	-18.57 ± 0.02	19.27 ± 0.01	D
GJ 438	90.7992 ± 0.0353	654.541 ± 0.044	-539.649 ± 0.040	3.21 ± 0.2600	39.72 ± 0.10	9.64 ± 0.24	-17.35 ± 0.04	D
GJ 447	296.3073 ± 0.0699	607.678 ± 0.137	-1223.323 ± 0.078	-31.07 ± 0.0009	17.94 ± 0.00	5.04 ± 0.00	-33.10 ± 0.00	D
GJ 450	114.1376 ± 0.0390	-273.164 ± 0.057	253.364 ± 0.047	0.27 ± 0.0014	-14.28 ± 0.01	4.70 ± 0.00	-3.67 ± 0.00	D
GJ 3708	78.3453 ± 0.0578	-213.094 ± 0.111	-184.359 ± 0.083	-9.09 ± 0.0015	-8.85 ± 0.01	-5.73 ± 0.01	-16.19 ± 0.01	D
GJ 9404	41.8403 ± 0.0441	-647.719 ± 0.069	79.007 ± 0.058	-0.83 ± 0.2200	-67.79 ± 0.08	-27.74 ± 0.03	-10.08 ± 0.22	D
GJ 465	112.7372 ± 0.0669	1095.877 ± 0.101	-2309.278 ± 0.125	51.19 ± 0.0014	94.83 ± 0.05	-66.09 ± 0.02	-28.51 ± 0.04	TR
GJ 476	55.0431 ± 0.0459	-449.276 ± 0.086	-319.343 ± 0.069	33.27 ± 0.017	-15.70 ± 0.02	-51.69 ± 0.04	21.03 ± 0.01	D
GJ 479	105.5122 ± 0.0645	-1034.452 ± 0.076	29.718 ± 0.053	-5.64 ± 0.0007	-42.65 ± 0.03	-19.23 ± 0.02	-2.20 ± 0.00	D
LHS 337	149.8423 ± 0.0755	-665.083 ± 0.146	-1312.565 ± 0.114	-	-	-	-	
GJ 480.1	124.2526 ± 0.1039	-782.177 ± 0.145	689.869 ± 0.285	-35.29 ± 0.0023	-47.91 ± 0.03	19.77 ± 0.01	11.94 ± 0.03	D
GJ 486	123.8215 ± 0.0623	-1008.602 ± 0.138	-459.800 ± 0.079	19.11 ± 0.0018	-20.60 ± 0.01	-39.84 ± 0.02	12.45 ± 0.00	D
GJ 488	93.8820 ± 0.0508	-29.855 ± 0.107	-397.051 ± 0.061	5.03 ± 0.011	9.63 ± 0.01	-17.67 ± 0.01	-4.94 ± 0.01	D
GJ 494	86.8570 ± 0.1515	-632.151 ± 0.502	-36.019 ± 0.187	-11.23 ± 0.1100	-29.46 ± 0.07	-18.71 ± 0.06	-10.10 ± 0.11	D
GJ 9440	59.3075 ± 0.0328	-298.530 ± 0.044	-142.685 ± 0.045	-11.70 ± 0.0017	-12.65 ± 0.01	-24.82 ± 0.01	-7.76 ± 0.00	D
GJ 514	131.2428 ± 0.0543	1127.507 ± 0.102	-1073.879 ± 0.066	14.56 ± 0.0007	57.40 ± 0.02	-8.20 ± 0.00	-3.57 ± 0.01	D
GJ 521A	74.8051 ± 0.0257	-42.466 ± 0.034	389.084 ± 0.038	-65.35 ± 0.0015	-13.79 ± 0.01	-7.64 ± 0.01	-68.10 ± 0.00	TR
GJ 526	183.9836 ± 0.0509	1776.019 ± 0.094	-1455.184 ± 0.065	15.81 ± 0.0030	61.15 ± 0.02	-1.83 ± 0.00	-2.67 ± 0.01	D
GJ 3804	89.2264 ± 0.0781	-307.301 ± 0.132	-552.535 ± 0.120	4.97 ± 0.1000	-0.01 ± 0.06	-31.04 ± 0.05	-13.76 ± 0.07	D
GJ 536	96.0398 ± 0.0872	-825.424 ± 0.154	598.112 ± 0.180	-25.90 ± 0.0006	-56.41 ± 0.04	2.09 ± 0.01	4.03 ± 0.03	D
GJ 3822	49.1748 ± 0.0521	98.758 ± 0.080	-140.545 ± 0.064	-8.08 ± 0.0015	11.90 ± 0.02	-4.30 ± 0.01	-13.39 ± 0.01	D
GJ 548A	61.1783 ± 0.0542	792.548 ± 0.092	-1116.601 ± 0.111	8.78 ± 0.2100	101.85 ± 0.11	-22.29 ± 0.04	-21.56 ± 0.20	TR
GJ 552	70.1774 ± 0.0505	-1054.730 ± 0.093	1299.485 ± 0.105	7.85 ± 0.0017	-98.17 ± 0.08	20.15 ± 0.02	52.92 ± 0.03	TD
GJ 551	768.5004 ± 0.2030	-3781.306 ± 0.085	769.766 ± 0.189	-22.40 ± 0.5000	-29.57 ± 0.35	1.99 ± 0.36	13.79 ± 0.02	D
GJ 553.1	92.0697 ± 0.1046	-407.965 ± 0.136	-398.937 ± 0.137	-1.76 ± 0.1000	-7.79 ± 0.07	-27.73 ± 0.04	-6.03 ± 0.07	D
GJ 555	160.1141 ± 0.1135	-355.037 ± 0.180	593.220 ± 0.180	-1.43 ± 0.0012	-13.85 ± 0.01	5.88 ± 0.01	13.95 ± 0.01	D
GJ 9492	91.7062 ± 0.2434	-337.591 ± 0.365	25.182 ± 0.503	18.80 ± 0.0017	-15.59 ± 0.05	1.17 ± 0.04	20.38 ± 0.03	D
GJ 569A	100.6811 ± 0.0528	279.340 ± 0.080	-117.959 ± 0.095	-7.22 ± 0.0009	7.90 ± 0.01	3.51 ± 0.01	13.46 ± 0.00	D
GJ 570B	168.7700 ± 21.5400	961.780 ± 20.680	-1677.830 ± 16.080	25.90 ± 2.0000	46.13 ± 3.79	-22.20 ± 2.12	-31.64 ± 6.06	D

Table A.2. Continued.

Star	π (mas)	μ_α (mas yr $^{-1}$)	μ_δ (mas yr $^{-1}$)	V_{rad} (km s $^{-1}$)	U (km s $^{-1}$)	V (km s $^{-1}$)	W (km s $^{-1}$)	Notes
GJ 581	158.7492 ± 0.0523	-1221.467 ± 0.093	-97.129 ± 0.079	-9.42 ± 0.0007	-25.07 ± 0.01	-25.65 ± 0.01	11.89 ± 0.01	D
GJ 588	169.0074 ± 0.0580	-1176.658 ± 0.109	-1030.896 ± 0.073	21.46 ± 0.0003	-0.67 ± 0.01	-48.84 ± 0.01	0.59 ± 0.00	D
GJ 606	75.2306 ± 0.0513	202.554 ± 0.114	-25.528 ± 0.060	-17.13 ± 0.010	-8.91 ± 0.01	6.58 ± 0.01	-18.34 ± 0.01	D
GJ 3942	59.0421 ± 0.0219	203.934 ± 0.045	61.990 ± 0.045	-19.37 ± 0.4800	-0.60 ± 0.05	-1.32 ± 0.33	-25.81 ± 0.34	D
GJ 618A	117.3560 ± 0.0598	-747.687 ± 0.143	988.207 ± 0.114	27.98 ± 0.0007	21.19 ± 0.00	0.76 ± 0.01	53.28 ± 0.03	TR
GJ 625	154.4710 ± 0.0273	432.073 ± 0.064	-171.668 ± 0.059	-13.06 ± 0.014	7.85 ± 0.00	-2.55 ± 0.00	-17.49 ± 0.00	D
GJ 628	232.2095 ± 0.0630	-94.027 ± 0.130	-1183.784 ± 0.080	-21.22 ± 0.0004	-122.92 ± 0.00	-21.13 ± 0.01	-20.60 ± 0.00	D
GJ 643	153.9189 ± 0.1310	-816.944 ± 0.415	-898.327 ± 0.154	15.84 ± 0.0018	19.54 ± 0.01	-33.83 ± 0.04	11.09 ± 0.02	D
GJ 649	96.3141 ± 0.0311	-115.479 ± 0.041	-507.887 ± 0.047	4.34 ± 0.0012	21.61 ± 0.01	-14.41 ± 0.01	1.28 ± 0.00	D
GJ 3997	73.1060 ± 0.0336	-150.004 ± 0.035	14.034 ± 0.043	-45.75 ± 0.2300	-16.88 ± 0.18	-48.61 ± 0.11	-21.86 ± 0.10	D
GJ 3998	55.0799 ± 0.0497	-137.311 ± 0.141	-347.315 ± 0.105	-31.00 ± 0.9000	-23.85 ± 0.71	-28.50 ± 0.40	1.39 ± 0.38	D
GJ 2128	66.1437 ± 0.0402	-278.769 ± 0.072	-67.201 ± 0.061	-215.545 ± 0.082	6.37 ± 0.007	9.49 ± 0.00	15.06 ± 0.01	TR
GJ 667C	138.0171 ± 0.0918	1131.612 ± 0.110	-829.843 ± 0.068	-19.52 ± 0.018	40.45 ± 0.02	-21.11 ± 0.00	-35.91 ± 0.03	D
GJ 671	81.7581 ± 0.0397	283.832 ± 0.071	-880.251 ± 0.068	-2.90 ± 0.004	-7.78 ± 0.00	-7.23 ± 0.00	-29.75 ± 0.01	D
GJ 674	219.8012 ± 0.0487	572.582 ± 0.102	-249.210 ± 0.069	-12.46 ± 0.0006	-3.40 ± 0.00	-13.25 ± 0.01	-20.21 ± 0.01	D
GJ 678.1A	98.8491 ± 0.0403	29.836 ± 0.076	-74.415 ± 0.106	470.338 ± 0.070	-22.94 ± 0.0007	-14.17 ± 0.00	25.76 ± 0.01	D
GJ 680	103.3500 ± 0.0545	-320.636 ± 0.074	-514.400 ± 0.063	-14.89 ± 0.0013	35.74 ± 0.02	-3.36 ± 0.01	-21.65 ± 0.01	D
GJ 685	69.8254 ± 0.0392	-706.117 ± 0.185	-1269.528 ± 0.071	-28.76 ± 0.0007	30.55 ± 0.00	-25.42 ± 0.00	-6.72 ± 0.00	D
GJ 687	219.7807 ± 0.0324	-937.912 ± 0.124	-9.51 ± 0.0010	-34.87 ± 0.0007	-40.05 ± 0.00	-18.61 ± 0.01	6.49 ± 0.00	D
GJ 682	199.7031 ± 0.0832	926.741 ± 0.050	984.697 ± 0.071	-2.25 ± 0.01	33.45 ± 0.01	35.51 ± 0.01	-21.13 ± 0.01	TR
GJ 686	122.5609 ± 0.0346	-19.501 ± 0.053	33.122 ± 0.056	4.16 ± 0.0149	-55.62 ± 0.01	3.11 ± 0.01	4.23 ± 0.01	D
GJ 694.2	46.5683 ± 0.0280	-1117.143 ± 0.327	-1353.816 ± 0.233	-42.94 ± 0.0008	-27.26 ± 0.04	20.15 ± 0.02	D	D
GJ 693	169.8613 ± 0.1184	-802.803 ± 0.638	10362.542 ± 0.360	-110.35 ± 0.0030	-141.11 ± 0.03	4.96 ± 0.04	18.47 ± 0.03	TR
GJ 699	547.4506 ± 0.2899	569.729 ± 0.096	-332.464 ± 0.082	32.69 ± 0.0005	33.07 ± 0.00	14.31 ± 0.00	-18.82 ± 0.01	D
GJ 701	129.3922 ± 0.0613	-618.435 ± 0.136	-347.100 ± 0.109	-34.80 ± 1.7000	-28.87 ± 1.65	-30.53 ± 0.40	12.74 ± 0.06	D
GJ 1224	125.5872 ± 0.0705	-40.230 ± 0.030	-448.534 ± 0.046	-0.40 ± 0.3300	39.23 ± 0.19	-25.16 ± 0.25	-14.32 ± 0.09	D
GJ 4057	43.7891 ± 0.0272	452.186 ± 0.049	363.668 ± 0.056	-31.51 ± 0.0013	-39.64 ± 0.01	-10.10 ± 0.01	-33.95 ± 0.01	D
GJ 720A	91.4293 ± 0.0709	-31.056 ± 0.107	354.209 ± 0.111	-34.14 ± 0.0033	-36.16 ± 0.01	-13.32 ± 0.01	4.55 ± 0.01	D
GJ 725A	283.9489 ± 0.0624	-1311.907 ± 0.181	1792.185 ± 0.217	-0.77 ± 0.0008	-24.49 ± 0.01	-11.88 ± 0.00	25.19 ± 0.01	D
GJ 725B	283.8624 ± 0.1065	-1400.023 ± 0.317	1862.407 ± 0.385	1.10 ± 0.0008	-25.30 ± 0.01	-10.86 ± 0.01	27.51 ± 0.01	D
GJ 729	336.1228 ± 0.0641	639.348 ± 0.127	-193.550 ± 0.105	-10.49 ± 0.0015	-12.02 ± 0.00	-1.00 ± 0.00	-7.30 ± 0.00	D
GJ 731	65.7639 ± 0.0459	-226.071 ± 0.077	-481.639 ± 0.086	-14.52 ± 0.0016	18.81 ± 0.02	-36.35 ± 0.02	-2.55 ± 0.01	D
GJ 740	90.0477 ± 0.0490	-196.301 ± 0.087	-1220.467 ± 0.092	10.43 ± 0.0006	47.34 ± 0.02	-41.31 ± 0.03	-19.89 ± 0.01	D
GJ 4092	35.4261 ± 0.0408	366.183 ± 0.080	-181.171 ± 0.081	-82.98 ± 0.0013	-61.82 ± 0.01	-52.65 ± 0.01	-57.28 ± 0.07	TR
GJ 1232	97.4518 ± 0.1596	-641.446 ± 0.687	-424.538 ± 0.474	-14.01 ± 0.0036	15.61 ± 0.06	-32.47 ± 0.05	17.27 ± 0.06	D
GJ 752A	169.1590 ± 0.0520	-579.043 ± 0.088	-1332.743 ± 0.081	35.88 ± 0.0004	53.48 ± 0.01	-7.78 ± 0.01	-5.00 ± 0.00	D
GJ 754	169.0921 ± 0.2165	659.330 ± 0.687	-2897.035 ± 0.332	16.00 ± 0.5000	-10.95 ± 0.45	-72.79 ± 0.12	-42.14 ± 0.21	TR
GJ 1236	94.1932 ± 0.0657	-740.028 ± 0.110	-444.907 ± 0.094	24.39 ± 0.0032	44.15 ± 0.02	-9.90 ± 0.02	20.89 ± 0.02	D
GJ 9689	32.6292 ± 0.0443	421.921 ± 0.057	19.177 ± 0.051	-68.36 ± 0.5600	-72.88 ± 0.32	-42.78 ± 0.45	-36.01 ± 0.13	TR
GJ 793	123.7545 ± 0.0219	443.220 ± 0.045	283.443 ± 0.043	10.58 ± 0.0014	-20.24 ± 0.00	9.01 ± 0.00	-5.23 ± 0.00	D
GJ 1256	104.8892 ± 0.0851	1321.004 ± 0.098	662.235 ± 0.110	-59.00 ± 5.0000	-83.46 ± 2.40	-27.51 ± 4.17	-14.81 ± 1.36	D
GJ 803	102.8295 ± 0.0486	281.424 ± 0.075	359.895 ± 0.054	-4.50 ± 0.2500	-10.02 ± 0.20	-16.06 ± 0.04	-10.26 ± 0.15	D
LHS 3583	93.7195 ± 0.0348	539.696 ± 0.068	-544.152 ± 0.067	970.06 ± 7.1111	518.69 ± 4.04	-643.71 ± 4.58	-509.03 ± 3.65	H

Table A.2. Continued.

Star	π (mas)	μ_α (mas yr $^{-1}$)	μ_δ (mas yr $^{-1}$)	V_{rad} (km s $^{-1}$)	U (km s $^{-1}$)	V (km s $^{-1}$)	W (km s $^{-1}$)	Notes
LP 816-60	178.1243 ± 0.0849	-309.217 ± 0.152	37.345 ± 0.097	16.31 ± 0.0017	16.62 ± 0.00	7.22 ± 0.00	-2.54 ± 0.01	D
GJ 821	84.7044 ± 0.0685	714.800 ± 0.1033	-1995.206 ± 0.064	-58.26 ± 0.0014	-26.54 ± 0.01	-125.61 ± 0.08	-31.30 ± 0.06	TD
BPM 96441	24.6435 ± 0.0349	-6.805 ± 0.050	-115.461 ± 0.057	5.29 ± 0.3000	17.44 ± 0.07	-1.51 ± 0.29	-14.72 ± 0.07	D
TYC 2710-691-1	21.9300 ± 0.5900	53.459 ± 1.620	-29.716 ± 1.893	-22.502 ± 0.089	-22.47 ± 0.8100	-9.37 ± 0.17	-22.79 ± 0.77	D
TYC 2703-706-1	26.7573 ± 0.0428	59.566 ± 0.084	-182.442 ± 0.217	-67.36 ± 0.3300	30.71 ± 0.12	-69.21 ± 0.32	22.42 ± 0.08	TR
GJ 4196	38.4522 ± 0.1050	-280.038 ± 0.142	-816.604 ± 0.064	13.16 ± 0.0003	8.90 ± 0.00	-20.66 ± 0.00	-6.15 ± 0.00	D
GJ 832	201.4073 ± 0.0429	-45.834 ± 0.071	-655.215 ± 0.045	-28.09 ± 0.2300	58.72 ± 0.04	-31.79 ± 0.23	-40.37 ± 0.04	TR
NLTT 52021	43.6391 ± 0.0296	-140.668 ± 0.048	-452.430 ± 0.124	-278.582 ± 0.137	18.38 ± 0.0006	31.50 ± 0.04	5.34 ± 0.01	D
GJ 846	94.7419 ± 0.1406	-246.000 ± 29.000	-246.000 ± 29.000	-22.125 ± 0.083	-15.28 ± 0.0007	-43.39 ± 0.02	-17.44 ± 0.01	D
LHS 3746	134.2900 ± 1.3100	814.000 ± 8.000	113.534 ± 0.081	232.713 ± 0.059	8.63 ± 0.5400	2.99 ± 0.03	16.15 ± 0.53	32.41 ± 0.12
GJ 849	113.6000 ± 0.0463	856.890 ± 0.118	-306.305 ± 0.108	24.00 ± 0.5000	-16.91 ± 0.24	-11.66 ± 0.19	-45.95 ± 0.40	D
NLTT 53166	42.1720 ± 0.0361	-210.821 ± 0.047	-718.314 ± 0.232	308.26 ± 116.4120	136.10 ± 51.24	91.95 ± 43.94	-262.23 ± 94.84	TR
GJ 1265	97.5087 ± 0.0711	308.434 ± 0.227	47.111 ± 0.076	5.34 ± 0.3000	-1.13 ± 0.03	8.37 ± 0.28	8.57 ± 0.10	H
LHS 3799	138.1782 ± 0.2484	-26.606 ± 0.053	95.464 ± 0.916	-16.17 ± 0.3300	-40.95 ± 0.88	-15.76 ± 0.29	0.43 ± 0.30	D
2MASS J22*	23.7791 ± 0.0509	256.835 ± 1.005	-458.775 ± 0.063	0.29 ± 0.0017	19.76 ± 0.00	3.60 ± 0.00	-1.71 ± 0.00	D
GJ 9793	31.8454 ± 0.6551	-706.152 ± 0.069	-673.638 ± 0.102	-1.60 ± 0.0005	-12.33 ± 0.01	-19.69 ± 0.01	-11.69 ± 0.01	D
GJ 873	198.0112 ± 0.0380	957.961 ± 0.117	-1059.318 ± 0.053	65.86 ± 0.0007	67.03 ± 0.01	-58.64 ± 0.01	3.63 ± 0.01	TR
GJ 876	213.8669 ± 0.0758	-1026.327 ± 0.053	-110.175 ± 0.064	-32.44 ± 0.2800	1.89 ± 0.01	-31.12 ± 0.22	12.75 ± 0.17	D
GJ 877	116.4127 ± 0.0291	24.678 ± 0.072	-283.998 ± 0.058	-27.33 ± 0.0005	32.49 ± 0.01	-16.63 ± 0.00	25.21 ± 0.00	D
GJ 4306	59.0165 ± 0.0581	-1034.803 ± 0.070	58.166 ± 0.071	15.98 ± 0.0018	34.85 ± 0.01	16.90 ± 0.01	0.47 ± 0.01	D
GJ 880	121.4918 ± 0.0507	-902.348 ± 0.101	1330.388 ± 0.076	8.82 ± 0.0020	-93.60 ± 0.01	-13.44 ± 0.00	-51.78 ± 0.01	TR
GJ 884	304.2190 ± 0.0451	6765.995 ± 0.071	715.742 ± 0.090	6.59 ± 0.0015	-46.59 ± 0.04	16.21 ± 0.01	-13.04 ± 0.02	D
GJ 887	67.0946 ± 0.0516	-1382.460 ± 0.106	-6.51 ± 0.0024	57.63 ± 0.06	-33.19 ± 0.03	-33.71 ± 0.04	TR	
GJ 891	94.6489 ± 0.0913	-536.693 ± 0.219	-281.952 ± 0.045	-33.19 ± 0.0012	21.31 ± 0.01	-28.11 ± 0.00	-13.61 ± 0.01	D
LHS 543	75.5654 ± 0.0333	-61.707 ± 0.048	-968.648 ± 0.054	-71.13 ± 0.0004	-8.81 ± 0.01	-70.14 ± 0.01	39.61 ± 0.01	TR
GJ 895	169.3585 ± 0.0595	992.665 ± 0.109	-379.249 ± 0.047	-9.01 ± 0.0008	-11.65 ± 0.00	-11.94 ± 0.01	16.45 ± 0.00	D
GJ 908	98.8631 ± 0.0279	243.926 ± 0.049	-127.221 ± 0.070	-1.90 ± 0.2400	-2.73 ± 0.04	14.10 ± 0.05	4.32 ± 0.23	D
LTT 9759	42.6784 ± 0.0532	-41.996 ± 0.100						
GJ 911								

Notes. * 2MASS J22353504+3712131; D: Thin disk, TD: Thick disk, TR: Thick disk, H: Halo

Table A.3. Planet host stars in the sample, along with the planetary properties.

Star	Planet	P (days)	a (au)	eccentricity	$m \sin i^\dagger$ (M_\oplus)
GJ 15A	b	11.4407	0.072	0.094	3.03
GJ 15A	c	7600	5.4	0.27	36
GJ 27.1	b	15.819	0.101	0.08	13
GJ 49	b	13.8508	0.0905	0.363	5.63
GJ 54.1	b	1.96876	0.01557	0	0.75
GJ 54.1	c	3.06008	0.0209	0.04	0.98
GJ 54.1	d	4.65627	0.02764	0.129	1.14
LP 771-96	b	5.35882	0.03807	0.19	2.2 [†]
GJ 176	b	8.7836	0.066	0	8.4
GJ 179	b	2288	2.41	0.21	260.61
GJ 180	b	17.133	0.092	0.07	6.49
GJ 180	c	24.329	0.129	0.09	6.4
GJ 180	d	106.3	0.309	0.14	7.56
LHS 1723	b	5.3636	0.03282	0.23	2.02
LHS 1723	c	40.54	0.1246	0.17	2.31
GJ 191	b	121.54	0.311	0.23	7
GJ 229	b	526.115	0.898	0.1	8.478
GJ 229	c	121.995	0.339	0.19	7.268
GJ 273	b	18.6498	0.091101	0.1	2.89
GJ 273	c	4.7234	0.036467	0.17	1.18
GJ 317	b	692	1.15	0.11	572.07
GJ 317	c	5312		0.308	489
GJ 357	b	3.93072	0.035		1.84 [†]
GJ 357	c	9.1247	0.061		3.4
GJ 357	d	55.661	0.204		6.1
GJ 411	b	12.9532	0.0785	0.22	2.99
GJ 433	b	7.3705	0.062	0.04	6.043
GJ 433	c	5094.105	4.819	0.12	32.422
GJ 433	d	36.059	0.178	0.07	5.223
GJ 436	b	2.64388312	0.0291	0.13827	22.1
GJ 447	b	9.8658	0.0496	0.116	1.4
GJ 494	b				1997.59 [†]
GJ 536	b	8.7076	0.06661	0.08	5.36
GJ 551	b	11.186	0.0485	<0.35	1.27
GJ 581	b	5.3686	0.04061	0	15.8
GJ 581	c	12.914	0.0721	0	5.5
GJ 581	d	3.149	0.02815	0	1.7
GJ 3942	b	6.905	0.0608	0.121	7.14
GJ 625	b	14.628	0.078361	0.13	2.82
GJ 628	b	4.8869	0.0375	0.15	1.91
GJ 628	c	17.8719	0.089	0.11	3.41
GJ 628	d	217.21	0.47	0.55	7.7
GJ 649	b	598.3	1.135	0.3	104.244
GJ 3998	b	2.64977	0.029	0	2.47
GJ 3998	c	13.74	0.089	0.049	6.26
GJ 667C	b	7.2004	0.0505	0.13	5.6
GJ 667C	c	28.14	0.125	0.02	3.8
GJ 667C	d	62.24	0.213	0.02	2.7
GJ 667C	e	39.026	0.156	0.03	2.7
GJ 667C	f	256.2	0.549	0.08	4.6
GJ 674	b	4.6938	0.039	0.2	11.09
GJ 685	b	24.16	0.1344	0	9
GJ 687	b	38.14	0.17	0.04	19
GJ 682	b	14.748	0.08	0.08	4.4
GJ 682	c	57.32	0.176	0.1	8.7
GJ 686	b	15.5314	0.0917	0.077	6.64
GJ 752A	b	105.9	0.3357	0.16	12.2
GJ 832	b	3657	3.56	0.08	216
GJ 832	c	35.68	0.163	0.18	5.4
GJ 849	b	1882	2.35	0.04	318

Table A.3. Continued.

Star	Planet	P (days)	a (au)	eccentricity	$m \sin i^\dagger$ (M_\oplus)
GJ 1265	b	3.6511	0.026	0.04	7.4
Gl 876	b	61.1166	0.208317	0.0324	723.2235 [†]
Gl 876	c	30.0881	0.12959	0.25591	226.9846 [†]
Gl 876	d	1.93778	0.02080665	0.207	6.83 [†]
Gl 876	e	124.26	0.3343	0.055	14.6 [†]

Notes. [†] True mass

Table A.4. Derived abundances, [X/H] (dex), for the M stars analyzed in this work.

Star	[Fe/H]	[C/H]	[Na/H]	[Mg/H]	[Al/H]	[Si/H]	[Ca/H]	[Sc/H]	[Ti/H]	[V/H]	[Cr/H]	[Mn/H]	[Co/H]	[Ni/H]	[Zn/H]
GJ 2	-0.12	-0.02	-0.05	-0.43	0.03	-0.01	-0.21	-0.31	-0.03	0.09	-0.05	-0.09	0.10	-0.08	-0.27
GJ 1	-0.33	-0.38	-0.12	-0.44	-0.07	-0.36	-0.27	-0.63	0.01	0.20	-0.26	-0.59	-0.29	-0.51	-0.74
GJ 1002	-0.01	-0.07	-0.33	0.01	-0.28	0.23	-0.04	0.32	-0.19	0.05	-0.02	0.24	0.03	0.27	0.64
GJ 3014	-0.36	0.01	-0.29	-0.51	-0.02	-0.01	-0.26	-0.28	-0.21	-0.10	-0.24	-0.22	0.08	-0.07	-0.50
GJ 12	0.07	0.00	-0.04	-0.22	-0.11	0.10	-0.14	-0.03	-0.04	0.10	-0.05	-0.06	0.10	0.03	-0.14
GJ 16	-0.01	0.01	0.03	-0.33	0.15	0.04	-0.25	-0.25	0.03	0.10	-0.01	0.04	0.26	-0.04	-0.19
GJ 15A	-0.34	-0.48	-0.06	-0.69	-0.18	-0.29	-0.20	-0.73	-0.03	0.17	-0.17	-0.53	-0.22	-0.45	-0.58
GJ 15B	-0.30	-0.33	-0.27	-0.47	-0.31	-0.08	-0.11	-0.32	-0.17	0.04	-0.26	-0.29	-0.10	-0.17	-0.28
GJ 1009	0.20	0.20	0.20	-0.07	0.22	0.17	-0.11	0.01	0.12	0.22	0.08	0.13	0.24	0.11	-0.12
GJ 21	-0.02	0.09	-0.17	-0.47	-0.06	0.05	-0.23	-0.21	-0.12	-0.02	-0.04	-0.06	0.11	0.00	-0.27
GJ 26	-0.22	-0.15	-0.05	-0.39	0.09	-0.09	-0.24	-0.36	-0.01	0.09	-0.19	-0.22	0.12	-0.20	-0.46
GJ 27.1	-0.03	-0.05	0.02	-0.29	0.04	-0.03	-0.16	-0.25	0.02	0.17	-0.07	-0.17	0.01	-0.12	-0.38
LHS 1134	0.01	-0.16	-0.09	-0.06	-0.02	0.03	-0.16	0.00	-0.05	0.12	0.00	0.00	0.03	-0.02	0.13
GJ 47	-0.15	-0.13	-0.13	-0.45	-0.07	-0.06	-0.23	-0.33	-0.08	0.03	-0.16	-0.21	0.08	-0.16	-0.41
GJ 49	0.06	0.23	-0.03	-0.27	0.13	0.16	-0.19	-0.05	-0.04	0.03	0.02	0.13	0.28	0.13	-0.15
GJ 1030	-0.10	0.12	0.02	-0.27	0.20	0.09	-0.16	-0.15	0.02	0.09	-0.07	0.03	0.24	0.03	-0.26
GJ 54.1	-0.04	-0.18	-0.26	-0.22	-0.27	-0.05	-0.08	-0.13	-0.10	0.11	-0.08	-0.17	-0.10	-0.10	-0.02
NLT T 4188	-0.73	-0.29	-0.54	-0.87	-0.42	-0.22	-0.19	-0.56	-0.36	-0.11	-0.33	-0.63	-0.43	-0.28	-0.59
L 707-74	0.12	-0.10	0.03	-0.19	-0.05	0.05	-0.17	-0.12	0.01	0.16	0.01	-0.04	0.10	-0.05	-0.10
GJ 70	-0.03	-0.13	-0.08	-0.33	0.08	-0.06	-0.29	-0.32	-0.02	0.07	-0.11	-0.08	0.20	-0.17	-0.32
GJ 3117	-0.02	0.07	-0.01	-0.27	0.16	0.06	-0.27	-0.16	0.00	0.08	-0.06	0.01	0.27	-0.02	-0.25
GJ 83.1	0.24	0.00	-0.15	-0.14	-0.11	0.09	-0.14	-0.14	0.02	-0.10	0.06	0.08	0.03	0.11	0.04
GJ 3126	0.09	0.01	0.00	-0.10	0.26	0.11	-0.27	-0.05	-0.04	0.02	0.00	0.15	0.36	0.03	-0.10
GJ 87	-0.49	-0.54	-0.21	-0.44	-0.05	-0.55	-0.39	-0.81	-0.01	0.18	-0.30	-0.71	-0.43	-0.69	-0.77
GJ 105B	-0.07	-0.14	-0.05	-0.12	0.01	0.00	-0.12	-0.06	-0.01	0.18	-0.06	-0.10	-0.02	-0.06	-0.05
LP 993-115	0.24	0.06	0.06	-0.14	0.06	0.05	-0.12	-0.07	0.02	0.14	0.11	0.09	0.12	-0.04	-0.22
GJ 3186	-0.15	-0.26	0.22	-0.33	0.23	-0.15	-0.34	-0.55	0.25	0.39	0.10	-0.03	0.13	-0.27	0.08
GJ 119A	-0.35	0.02	0.11	-0.31	0.22	-0.04	-0.06	-0.31	0.16	0.27	-0.16	-0.15	0.04	-0.11	-0.34
GJ 119B	-0.23	0.15	0.04	-0.21	0.26	0.06	-0.12	-0.10	0.06	0.13	-0.20	-0.11	0.19	-0.01	-0.47
LHS 1481	-0.26	-0.36	-0.16	-0.51	-0.40	-0.15	-0.15	-0.43	-0.09	0.15	-0.21	-0.45	-0.24	-0.27	-0.37
LP 771-96	0.06	-0.13	-0.06	-0.21	-0.08	-0.01	-0.23	-0.16	-0.03	0.13	-0.01	-0.08	0.04	-0.09	-0.09
LHS 1513	-0.10	-0.14	-0.05	-0.19	-0.02	-0.04	-0.13	-0.15	0.00	0.17	-0.12	-0.19	-0.04	-0.12	-0.23
TYC 1795-941-1	0.04	0.09	-0.18	-0.42	-0.10	0.27	-0.15	0.07	-0.15	0.04	0.22	0.25	0.12	0.27	0.54
GJ 1057	-0.10	-0.15	-0.10	-0.02	-0.01	0.05	0.01	0.06	-0.04	0.16	-0.04	-0.01	-0.07	0.03	0.17
NLT T 10614	-0.04	0.06	0.04	-0.33	0.13	0.06	-0.19	-0.22	0.04	0.11	0.00	0.03	0.22	-0.01	-0.15
GJ 1065	0.15	0.01	-0.01	-0.17	-0.02	0.04	-0.21	-0.09	0.00	0.13	0.02	-0.05	0.03	0.10	-0.14
GJ 145	0.17	0.26	-0.25	-0.44	0.00	0.11	-0.10	-0.10	-0.19	-0.07	0.20	0.00	0.08	0.09	-0.14
GJ 150.1B	-0.12	0.12	-0.07	-0.39	0.01	0.09	-0.15	-0.06	0.03	-0.11	-0.07	0.12	0.04	-0.34	-0.34
GJ 156	0.18	0.15	0.38	-0.01	0.33	0.30	0.09	0.10	0.25	0.37	0.10	0.29	0.32	0.21	0.15
GJ 156.1	-0.14	-0.03	0.02	-0.23	-0.28	-0.03	-0.26	-0.28	0.06	0.14	-0.04	0.02	0.18	-0.10	-0.17
GJ 162	-0.29	-0.11	-0.05	-0.59	-0.07	-0.05	-0.10	-0.42	-0.03	0.12	-0.14	-0.27	-0.03	-0.14	-0.41
GJ 1068	-0.01	-0.14	-0.23	-0.12	-0.24	0.09	-0.11	0.06	-0.12	0.11	-0.03	0.07	-0.02	0.08	0.32
GJ 166C	0.35	-0.07	0.04	-0.17	0.12	-0.10	-0.11	-0.27	0.04	0.19	0.16	-0.18	0.04	-0.22	-0.35

Table A.4. Continued.

Star	[Fe/H]	[C/H]	[Na/H]	[Mg/H]	[Al/H]	[Si/H]	[Ca/H]	[Sc/H]	[Ti/H]	[V/H]	[Cr/H]	[Mn/H]	[Co/H]	[Ni/H]	[Zn/H]
GJ 169	0.28	0.00	0.14	0.24	0.35	0.17	-0.21	0.11	0.17	0.31	0.53	0.32	0.16	0.72	
GJ 173	0.00	-0.08	-0.01	-0.22	0.06	-0.09	-0.29	0.03	0.18	-0.02	-0.14	-0.01	-0.18	-0.27	
GJ 176	0.10	0.12	0.05	-0.11	0.12	0.06	-0.16	-0.06	0.04	0.13	0.00	0.00	0.14	0.00	-0.22
GJ 179	0.10	0.04	0.06	-0.06	0.16	0.09	-0.17	0.00	0.03	0.16	0.05	0.04	0.15	0.03	-0.05
GJ 180	-0.16	-0.29	-0.08	-0.33	-0.04	-0.24	-0.30	-0.47	-0.01	0.18	-0.10	-0.34	-0.16	-0.35	-0.41
GJ 1074	-0.35	-0.11	-0.15	-0.58	-0.10	-0.05	-0.13	-0.39	-0.10	0.07	-0.15	-0.27	-0.09	-0.13	-0.37
LHS 1723	-0.09	-0.18	-0.19	-0.24	-0.19	-0.06	-0.12	-0.17	-0.07	0.14	-0.10	-0.21	-0.10	-0.13	-0.12
LHS 1731	0.05	-0.10	-0.01	-0.16	-0.03	0.01	-0.18	-0.12	0.01	0.16	-0.01	-0.06	0.04	-0.06	-0.08
GJ 184	-1.08	-0.69	-0.44	-0.98	-0.35	-0.60	-0.14	-1.02	-0.18	0.09	-0.65	-1.14	-0.70	-0.76	-1.24
GJ 191	-0.77	-0.82	-0.44	-1.07	-0.66	-0.53	-0.15	-1.01	-0.25	0.08	-0.66	-1.19	-0.65	-0.77	-1.33
GJ 203	-0.05	-0.10	-0.09	-0.22	-0.11	0.02	-0.15	-0.09	-0.05	0.12	-0.08	-0.14	-0.01	-0.05	-0.14
GJ 205	0.43	0.32	0.36	0.11	0.40	0.30	-0.06	0.16	0.22	0.28	0.21	0.42	0.45	0.25	0.11
GJ 3352	-0.46	-0.36	-0.20	-0.48	0.01	-0.18	-0.29	-0.54	-0.11	0.07	-0.14	-0.24	-0.09	-0.27	-0.20
GJ 3356	0.03	0.04	0.05	-0.13	0.09	0.07	-0.13	-0.04	0.04	0.17	-0.02	-0.05	0.10	0.00	-0.17
GJ 208	0.27	0.15	0.02	-0.18	0.10	0.14	-0.11	-0.01	0.01	0.09	0.05	0.09	0.23	0.07	-0.16
GJ 213	-0.36	-0.31	-0.17	-0.23	-0.14	-0.15	-0.08	-0.23	-0.04	0.19	-0.23	-0.35	-0.24	-0.22	-0.21
GJ 229	-0.08	-0.11	0.04	-0.18	0.08	-0.10	-0.20	-0.30	0.08	0.23	0.00	-0.11	-0.06	-0.17	-0.15
TYC 3379-1077-1	-0.26	0.23	-0.09	-0.40	-0.04	0.29	0.15	0.07	-0.12	0.02	-0.07	0.05	0.07	0.29	-0.05
TYC 743-1836-1	-0.06	0.11	0.16	-0.35	0.03	0.16	0.01	-0.14	0.14	0.35	0.24	0.15	0.00	0.15	0.37
HIP 31293	0.20	0.11	0.02	-0.09	0.08	0.12	-0.20	0.03	0.01	0.12	0.06	0.07	0.18	0.06	-0.07
HIP 31292	0.20	0.11	0.02	-0.09	0.08	0.12	-0.20	0.03	0.01	0.12	0.06	0.07	0.18	0.06	-0.07
G 108-21	-0.04	0.03	0.04	-0.18	0.06	0.05	-0.15	0.05	-0.07	0.05	0.19	-0.09	-0.12	0.07	-0.03
GJ 250B	0.07	0.02	-0.01	-0.19	0.04	-0.01	-0.26	-0.17	0.02	0.16	0.00	-0.07	0.06	-0.08	-0.22
GJ 272	-0.30	-0.06	-0.18	-0.43	0.00	-0.01	-0.20	-0.30	-0.12	0.03	-0.10	-0.11	0.01	-0.06	-0.22
GJ 273	-0.12	-0.15	-0.09	-0.16	-0.01	-0.06	-0.17	-0.14	-0.01	0.17	-0.09	-0.17	-0.06	-0.13	-0.14
GJ 1097	0.14	-0.01	0.09	-0.09	0.15	0.05	-0.22	-0.09	0.06	0.19	0.06	0.04	0.15	-0.03	-0.09
StKM 1-650	-0.21	0.13	-0.03	-0.33	0.07	0.21	0.03	-0.03	-0.07	0.07	0.04	0.12	0.09	0.21	0.10
LHS 1935	0.13	-0.13	-0.02	-0.14	0.01	-0.01	-0.27	-0.15	0.00	0.15	0.04	-0.01	0.09	-0.09	-0.03
GJ 285	0.78	0.13	0.27	-0.26	0.32	-0.23	-0.02	-0.54	0.19	0.25	0.39	-0.41	0.10	-0.43	-1.00
GJ 299	-0.16	-0.32	-0.27	-0.25	-0.31	-0.06	-0.19	-0.16	-0.12	0.12	-0.15	-0.17	-0.12	-0.12	0.08
GJ 300	0.07	-0.05	0.12	-0.02	0.20	0.09	-0.07	0.01	0.06	0.21	0.05	0.04	0.12	0.02	0.01
GJ 2066	-0.31	-0.18	-0.08	-0.32	-0.06	-0.21	-0.20	-0.40	0.02	0.20	-0.20	-0.40	-0.21	-0.30	-0.48
GJ 317	-0.07	0.05	0.09	-0.05	0.18	0.06	-0.08	-0.01	0.09	0.21	-0.04	-0.05	0.07	0.00	-0.15
NLT T 21156	-0.12	0.28	-0.20	-0.37	0.00	0.13	-0.13	-0.04	-0.16	-0.11	-0.16	-0.11	0.20	0.09	-0.49
GJ 1123	0.00	-0.01	-0.01	0.03	0.09	0.13	-0.01	0.15	-0.01	0.14	0.00	0.05	0.05	0.10	0.11
GJ 341	-0.20	-0.16	-0.08	-0.42	-0.08	-0.11	-0.15	-0.37	-0.03	0.15	-0.18	-0.35	-0.13	-0.22	-0.53
GJ 1125	0.03	0.01	-0.01	-0.16	-0.01	0.07	-0.15	-0.04	0.00	0.15	-0.04	-0.06	0.07	0.00	-0.14
GJ 357	-0.11	-0.30	-0.05	-0.28	-0.03	-0.18	-0.32	-0.41	-0.01	0.17	-0.05	-0.27	-0.09	-0.29	-0.27
GJ 358	0.26	0.11	0.08	-0.12	0.12	0.05	-0.18	-0.09	0.07	0.18	0.09	-0.01	0.15	-0.03	-0.23
GJ 361	-0.03	-0.02	-0.07	-0.27	-0.01	-0.07	-0.26	-0.24	-0.01	0.13	-0.07	-0.18	-0.02	-0.14	-0.35
GJ 367	0.13	0.08	0.13	-0.12	0.15	0.07	-0.15	-0.09	0.09	0.20	0.01	0.16	-0.01	-0.01	-0.22
GJ 1129	0.09	-0.06	0.06	-0.04	0.13	0.08	-0.15	0.00	0.03	0.18	0.04	0.05	0.12	0.01	0.04
GJ 382	0.29	0.18	0.15	-0.04	0.21	0.13	-0.19	0.00	0.10	0.18	0.11	0.17	0.27	0.07	-0.09
GJ 388	0.50	0.16	0.13	-0.24	0.17	-0.08	-0.14	-0.31	0.10	0.18	0.19	-0.21	0.14	-0.21	-0.66
GJ 390	-0.01	0.00	0.04	-0.23	0.07	0.07	-0.02	-0.18	-0.04	0.20	-0.05	-0.12	0.02	-0.10	-0.31

Table A.4. Continued.

Star	[Fe/H]	[C/H]	[Na/H]	[Mg/H]	[Al/H]	[Si/H]	[Ca/H]	[Sc/H]	[Ti/H]	[V/H]	[Cr/H]	[Mn/H]	[Co/H]	[Ni/H]	[Zn/H]
GJ 393	-0.12	-0.14	-0.10	-0.28	-0.05	-0.17	-0.28	-0.34	0.00	0.16	-0.10	-0.27	-0.12	-0.24	-0.35
GJ 399	0.01	0.16	0.08	-0.20	0.26	0.17	-0.17	-0.03	0.02	0.05	-0.08	0.10	0.41	0.09	-0.27
LHS 288	-0.28	-0.21	-0.56	-0.18	-0.63	0.15	-0.01	0.23	-0.26	0.05	-0.26	0.02	-0.14	0.19	0.58
GJ 402	0.23	0.04	0.10	0.02	0.19	0.17	-0.13	0.10	0.03	0.15	0.11	0.19	0.24	0.11	0.12
GJ 406	0.24	-0.05	-0.15	-0.20	-0.01	-0.25	0.15	-0.36	-0.03	0.18	0.18	-0.45	-0.27	-0.33	-0.52
GJ 408	-0.02	-0.01	-0.07	-0.29	0.03	0.05	-0.21	-0.15	-0.03	0.04	-0.11	-0.04	0.22	-0.03	-0.25
GJ 410	0.21	0.10	-0.03	-0.24	0.05	0.04	-0.20	-0.15	-0.02	0.07	0.01	-0.05	0.14	-0.05	-0.36
GJ 411	-0.27	-0.49	-0.21	-0.46	0.04	-0.32	-0.41	-0.64	-0.10	-0.01	-0.26	-0.40	0.01	-0.49	-0.63
GJ 412A	-0.78	-0.67	-0.25	-0.97	-0.44	-0.43	-0.04	-0.93	-0.15	0.13	-0.45	-0.96	-0.57	-0.62	-0.98
GJ 413.1	0.12	0.03	0.06	-0.16	0.11	0.02	-0.22	-0.14	0.05	0.17	0.02	-0.02	0.11	-0.06	-0.22
GJ 414B	0.23	0.25	0.23	-0.07	0.39	0.21	-0.20	0.00	0.16	0.17	0.13	0.33	0.49	0.15	0.02
GJ 3649	-0.29	-0.06	0.01	-0.45	0.05	-0.03	-0.12	-0.36	0.03	0.17	-0.12	-0.19	0.03	-0.12	-0.36
GJ 433	-0.06	-0.07	-0.02	-0.28	0.01	-0.08	-0.22	-0.29	0.02	0.17	-0.07	-0.21	-0.04	-0.17	-0.37
GJ 436	0.19	0.14	0.04	-0.11	0.13	0.10	-0.22	0.00	0.03	0.12	0.03	0.05	0.20	0.04	-0.17
GJ 438	-0.16	-0.32	-0.09	-0.46	-0.11	-0.22	-0.25	-0.52	-0.04	0.15	-0.15	-0.42	-0.17	-0.36	-0.57
GJ 447	-0.08	-0.26	-0.16	-0.11	-0.08	-0.04	-0.18	-0.11	-0.07	0.14	-0.05	-0.06	-0.05	-0.09	0.12
GJ 450	-0.06	-0.07	-0.13	-0.51	-0.10	-0.08	-0.26	-0.38	-0.06	0.05	-0.07	-0.20	0.04	-0.17	-0.37
GJ 3708	0.02	-0.09	0.00	-0.17	0.04	-0.04	-0.23	-0.19	0.02	0.18	0.00	-0.11	0.01	-0.12	-0.16
GJ 9404	0.16	0.21	0.37	-0.07	0.35	0.30	0.01	0.03	0.24	0.36	0.34	0.49	0.34	0.29	0.56
GJ 465	-0.36	-0.42	-0.17	-0.56	-0.30	-0.29	-0.22	-0.58	-0.06	0.18	-0.29	-0.60	-0.31	-0.43	-0.63
GJ 476	-0.50	-0.16	-0.11	-0.43	0.13	-0.22	-0.25	-0.48	0.00	0.11	-0.36	-0.44	-0.03	-0.33	-0.75
GJ 479	0.26	0.10	0.08	-0.07	0.16	0.08	-0.23	-0.04	0.05	0.16	0.11	0.09	0.21	0.01	-0.09
LHS 337	-0.18	-0.27	-0.19	-0.18	-0.19	-0.03	-0.09	-0.08	-0.08	0.15	-0.13	-0.15	-0.14	-0.08	0.08
GJ 480.1	0.06	-0.21	-0.08	-0.22	-0.14	-0.01	-0.22	-0.18	-0.06	0.13	-0.01	-0.06	0.03	-0.10	-0.02
GJ 486	0.01	-0.03	-0.01	-0.09	0.08	0.04	-0.15	-0.03	0.00	0.15	-0.01	-0.04	0.05	-0.02	-0.07
GJ 488	0.31	0.12	0.34	0.00	0.35	0.28	-0.01	0.05	0.20	0.32	0.19	0.37	0.35	0.19	0.20
GJ 494	0.44	0.09	0.13	-0.23	0.20	-0.05	-0.20	-0.33	0.10	0.21	0.21	-0.09	0.14	-0.18	-0.46
GJ 9440	0.30	0.37	0.31	0.00	0.41	0.36	-0.08	0.16	0.17	0.18	0.20	0.50	0.56	0.32	0.20
GJ 514	-0.23	-0.20	-0.14	-0.39	-0.10	-0.19	-0.24	-0.42	-0.04	0.13	-0.17	-0.37	-0.19	-0.28	-0.48
GJ 521A	-0.46	-0.49	-0.22	-0.45	0.12	-0.42	-0.41	-0.74	-0.06	0.07	-0.31	-0.49	-0.12	-0.57	-0.70
GJ 526	-0.20	-0.23	-0.03	-0.34	0.07	-0.23	-0.25	-0.47	0.04	0.19	-0.20	-0.40	-0.12	-0.36	-0.65
GJ 3804	0.00	-0.06	-0.05	-0.11	0.05	0.02	-0.21	-0.06	-0.02	0.14	0.00	-0.05	0.03	-0.04	-0.05
GJ 536	-0.26	-0.32	-0.15	-0.33	0.00	-0.30	-0.35	-0.54	-0.02	0.16	-0.15	-0.39	-0.21	-0.41	-0.46
GJ 3822	0.06	0.25	0.09	-0.23	0.16	0.25	-0.05	0.01	0.03	0.13	0.14	0.27	0.26	0.24	0.15
GJ 548A	0.37	0.34	0.48	0.01	0.41	0.41	0.07	0.16	0.31	0.39	0.42	0.63	0.46	0.39	0.64
GJ 552	0.05	0.16	0.10	-0.18	0.26	0.12	-0.16	-0.08	0.07	0.10	-0.03	0.10	0.34	0.05	-0.24
GJ 551	0.05	-0.13	-0.23	-0.03	-0.09	-0.01	0.01	0.01	-0.10	0.12	0.07	-0.05	-0.13	-0.02	0.20
GJ 553.1	0.10	-0.05	0.04	-0.08	0.12	0.05	-0.18	-0.06	0.03	0.17	0.05	0.01	0.10	-0.03	-0.04
GJ 555	0.12	-0.02	0.11	0.01	0.22	0.11	-0.10	0.05	0.05	0.19	0.08	0.09	0.14	0.04	0.06
GJ 9492	-0.28	-0.03	-0.26	-0.50	-0.14	0.02	-0.11	-0.20	-0.23	-0.12	-0.27	-0.30	0.02	-0.06	-0.59
GJ 569A	0.18	0.04	-0.05	-0.26	0.04	-0.09	-0.27	-0.29	0.00	0.12	0.04	-0.19	0.03	-0.19	-0.45
GJ 570B	-0.15	-0.07	-0.02	-0.28	-0.01	-0.07	-0.15	-0.27	0.03	0.20	-0.11	-0.22	-0.09	-0.15	-0.34
GJ 581	0.07	-0.10	-0.02	-0.18	0.00	-0.01	-0.23	-0.16	0.00	0.16	0.01	-0.07	0.05	-0.09	-0.12
GJ 588	0.12	0.09	0.13	0.01	0.22	0.05	-0.17	-0.04	0.11	0.20	0.07	0.08	0.16	0.00	-0.06
GJ 606	-0.09	0.03	-0.20	-0.40	-0.02	0.01	-0.29	-0.22	-0.13	-0.05	-0.08	-0.07	0.15	-0.05	-0.27

Table A.4. Continued.

Star	[Fe/H]	[C/H]	[Na/H]	[Mg/H]	[Al/H]	[Si/H]	[Ca/H]	[Sc/H]	[Ti/H]	[V/H]	[Cr/H]	[Mn/H]	[Co/H]	[Ni/H]	[Zn/H]
GJ 3942	0.16	0.21	-0.03	-0.29	0.07	0.21	-0.14	0.00	-0.05	0.04	0.15	0.24	0.25	0.19	0.11
GJ 618A	0.11	0.04	0.09	-0.10	0.12	0.07	-0.16	-0.05	0.06	0.18	0.04	0.02	0.13	0.00	-0.12
GJ 625	-0.19	-0.40	-0.06	-0.60	-0.18	-0.16	-0.20	-0.57	-0.05	0.11	-0.15	-0.34	-0.03	-0.31	-0.43
GJ 628	-0.03	-0.20	-0.02	-0.10	0.07	-0.06	-0.21	-0.17	0.02	0.19	-0.01	-0.08	-0.01	-0.14	-0.03
GJ 643	-0.03	-0.17	-0.09	-0.19	-0.10	0.00	-0.16	-0.12	-0.04	0.15	-0.05	-0.10	-0.02	-0.07	-0.03
GJ 649	-0.23	-0.09	-0.13	-0.51	-0.10	-0.08	-0.17	-0.39	-0.07	0.10	-0.10	-0.25	-0.10	-0.15	-0.37
GJ 3997	-0.39	-0.52	-0.21	-0.84	-0.29	-0.26	-0.16	-0.73	-0.17	0.05	-0.23	-0.58	-0.26	-0.43	-0.66
GJ 3998	0.04	-0.03	0.05	-0.29	0.18	0.05	-0.25	-0.25	0.03	0.10	0.03	0.09	0.27	-0.04	-0.11
GJ 2128	-0.23	-0.16	-0.17	-0.39	0.01	-0.08	-0.28	-0.33	-0.10	-0.01	-0.18	-0.20	0.09	-0.18	-0.38
GJ 667C	-0.07	-0.29	-0.07	-0.41	-0.12	-0.11	-0.25	-0.39	-0.04	0.16	-0.10	-0.27	-0.07	-0.25	-0.34
GJ 671	-0.49	-0.44	-0.20	-0.55	-0.07	-0.27	-0.32	-0.61	-0.08	0.08	-0.31	-0.46	-0.07	-0.41	-0.55
GJ 674	0.05	-0.09	-0.09	-0.22	-0.06	-0.08	-0.28	-0.23	-0.02	0.13	0.00	-0.14	-0.02	-0.15	-0.19
GJ 678.1A	-0.27	-0.36	-0.15	-0.43	-0.08	-0.24	-0.24	-0.52	-0.07	0.13	-0.17	-0.41	-0.22	-0.36	-0.49
GJ 680	0.08	-0.09	0.00	-0.20	0.06	-0.05	-0.28	-0.25	0.01	0.15	0.00	-0.09	0.06	-0.15	-0.24
GJ 685	-0.07	0.12	-0.21	-0.38	-0.04	0.08	-0.16	-0.12	-0.15	-0.04	-0.03	0.00	0.07	0.06	-0.17
GJ 687	0.05	0.01	-0.03	-0.13	0.22	0.06	-0.24	-0.07	-0.02	0.05	-0.06	0.06	0.26	-0.02	-0.20
GJ 682	0.20	-0.03	0.13	0.04	0.25	0.13	-0.13	0.05	0.05	0.18	0.12	0.17	0.22	0.06	0.11
GJ 686	-0.30	-0.30	-0.22	-0.59	-0.17	-0.20	-0.14	-0.52	-0.15	0.01	-0.23	-0.44	-0.19	-0.31	-0.64
GJ 694.2	0.02	0.07	0.13	-0.35	0.11	0.17	-0.03	-0.14	0.05	0.16	0.10	0.12	0.19	0.11	0.01
GJ 693	-0.10	-0.30	-0.14	-0.22	-0.09	-0.15	-0.30	-0.31	-0.05	0.13	-0.07	-0.19	-0.08	-0.24	-0.11
GJ 699	-0.28	-0.58	-0.30	-0.36	-0.22	-0.14	-0.29	-0.38	-0.15	0.04	-0.31	-0.20	0.07	-0.28	-0.10
GJ 701	-0.31	-0.24	-0.20	-0.45	-0.19	-0.23	-0.22	-0.46	-0.08	0.11	-0.23	-0.47	-0.27	-0.32	-0.57
GJ 1224	0.28	-0.10	-0.11	-0.24	-0.04	-0.13	-0.13	-0.31	-0.04	0.13	0.11	-0.24	-0.02	-0.24	-0.36
GJ 4057	0.02	0.03	0.15	-0.41	0.07	0.16	-0.02	-0.18	0.07	0.21	0.14	0.10	0.15	0.09	0.08
GJ 720A	-0.17	-0.21	-0.06	-0.42	0.06	-0.12	-0.26	-0.43	0.01	0.17	0.02	-0.11	-0.04	-0.20	-0.07
GJ 141-29	0.40	-0.08	0.03	-0.22	0.12	-0.17	-0.19	-0.38	0.03	0.16	0.19	-0.26	0.05	-0.31	-0.50
GJ 725A	-0.21	-0.23	-0.11	-0.33	0.05	-0.12	-0.22	-0.33	-0.04	0.06	-0.23	-0.25	0.07	-0.24	-0.45
GJ 725B	-0.24	-0.35	-0.14	-0.36	-0.03	-0.12	-0.20	-0.34	-0.06	0.09	-0.26	-0.26	0.05	-0.25	-0.37
GJ 729	0.06	-0.25	-0.16	-0.30	-0.20	-0.21	-0.18	-0.41	-0.04	0.13	-0.02	-0.32	-0.11	-0.31	-0.32
GJ 731	-0.31	-0.37	-0.14	-0.68	-0.16	-0.18	-0.16	-0.58	-0.09	0.11	-0.09	-0.37	-0.20	-0.30	-0.35
GJ 740	-0.06	0.01	0.17	-0.35	0.13	0.08	-0.04	-0.25	0.12	0.27	0.08	0.03	0.09	0.00	-0.03
GJ 4092	-0.25	-0.26	-0.10	-0.23	0.22	-0.08	-0.27	-0.33	-0.03	0.10	-0.04	0.04	0.09	-0.14	0.05
GJ 1232	0.06	-0.08	0.00	0.05	0.08	-0.11	0.08	-0.06	0.11	0.03	0.08	0.05	0.05	0.05	0.17
GJ 752A	-0.04	0.06	0.03	-0.12	0.13	-0.01	-0.20	-0.12	0.05	0.17	-0.04	-0.09	0.05	-0.07	-0.24
GJ 754	-0.25	-0.34	-0.23	-0.16	-0.17	-0.11	-0.13	-0.16	-0.09	0.15	-0.14	-0.20	-0.19	-0.16	0.06
GJ 1236	0.00	-0.16	-0.07	-0.26	-0.14	-0.01	-0.19	-0.18	-0.05	0.13	-0.04	-0.14	0.00	-0.10	-0.13
GJ 9689	0.05	0.05	0.04	-0.15	0.29	0.12	-0.25	-0.12	0.04	0.12	0.12	0.28	0.32	0.07	0.20
GJ 793	0.01	-0.01	-0.04	-0.33	0.04	0.03	-0.23	-0.19	-0.01	0.07	-0.11	-0.06	0.25	-0.07	-0.31
GJ 1256	0.15	-0.09	-0.02	0.04	0.14	0.11	-0.14	0.07	-0.03	0.12	0.09	0.15	0.16	0.05	0.21
GJ 803	0.28	-0.03	0.00	-0.27	0.14	-0.33	-0.25	-0.57	0.09	0.19	0.18	-0.37	-0.13	-0.44	-0.65
LHS 3583	0.24	0.05	0.01	-0.11	0.06	0.11	-0.23	-0.01	-0.01	0.09	0.07	0.08	0.20	0.03	-0.07
LP 816-60	-0.11	-0.18	-0.11	-0.11	-0.05	-0.03	-0.13	-0.08	0.14	-0.03	-0.10	-0.05	-0.08	0.01	-0.01
GJ 821	-0.54	-0.80	-0.38	-0.71	-0.32	-0.62	-0.44	-1.00	-0.15	0.12	-0.39	-0.88	-0.54	-0.81	-0.90
BPM 96441	0.11	0.22	0.38	-0.14	0.28	0.38	0.10	0.07	0.22	0.38	0.38	0.48	0.28	0.36	0.67
TYC 2710-691-1	-0.12	0.00	-0.10	-0.55	-0.23	0.08	-0.13	-0.20	-0.03	0.23	0.22	-0.01	-0.16	0.08	0.41

Table A.4. Continued.

Star	[Fe/H]	[C/H]	[Na/H]	[Mg/H]	[Al/H]	[Si/H]	[Ca/H]	[Sc/H]	[Ti/H]	[V/H]	[Cr/H]	[Mn/H]	[Co/H]	[Ni/H]	[Zn/H]
TYC 2703-706-1	0.46	0.25	0.09	-0.40	0.18	-0.01	-0.19	-0.35	0.10	0.19	0.37	0.00	0.20	-0.09	-0.24
GJ 4196	-0.89	-0.97	-0.30	-0.84	-0.14	-0.80	-0.55	-1.30	-0.01	0.24	-0.44	-1.00	-0.52	-1.01	-0.88
GJ 832	-0.01	-0.06	-0.03	-0.18	0.03	-0.10	-0.24	-0.03	0.15	-0.04	-0.15	-0.02	-0.16	-0.26	-0.33
NLT T 52021	-0.19	0.07	-0.07	-0.36	0.16	0.04	-0.25	-0.22	-0.04	0.02	-0.12	-0.05	0.23	-0.03	-0.30
GJ 846	0.04	-0.01	0.06	-0.25	0.09	0.05	-0.12	-0.17	0.04	0.17	-0.05	-0.06	0.10	-0.05	-0.30
LHS 3746	0.20	0.01	0.04	-0.05	0.06	0.13	-0.16	0.05	0.01	0.14	0.07	0.12	0.18	0.07	0.08
GJ 849	0.32	0.17	0.20	0.11	0.34	0.19	-0.20	0.12	0.11	0.18	0.17	0.30	0.36	0.14	0.12
NLT T 53166	-0.62	-0.41	-0.43	-0.92	-0.35	-0.19	-0.07	-0.59	-0.35	-0.13	-0.42	-0.68	-0.32	-0.33	-0.87
GJ 1265	-0.11	-0.27	-0.19	-0.11	-0.11	-0.04	-0.14	-0.07	-0.08	0.14	-0.06	-0.08	-0.10	-0.08	0.15
LHS 3799	0.38	0.06	0.10	-0.10	0.18	0.00	0.02	-0.14	0.06	0.19	0.20	-0.11	0.08	-0.10	-0.33
2MASS J2222*	-0.21	-0.07	-0.11	-0.58	-0.22	0.03	-0.15	-0.28	-0.04	0.20	0.15	-0.09	-0.16	0.01	0.27
GJ 9793	0.24	0.31	0.06	-0.25	0.12	0.42	0.00	0.19	-0.02	0.13	0.34	0.48	0.32	0.43	0.57
GJ 873	0.55	0.07	0.08	-0.31	0.18	-0.12	-0.10	-0.41	0.06	0.10	0.18	-0.25	0.25	-0.29	-0.77
GJ 876	0.08	-0.03	0.08	-0.04	0.18	0.08	-0.14	-0.01	0.05	0.19	0.05	0.05	0.13	0.01	-0.01
GJ 877	0.00	0.10	0.01	-0.16	0.07	0.05	-0.15	-0.04	0.02	0.15	-0.07	-0.10	0.07	-0.01	-0.28
GJ 4306	0.13	0.03	0.18	-0.25	0.25	0.10	-0.23	-0.22	0.13	0.21	0.14	0.21	0.33	0.01	0.06
GJ 880	0.08	-0.04	0.06	-0.08	0.19	-0.02	-0.26	-0.19	0.06	0.17	0.06	0.04	0.11	-0.09	-0.09
GJ 884	-0.28	-0.18	-0.13	-0.35	-0.08	-0.06	-0.07	-0.25	-0.04	0.15	-0.17	-0.26	-0.17	-0.14	-0.24
GJ 887	0.08	-0.10	0.06	-0.27	0.08	-0.02	-0.16	-0.26	0.03	0.15	-0.06	-0.13	0.09	-0.14	-0.41
GJ 891	-0.11	-0.16	-0.09	-0.34	-0.08	-0.16	-0.28	-0.38	-0.01	0.17	-0.08	-0.29	-0.13	-0.25	-0.37
LHS 543	0.33	0.18	0.14	0.10	0.30	0.25	-0.13	0.23	0.05	0.13	0.17	0.28	0.33	0.20	0.14
GJ 895	0.03	0.23	0.00	-0.27	0.18	0.30	-0.04	0.04	-0.10	-0.03	-0.01	0.20	0.35	0.24	-0.18
GJ 908	-0.78	-0.85	-0.46	-0.79	-0.22	-0.67	-0.44	-1.09	-0.21	0.01	-0.52	-0.93	-0.49	-0.86	-1.06
LTT 9759	0.35	0.25	0.20	0.04	0.32	0.21	-0.20	0.11	0.11	0.17	0.16	0.27	0.37	0.15	-0.01
GJ 911	0.08	-0.03	0.08	-0.26	0.09	0.10	-0.12	-0.13	0.01	0.12	-0.06	-0.06	0.18	-0.02	-0.33

Notes. * 2MASS J22353504+3712131.